CONFORMATION AND ELECTRONIC CONFIGURATION OF COMPLEXES WITH MULTIPLE DIMETAL UNITS

A Dissertation

by

QINLIANG ZHAO

Submitted to the Office of Graduate Studies of
Texas A&M University
in partial fulfillment of the requirements for the degree of

DOCTOR OF PHILOSOPHY

August 2007

Major Subject: Chemistry

CONFORMATION AND ELECTRONIC CONFIGURATION OF COMPLEXES WITH MULTIPLE DIMETAL UNITS

A Dissertation

by

QINLIANG ZHAO

Submitted to the Office of Graduate Studies of
Texas A&M University
in partial fulfillment of the requirements for the degree of

DOCTOR OF PHILOSOPHY

Approved by:

Co-Chairs of Committee,	Carlos A. Murillo
	Marcetta Y. Darensbourg
Committee Members,	Eric E. Simanek
	Max D. Summers
Head of Department,	David H. Russell

August 2007

Major Subject: Chemistry

ABSTRACT

Conformation and Electronic Configuration of Complexes

with Multiple Dimetal Units. (August 2007)

Qinliang Zhao, B.S., Zhejiang University

Co-Chairs of Advisory Committee: Dr. C. A. Murillo
Dr. M. Y. Darensbourg

By using the building blocks $Mo_2(DAniF)_3(O_2CCH_3)$ (DAniF = *N*,*N*′-di-*p*-anisylformamidinate) and $[Mo_2(cis\text{-}DAniF)_2(NCCH_3)_4](BF_4)_2$, a series of complexes with multiple dimolybdenum units, bridged by a variety of linkers and having various oxidation states, has been synthesized and studied by various physical and chemical methods.

The isomeric neutral diamidate-bridged molecules, α– and β–$(DAniF)_3Mo_2(ArN(O)CC(O)NAr)Mo_2(DAniF)_3$ (Ar = *p*-anisyl), have been oxidized to give the PF_6 salts of the four cations α^{1+}, α^{2+}, β^{1+}, β^{2+}; all four structures together with supporting evidence show that in α^{1+} and α^{2+} the unpaired electrons are localized while in β^{1+} and β^{2+} they are delocalized in the time scale of these experiments.

It is also found that a hydroxide bridged complex having a $[Mo_2](\mu\text{-}OH)_2[Mo_2]$ core undergoes a oxidative deprotomation, both in solution and in crystals, to a compound with a $[Mo_2](\mu\text{-}O)_2[Mo_2]$ core. A probable key intermediate with one OH and one O bridge has also been characterized.

One electron oxidation of the tetrabridged compounds $[Mo_2(cis\text{-}DAniF)_2]_2(\mu\text{-}X)_4$, where X is a halogen atom (Cl, Br, I), produces a decrease of about 0.24 Å in the separation between the midpoints of the multiply bonded dimolybdenum units. DFT

calculations suggest partial bond formation during the oxidation, which is consistent with NIR, EPR and electrochemical measurements.

Additionally, a pair of isomeric cyclic triads containing three $[Mo_2(cis\text{-}DAniF)_2]^{2+}$ units, bridged by six fluoride anions, have been synthesized and crystallographically characterized. The symmetry of the α isomer is C_{2v} because the three $[Mo_2]$ units are oriented in two orthogonal directions while that of the other isomer is D_{3h} because the three $[Mo_2]$ units are parallel. No direct interconversion between isomers has been detected by heating or irradiation of solutions but oxidation of the α isomer first generates an α^+ species that changes to β^+.

Finally, reaction of $[Mo_2(cis\text{-}DAniF)_2(NCCH_3)_4](BF_4)_2$ and $Bu^n{}_4NBH_4$ in ether gives $[Mo_2(cis\text{-}DAniF)_2]_2(\mu\text{-}H)_4$ (**14**), a compound whose Mo_4H_4 core may be described as an elongated tetrahedron in which the four H atoms are along the four long edges and the Mo_2 units along the short edges.

DEDICATION

This work is dedicated to:

The memory of my graduate research advisor Professor F. A. Cotton

My husband, Zhijun (Jim) Jiang and my son, Jason Tom Jiang

ACKNOWLEDGEMENTS

I sincerely thank Prof. F. A. Cotton and Carlos A. Murillo for their guidance, encouragement and support during my graduate studies. I would like to thank them for giving me the opportunity to work on highly challenging and rewarding projects.

I thank Dr. Chun Y. Liu, my mentor, and Dr. Rongmin Yu, for their guidance and helpful discussions as I worked on these projects. Their wealth of synthetic knowledge has made this road less difficult to travel.

I truly appreciate the help of Dr. Xiaoping Wang concerning X-ray crystallography and Dr. Dino Villagrán's instruction and assistance with theoretical calculations. The assistance and advice they have provided have been of great help to carry out my research projects.

I greatly appreciate Dr. Zhong Li's advice and helpful discussions related to my research projects. I thank Dr. Sergey Ibragimov for introducing me to EPR measurements and Mr. Mark D. Young for magnetic susceptibility measurements.

I also thank Mrs. Julie A. Zercher for assistance and advice on the preparation of manuscripts. I would like to thank all the members of the LMSB, past and present, friends and family for their support and encouragement through the years.

Finally, I would like to express special thanks to my husband Zhijun (Jim) Jiang and my son Jason for their love. Their support was very important accomplishing my graduate program.

TABLE OF CONTENTS

LIST OF TABLES

TABLE . Page

LIST OF FIGURES

FIGURE Page

FIGURE Page

FIGURE Page

CHAPTER I

INTRODUCTION*

Mixed valence (MV) systems are a class of inorganic compounds which contain two or more atoms of the same elements in different formal oxidation states. This concept has recently been of interest for the development of highly conducting materials, energy storage devices and molecular electronic applications, for example, molecular wires and molecular switches.[1] It is also of significance in a variety of interdisciplinary areas for reasons that include augmenting fundamental knowledge of chemistry, searching for better understanding of important biochemical redox and electron transfer processes, and fabrication of nanoscale structures in materials science.[2]

Mixed-valence chemistry has long focused on electronic interactions between adjacent, especially covalently connected, metal centers joined by a linker.[3] The most intensively studied MV systems are those complexes containing two structurally identical metal-containing units linked by a symmetrical organic group, where each metal atom has different formal oxidation numbers and the odd electron may be localized on one end or move back and forth between the two metal centers. [4] The earliest systematically studied example is the pyrazine-bridged Ru dimer,

---

This dissertation follows the format and style of *Inorganic Chemistry*.

* Reproduced in part with permission from *Inorg. Chem.* **2007**, *46*, 2604, Cotton, F. A.; Liu, C. Y.; Murillo, C. A.; Zhao, Q., "Electronic Localization versus Delocalization Determined by the Binding of the Linker in an Isomer Pair," Copyright 2007 American Chemical Society.

$\{[Ru(NH_3)_5](pyz)[Ru(NH_3)_5]\}^{5+}$, pyz = pyrazine, (**I** in Figure 1), also known as the Creutz-Taube (C-T) ion.[5] The C-T ion has been used as a prototype for hundreds of compounds to study issues such as the location of the odd electron in compounds of this type, the extent of the electronic communication between the two metal centers mediated by the linkers, and the pathway of electron transfer from one end (donor) to the other (acceptor).

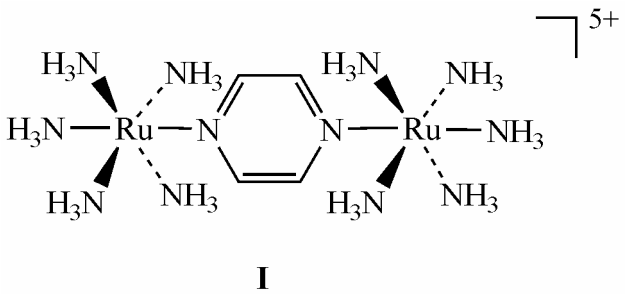

I

Figure 1. The Creutz-Taube (C-T) Ion.

Since the C-T ion was synthesized in the late 1960s,[5] a host of other such systems have been investigated.[4,6] Various chemical and physical methods such as X-ray structure analysis, electrochemical studies, spectroscopic and magnetic measurements have been used to probe the electronic communication between the two redox sites. Depending on the ability of the linker to transmit electronic communication, mixed valence systems have conventionally been divided into three different classes in the widely accepted Robin-Day categories,[7] that is, Class I (no interaction, localized valency), Class II (weak to medium coupling, valence trapped), and Class III (strong interaction, delocalized). Earlier work by Hush[8] illustrated the three classes of mixed valence compounds by a classical potential energy configuration diagram shown in

Figure 2, in which the *X* axis is a coordinate expressing the Ru_a^{III}-N distance as the sum of Ru_a-N and Ru_b-N is held constant. The systems vary from completely localized systems (Class I) to intermediate (Class II) to completely delocalized (Class III). For compounds in Classes I and II, there are two potential energy minima and the odd electron is energetically favored to be localized on one of the two metal centers because of the presence of large energy barrier (E_{th}) for thermal electron transfer. Whereas in Class III compounds, due to the strong electron coupling, this energy barrier does not exist, $E_{th} = 0$, and the odd electron is present actually equally on both metal centers which are indistinguishable.

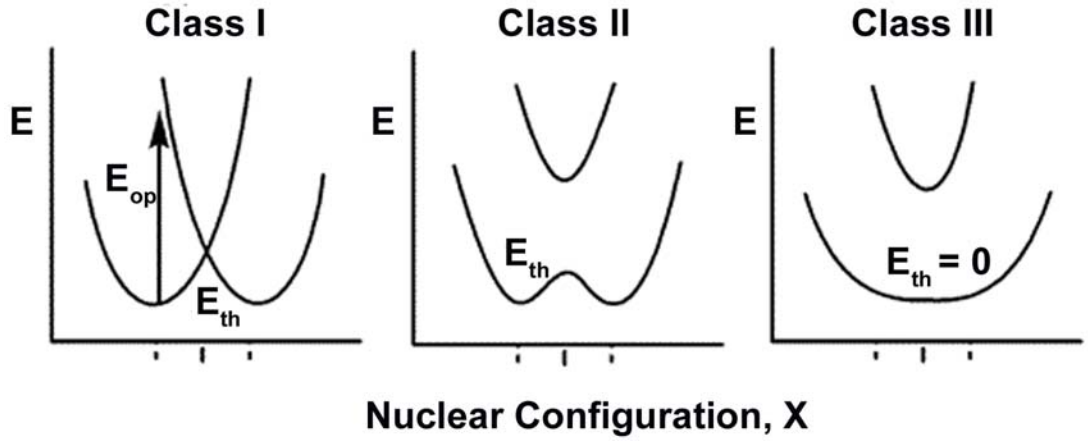

Figure 2. Potential energy configuration curves for the three classes of mixed valence compounds classified by Robin and Day.

Intense studies on the C-T complex and other similar compounds have aimed at answering the question of whether the unpaired electron is localized or delocalized. At least for the two extreme situations, fully localized (Class I) and delocalized (Class III),

different structure parameters for the molecules are expected in that the molecules in Class I have two distinct metal centers but those in Class III should have two indistinguishable ends. However, no satisfactory results were ever obtained from crystallographic studies even though assiduous and skillful efforts were made.[9] In dinuclear compounds, where a single metal serves as the redox site, the donor and acceptor differ by one electron which was actually removed from an essentially non-bonding orbital, thus large changes in structural parameters are not expected. In addition, bond distances between the heavy metal atoms and light ligand atoms (typically N or O) have relatively high estimated standard deviations, which may blur the structural difference between the two ends. The lack of direct structural evidence to evaluate a system has delayed progress in this area. Therefore, there is still a need to develop complex systems in which both integral data collections and unambiguous data analysis may be accomplished.

Recently, we[10] and others[11] have extended the concept of mixed valence systems to the field of covalently bonded dimetal units by employing two or more dimetal units, typically two Mo_2^{4+} species joined by an appropriate linker. In such compounds, quadruply bonded Mo_2^{4+} units often act as redox sites. By careful selection of the linker, it is possible to control the geometric conformation of the assembled molecules, regulate the electronic configuration, and modify their chemical properties. The compounds that have been most studied could be generically formulated as $[Mo_2]L[Mo_2]$ shown in Figure 3, where $[Mo_2]$ is an abbreviation for an Mo_2^{4+} core supported by two or three *N*,*N*'-di(*p*-anisyl)formamidinate (DAniF) anions, and L is the linker capable of binding

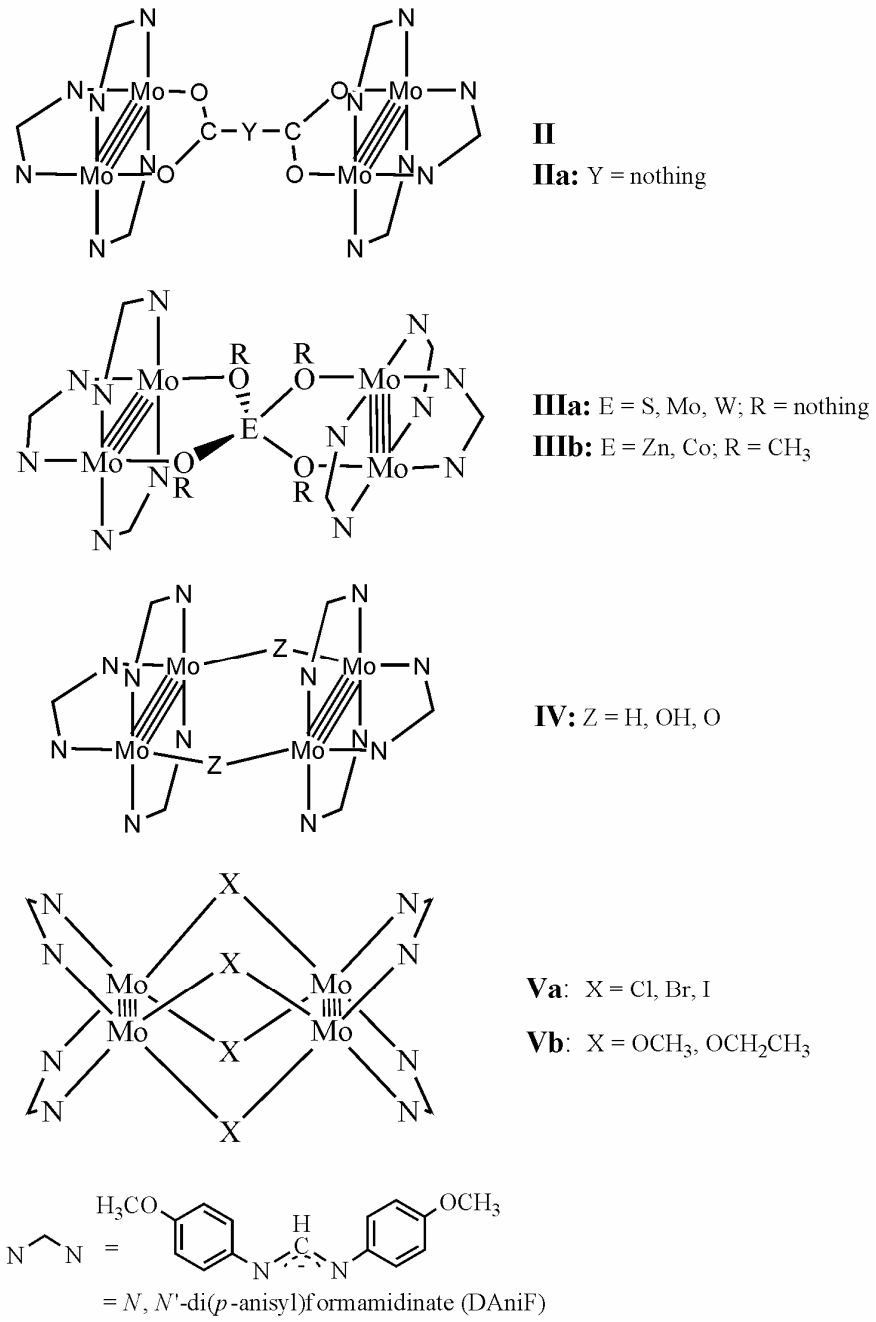

Figure 3. Representatives' examples of complexes with two covalently bonded dimolybdenum units.

the $[Mo_2]$ units. In addition to organic linkers such as dicarboxylate, $^{-}O_2C–Y–CO_2^{-}$ (**II**),[12] and diamidate,[13] a variety of inorganic species have been used to link two dimetal units. These include polyatomic anions EO_4^{2-} (**IIIa**, E = S, Mo and W), [14] $E(OCH_3)_4^{2-}$ (**IIIb**, E = Zn or Co),[15] single atom hydride H^- (**IV**),[16] hydroxide OH^- (**IV**),[17] halides X (**Va**, X = Cl^-, Br^- and I^-),[17b] and alkoxides ^{-}OR (**Vb**, R = CH_3, CH_2CH_3).[18]

To some extent, a covalently bonded dimetal unit behaves like a single metal ion and the tetranuclear complexes $[M_2]L[M_2]$ have a basic kinship with the binuclear Creutz-Taube ion. For instance, the $[M_2]$ unit is an electrochemically addressable redox center in which one-electron oxidation from $[M_2]$ units occurs reversibly, and the "dimer of dimers" displays two successive redox couples with varying potential separations as shown in Figure 4. The potential separation ($\Delta E_{1/2}$) between two redox waves has been used to estimate the electronic coupling between the two metal centers. Similarly to binuclear complexes with two redox sites, a constant for the comproportionation equilibrium (Eq. 1) involving dimetal species at three different oxidation levels can be derived from the $\Delta E_{1/2}$ value.[19]

$$[M_2](L)[M_2] + \{[M_2](L)[M_2]\}^{2+} \rightleftharpoons 2\{[M_2](L)[M_2]\}^{+} \qquad \text{(eq. 1)}$$

$$K_c = e^{\Delta E_{1/2}/25.69}$$

The comproportionation constant, K_c, which is exponentially related to $\Delta E_{1/2}$, measures the thermodynamic stability of the mixed-valence species, formally $\{[M_2]L[M_2]\}^{+}$, and has also been used to evaluate the extent of electronic communication between the redox sites.[12] However, it must be pointed out that the value

of $\Delta E_{1/2}$ or K_c, even though to some extent it reflects the electronic coupling strength between the two metal centers, it does not provide all necessary information. Data from structural analysis, spectroscopic and magnetic measurements are also required to explain the extent of the electronic communication in the MV systems.

Because localized $\{[M_2]L[M_2]\}^+$ species have two distinct $[M_2]$ units, they are better described by the formula $[M_2]^{1+}L[M_2]^0$ and delocalized systems may be represented by $[M_2]^{0.5+}L[M_2]^{0.5+}$, as shown in Figure 4.

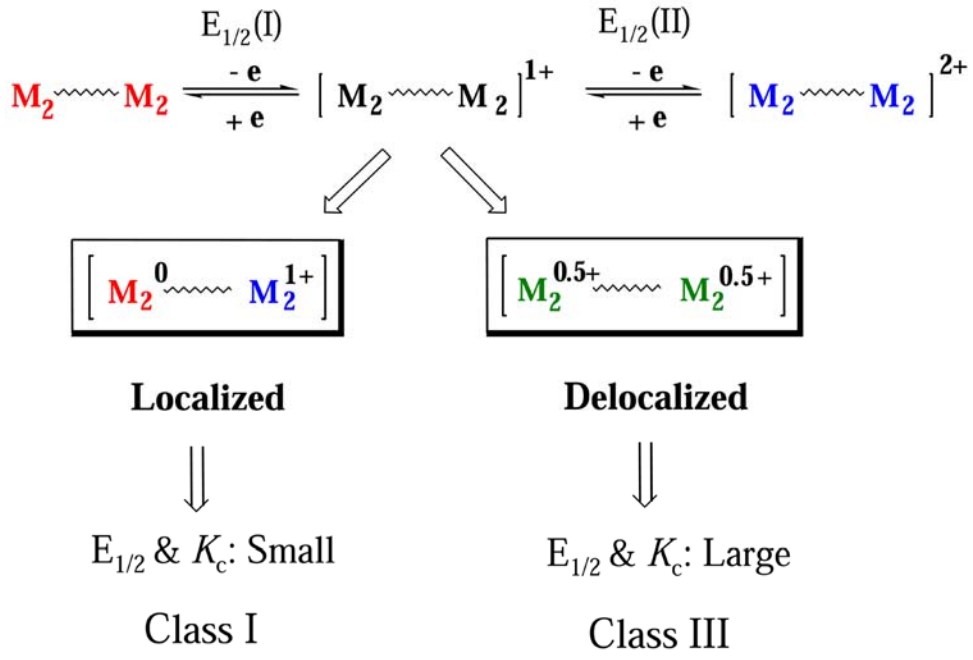

Figure 4. Redox processes for complexes with two dimetal units serving as the redox sites.

Typically, there are at least two important advantages in having compounds with dimetal units as the redox sites. Firstly, the electronic properties of many dimetal units have been very well studied.[10] This is particularly true for the multiply bonded [Mo_2] units which have a $\sigma^2\pi^4\delta^n$ (n = 0, 1, 2) electronic configuration shown in Figure 5 based on MO theory. The effect of the change of one electron in the dimetal unit can be monitored directly by the change in metal–metal bond distances from the X-ray analysis, thus affording a uniquely practical criterion for determination of the bond order or oxidation state of the dimetal center.[20] Secondly, electronic spectra, especially the position of δ-δ^* transitions, can be used to track the variation in electronic structure of the metal unit. In addition, a dimetal unit such as [Mo_2] differs from a mononuclear ion in coordination binding mode and electronic configuration, which endow the dimolybdenum molecules with unique structural and electronic features that greatly facilitate the study of mixed-valence chemistry.

Our studies on various compounds of the type [Mo_2]L[Mo_2] have shown that orbital interactions in the equatorial binding mode for an [Mo_2] unit may be constrained, by symmetry considerations, to occur between the metal based δ and the linker π^* orbitals. Thus the nature of the π^* orbitals, energy difference in linker π^* and metal δ orbitals, and conformation of the bridging groups play an important role in mediating the electronic coupling strength.[12c] The MV species may vary from being localized to being fully delocalized, depending on the efficiency of the linker in allowing electronic communication between the metal centers. For example, fully localized (Class I) mixed-valence compounds $[Mo_2]^0(OCH_3)_2E(OCH_3)_2[Mo_2]^{1+}$ (**IIIb** in Figure 3, E = Zn, Co)

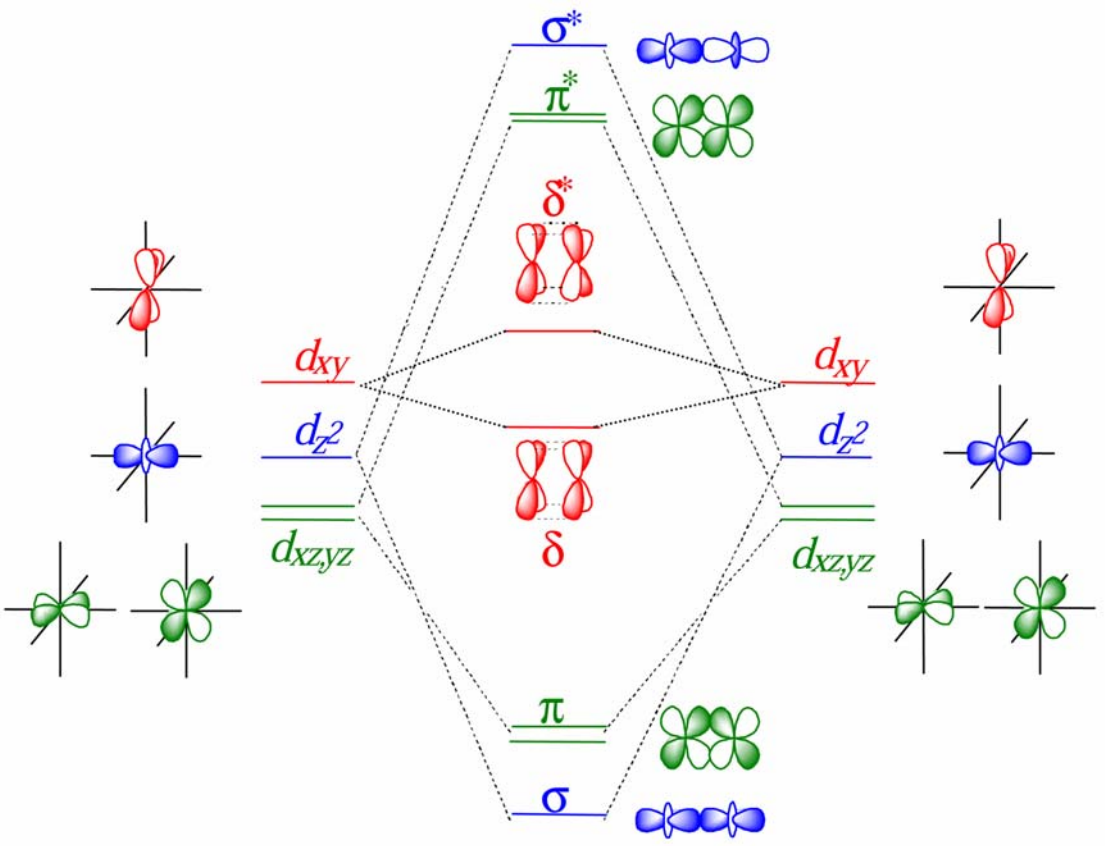

Figure 5. Molecular orbital diagram for a multiply bonded [Mo_2] unit.

were obtained because of the lack of symmetry allowed orbital interaction between the metal δ and linker π^* orbitals.[15] In the oxalate-linked compound $[Mo_2](O_2C–CO_2)[Mo_2]$ (**IIa** in Figure 3, Y = nothing), there are two essentially parallel dimetal units separated by a short distance, ca. 7.0 Å, which are only moderately coupled, in part because the metal δ to ligand π^* orbitals interactions must traverse through the C–C σ bond.[12a] When certain large conjugated linkers are introduced, for instance, tetraazatetracene[21] and dioxolene,[22] strong metal to metal interactions are observed and the resulting MV complexes are delocalized (Class III).

Although a large number of MV systems have been developed and studied for electronic coupling, few systems are fully characterized. The main goal of my graduate research is to gain more insight into the fundamental issues of electronic coupling by taking advantage of dimetal units. It includes syntheses of neutral complexes by employing a variety of linkers and building blocks, searching for comparable coupling systems with minimum variables, and full characterization of the neutral complexes and their oxidized MV species using various chemical and physical methods.

This dissertation presents the assembly of dimolybdenum units, $[Mo_2(cis\text{-}DAniF)_2]^{2+}$ and $[Mo_2[DAniF)_3]^{+}$, with various linkers which include oxamidate, hydroxide, oxide, halide and hydride anions, and the study of their conformation and electronic configuration. In Chapter II, the impact of the linkage isomers on the electronic coupling between the two dimetal centers is disscussed. It is found that variations of the binding modes of the linker can modify the mixed valence complex from an electron localized system to a delocalized system. Chapter III deals with a

hydroxide bridged complex having a $[Mo_2](\mu\text{-}OH)_2[Mo_2]$ core that undergoes a oxidative deprotomation, both in solution and in crystals, to a compound with a $[Mo_2](\mu\text{-}O)_2[Mo_2]$ core. In Chapter IV, a general methodology, using a designed building block, is developed for the synthesis of the tetrabridged compounds $[Mo_2(cis\text{-}DAniF)_2]_2(\mu\text{-}X)_4$, where X is a halogen atom (Cl, Br, I). All the experimental results and theoretical calculations indicate that the strong electronic coupling is principally due to direct overlap between the δ orbitals from the adjacent dimetal units. Chapter V covers the syntheses of a pair of isomeric cyclic triads containing three quadruply bonded $[Mo_2]$ units, $[Mo_2(cis\text{-}DAniF)_2]^{2+}$, bridged by six fluoride anions. The symmetry of the α isomer is C_{2v} because the three $[Mo_2]$ units are oriented in two orthogonal directions while that of the other is D_{3h} because the three $[Mo_2]$ units are parallel. Remarkably, no interconversion between isomers have been detected by heating or irradiation of solutions but oxidation of the α isomer first generates an α^+ species that changes to β^+. In Chapter VI, the assembly of the building block $[Mo_2(cis\text{-}DAniF)_2]^{2+}$ and hydride anions, H^-, gave a tetranuclear complex with a Mo_4H_4 core that may be described as an elongated tetrahedron in which the four H atoms are along the four long edges and the Mo_2 units along the short edges.

CHAPTER II

MODIFICATION OF ELECTRONIC COMMUNICATION VIA THE LINKAGE ISOMERS*

Prior work in this laboratory has reported that when a diaryloxamidate group, $[ArNC(O)C(O)NAr]^{2-}$ (Ar = phenyl or *p*-anisyl), serves as linker, two geometric isomers can be isolated.[13a] The two isomers, designated as α and β as shown in Figure 6, entail different binding modes of the oxamidate ligand. The α compound has two Mo_2^{4+} units linked by the oxamidate in three-atom bridging mode, similar to the oxalate (**IIa** in Figure 3 of Chapter I and the unsubstituted oxamidate analogues, [13b] but differing in that the two amidate groups are orthogonal. In the β isomer, the oxamidate linker adopts a four-atom (NCCO) bridging mode with respect to each $[Mo_2]$ unit, thus giving a molecule with two essentially parallel Mo–Mo quadruple bonds. From their structures, it was expected that the electronic coupling effects between these two molecules should be quite different. DFT calculations[13a] have shown that in the α form, the orbital interaction between two dimetal units is virtually none because of the orthogonality of the two Mo_2 units, but for the β isomer, delocalized molecular orbitals spread across between two Mo_2 centers with significant involvement of the ligand π* orbitals as shown in Figure 7.

---

* Reproduced in part with permission from *Inorg. Chem.* **2007**, *46*, 2604, Cotton, F. A.; Liu, C. Y.; Murillo, C. A.; Zhao, Q., "Electronic Localization versus Delocalization Determined by the Binding of the Linker in an Isomer Pair," Copyright 2007 American Chemical Society.

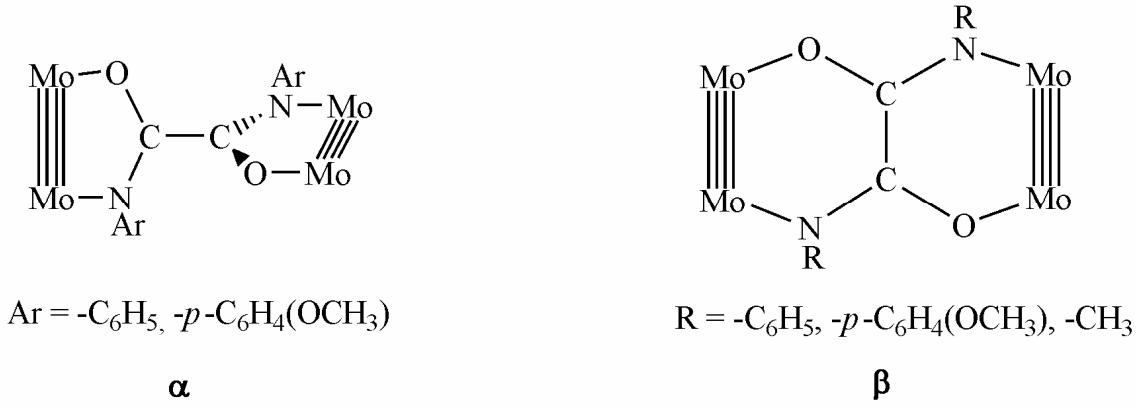

Figure 6. Core structure of the oxamidate bridged isomer pair.

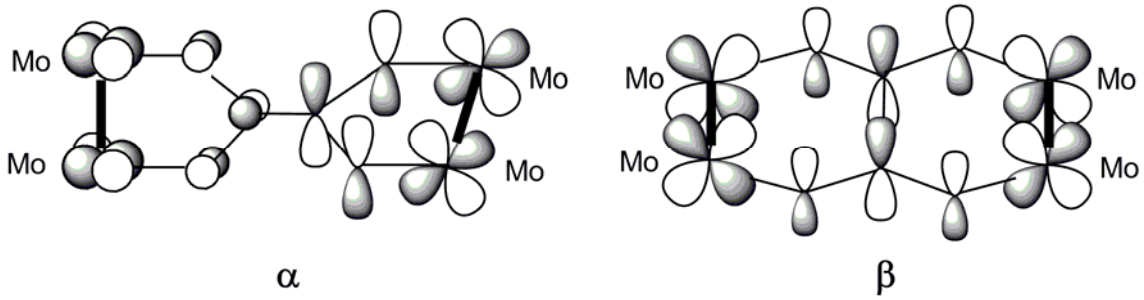

Figure 7. Frontier orbital interaction between the Mo_2 units (δ) and linker (π^*) for the isomer pair.

Indeed, in the primary study in which we were unable to isolate pure crystalline oxidized products, [13a] we have found that while the separation of oxidation potentials ($\Delta E_{1/2}$) for the α isomer is ca.190 mV, it is ca. 530 mV for the β form. From these values, comproportionation constants (K_c)[19] of ca. 10^3 and 10^6 are derived for these two compounds, respectively. Furthermore, the difference between them in electronic structure is also manifested in their electronic spectra.[13a]

This chapter shows that syntheses of the neutral α and β isomers have been improved to allow isolation of the corresponding MV species $\{[Mo_2](L)[Mo_2]\}^+$, as well as the preparation of the corresponding doubly oxidized species having two linked Mo_2^{5+} units. The compounds newly synthesized include α–$[Mo_2(DAniF)_3]_2$(*N*,*N*′-di-*p*-anisyloxamidate)(PF_6) (**1**), β–$[Mo_2(DAniF)_3]_2$(*N*,*N*′-di-*p*-anisyloxamidate)(PF_6) (**2**), α–$[Mo_2(DAniF)_3]_2$ (*N*,*N*′-di-*p*-anisyloxamidate)(PF_6)$_2$ (**3**), and β–$[Mo_2(DAniF)_3]_2$(*N*,*N*′-di-*p*-anisyloxamidate)(PF_6)$_2$ (**4**). X–ray crystallographic analyses show unambiguously that the MV species in the α form (**1**) has an unsymmetrical molecular structure with the Mo–Mo bond distances corresponding to a localized Mo_2^{4+} unit and a delocalized Mo_2^{5+} unit, whereas in the β form (**2**), there are two essentially identical $[Mo_2]$ units. Consistently, these compounds also exhibit different features in the near-IR (NIR) spectra: while compound **1** has a featureless spectrum in this region, compound **2** presents an intense absorption at low energy which might conventionally be termed a metal-to-metal intervalence charge-transfer, but which is better described as a HOMO–1 → SOMO transition in a fully delocalized molecule.[13a] The two doubly oxidized compounds in the pair also exhibit different magnetic behaviors. The α species **3** is

paramagnetic because of the weakness of interactions of the two localized Mo_2^{5+} units, but the β form, **4**, is diamagnetic due to the pairing of the electrons in the two Mo_2^{5+} units. The two mixed-valence complexes **1** and **2** are unambiguously assigned to Class I and Class III, respectively.

EXPERIMENTAL SECTION

Materials and Methods. Solvents were dried and then distilled under N_2 following conventional methods or purified under argon using a Glass Contour solvent purification system. The syntheses of **1–4** were conducted under N_2 using Schlenk line techniques. $Mo_2(DAniF)_3(O_2CCH_3)$,[13a] *N*,*N*′-di-*p*-anisyloxamide[13a] and HDAniF[23] were prepared by following published methods; 0.5 M solution of $NaOCH_3$ in methanol**,** purchased from Aldrich, were used as received. Ferrocenium hexafluorophosphate, $(Cp_2Fe)PF_6$, was purified by recrystallization from acetone/hexane prior to use.

Physical Measurements. Elemental analyses were performed by Robertson Microlit Laboratories, Madison, New Jersey. ^{1}H NMR spectra were recorded at 25 °C on a Mercury-300 NMR spectrometer with chemical shifts (δ ppm) referenced to $CDCl_3$. Electronic spectra in the UV−vis range were measured in the range of 200 to 800 nm on a Shimadzu UV−2501PC spectrophotometer. The NIR spectra were obtained from a Bruker TEASOR 27 spectrometer. EPR spectra were recorded using a Bruker ESP300 spectrometer, and the simulations of the spectra were performed using the program WIN-EPR SimFonia from Bruker. Measurement of magnetic susceptibility was performed on a SQUID magnetometer.

Improved Preparation of α–[Mo_2(DAniF)$_3$]$_2$(*N*,*N*′-di-*p*-anisyloxamidate). $Mo_2(DAniF)_3(O_2CCH_3)$ (0.51 g, 0.50 mmol) and *N*,*N*′-di-*p*-anisyloxamide (0.075 g, 0.25 mmol) were mixed in 20 mL of tetrahydrofuran. To the mixture, with stirring, was added 1.0 mL of a $NaOCH_3$ solution (0.50 M in CH_3OH), giving an orange solution. After stirring at ambient condition for 48 h, a yellow solid formed. The solvent was removed by evaporation under vacuum. The residue was extracted by dichloromethane, then, filtered through a Celite-packed frit. The volume of the filtrate was reduced to about 5 mL. A yellow solid was produced by addition of hexanes (ca. 30 mL) to the concentrated solution. Finally, the solid product was collected by filtration and dried under vacuum. Yield: 0.46 g (82%). This material was used for the oxidation reactions without further purification.

Improved Preparation of β–[Mo_2(DAniF)$_3$]$_2$(*N*,*N*′-di-*p*-anisyloxamidate). $Mo_2(DAniF)_3(O_2CCH_3)$ (0.51 g, 0.50 mmol) and *N*,*N*′-di-*p*-anisyloxamide (0.075 g, 0.25 mmol) were mixed in 20 mL of tetrahydrofuran. To the mixture, with stirring, was added 1.0 mL of a $NaOCH_3$ solution (0.5 M in CH_3OH), giving an orange solution. The solution was stirred for 30 min and then, the solvent was removed by evaporation under vacuum. The residue was extracted with dichloromethane (ca. 20 mL) and filtered through a Celite-packed frit. With stirring, the filtrate was transferred, through a cannula, to hot enthanol, generating a red precipitate. The mixture was stirred at ~ 80 °C for 30 min; then filtered while it was hot. The red solid was washed with 10 mL of hot ethanol and finally, dried under vacuum. Yield: 0.23 g (41%). This material was used for the oxidation reaction without further purification.

Preparation of α–[Mo_2(DAniF)$_3$]$_2$(*N*,*N*′-di-*p*-anisyloxamidate)PF_6, 1. A yellow solution of α–[Mo_2(DAniF)$_3$]$_2$(*N*,*N*′-di-*p*-anisyloxamidate) (0.140 g, 0.063 mmol) in 10 mL of CH_2Cl_2 and a blue solution having 1 equiv of $(Cp_2Fe)PF_6$ in 10 mL of CH_2Cl_2 were prepared separately and cooled to −78 °C. The two solutions were mixed by transferring the oxidizing reagent to the dimolybdenum complex using a cannula. After the resultant solution was stirred at −78 °C for 30 min, 60 mL of pre-cooled hexanes were added by syringe to produce a dark brown precipitate. After the solvent was decanted, the solid residue was washed with 20 mL of hexanes and then dried under vacuum. The solid was dissolved in dichloromethane and the solution was then layered with hexanes. Large dark crystals were obtained after diffusion for a period of three days. Yield: 0.081 g (54%). UV–vis in CH_2Cl_2, λ_{max} (nm) (ε, $M^{-1}cm^{-1}$): 442 (3.3×10^3). Anal. calcd. for $C_{106}H_{104}F_6Mo_4N_{14}O_{16}P$ (**1**): C, 53.97; H, 4.44; N, 8.31. Found: C, 54.09; H, 4.18; N, 8.21.

Preparation of β–[Mo_2(DAniF)$_3$]$_2$(*N*,*N*′-di-*p*-anisyloxamidate)PF_6, 2. This black compound was synthesized using a procedure similar to that for **1**, where red β–[Mo_2(DAniF)$_3$]$_2$(*N*,*N*′-di-*p*-anisyloxamidate) and 1 equiv of Cp_2FePF_6 were used as the starting materials. Large block-shaped crystals of **2**·3.5CH_2Cl_2 were obtained. Yield: 0.071 g (89%). NIR (KBr, cm^{-1}): 4730 (vs). UV–vis in CH_2Cl_2, λ_{max} (nm) (ε, $M^{-1}cm^{-1}$): 433 (3.4×10^3), 566 (1.3×10^3), 630 (7.2×10^3). Anal. calcd. for $C_{107}H_{106}Cl_2F_6Mo_4N_{14}O_{16}P$ (**2**·CH_2Cl_2): C, 52.59; H, 4.37; N, 8.02. Found: C, 52.38; H, 3.97; N, 7.94.

Preparation of α–[Mo_2(DAniF)$_3$]$_2$(*N*,*N*′-di-*p*-anisyloxamidate)$(PF_6)_2$, 3. This

compound was prepared similarly to **1** using α–$[Mo_2(DAniF)_3]_2$(*N*,*N*′-di-*p*-anisyloxamidate) (0.12 g, 0.055 mmol) and 2 equiv of $(Cp_2Fe)PF_6$ (0.036 g, 0.11 mmol) in 15 mL of CH_2Cl_2. Small black crystals were obtained. Yield: 0.077 g (56%). UV–vis in CH_2Cl_2, λ_{max} (nm) (ε, $M^{-1}cm^{-1}$): 450 (8.7×10^4). Anal. calcd. for $C_{106}H_{104}F_{12}Mo_4N_{14}O_{16}P_2$ (**3**): C, 50.85; H, 4.19; N, 7.83. Found: C, 50.50; H, 3.74; N, 7.70.

Preparation of β–$[Mo_2(DAniF)_3]_2$(*N*,*N*′-di-*p*-anisyloxamidate)$(PF_6)_2$, 4. This black compound was synthesized using a procedure similar to that for **2**, using two equiv of oxidizing regent. Small block-shaped crystals of **4**·$2CH_2Cl_2$ were obtained. Yield: 0.069 g (82%). ^{1}H NMR at 25 °C (δ, ppm in $CDCl_3$): 6.62 (d, 4H, aromatic C─*H*), 6.41 (m, 24H, aromatic C─*H*), 6.11 (m, 24H, aromatic C─*H*), 5.85 (d, 4H, aromatic C─*H*), 3.77 (s, 6H, ─OC*H*$_3$), 3.65 (s, 12H, ─OC*H*$_3$), 3.56 (s, 12H, ─OC*H*$_3$), 3.50 (s, 6H, ─OC*H*$_3$), 3.47 (s, 6H, ─OC*H*$_3$). ^{1}H NMR at –50 °C (δ, ppm in $CDCl_3$): 8.93 (s, 6H, ─NC*H*N─), 6.57 (d, 4H, aromatic C─*H*), 6.42 (m, 24H, aromatic C─*H*), 6.05 (m, 24H, aromatic C─*H*), 5.86 (d, 4H, aromatic C─*H*), 3.77 (s, 6H, ─OC*H*$_3$), 3.66 (s, 12H, ─OC*H*$_3$), 3.54 (s, 12H, ─OC*H*$_3$), 3.48 (s, 6H, ─OC*H*$_3$), 3.45 (s, 6H, ─OC*H*$_3$). UV–vis in CH_2Cl_2, λ_{max} (nm) (ε, $M^{-1}cm^{-1}$): 464 (1.0×10^4), 598 (787), 731 (1.3×10^4), 876 (7.2×10^3). Anal. calcd. for $C_{107}H_{106}Cl_2F_{12}Mo_4N_{14}O_{16}P_2$ (**4**·CH_2Cl_2): C, 49.65; H, 4.13; N, 7.58. Found: C, 49.25; H, 4.35; N, 7.13.

X−ray Structure Determinations. Single crystals suitable for X-ray analysis were mounted and centered on the tips of cryoloops. Then each crystal was attached to a goniometer head. Data for **1**·4CH_2Cl_2, **2**·3.5CH_2Cl_2, **3**·3CH_2Cl_2 and **4**·2CH_2Cl_2 were collected at −60 °C on a BRUKER SMART 1000 CCD area detector system. Cell parameters were determined using the program SMART.[24] Data reduction and integration were performed with the software package SAINT,[25] while absorption corrections were applied using the program SADABS.[26] The positions of the heavy atoms were found via direct methods using the program SHELXTL.[27] Subsequent cycles of least-squares refinement followed by difference Fourier syntheses revealed the positions of the remaining non-hydrogen atoms. Hydrogen atoms were added in idealized positions. Non-hydrogen atoms, except some atoms from disordered methoxyl groups and solvent molecules, were refined with anisotropic displacement parameters. Crystallographic data for **1**·4CH_2Cl_2, **2**·3.5CH_2Cl_2, **3**·3CH_2Cl_2, and **4**·2CH_2Cl_2 are given in Table I and selected bond distances and angles in Table II.

Table I. X−ray Crystallographic Data of **1**·4CH_2Cl_2, **2**·3.5CH_2Cl_2, **3**·3CH_2Cl_2 and **4**·2CH_2Cl_2

compound	**1**·4CH_2Cl_2	**2**·3.5CH_2Cl_2	**3**·3CH_2Cl_2	**4**·2CH_2Cl_2
empirical formula	$C_{110}H_{112}Cl_8F_6Mo_4N_{14}O_{16}P$	$C_{109.5}H_{111}Cl_7F_6Mo_4N_{14}O_{16}P$	$C_{109}H_{110}Cl_6F_{12}Mo_4N_{14}O_{16}P_2$	$C_{108}H_{108}Cl_4F_{12}Mo_4N_{14}O_{16}P_2$
fw	2698.47	2656.00	2758.51	2673.58
space group	$P2_1/c$ (No.14)	$P\bar{1}$ (No. 2)	$P\bar{1}$ (No. 2)	$P\bar{1}$ (No. 2)
a (Å)	14.2863(7)	16.186(3)	15.905(4)	16.489(5)
b (Å)	15.7924(8)	18.231(3)	19.349(5)	17.873(5)
c (Å)	52.946(3)	21.990(4)	21.638(5)	20.498(6)
α (deg)	90	93.145(3)	72.397(5)	74.728(5)
β (deg)	93.432(2)	110.568(3)	79.210(5)	75.070(5)
γ (deg)	90	108.078(3)	69.398(4)	80.877(6)
V (Å^3)	11924(1)	5677(2)	5917(2)	5604(3)
Z	4	2	2	2
T (K)	213	213	213	213
d_{calcd} (g/cm^3)	1.503	1.554	1.548	1.584
μ (mm^{-1})	0.680	0.690	0.663	0.651
R1[a] (wR2[b])	0.077 (0.133)	0.064 (0.138)	0.086 (0.166)	0.090 (0.165)

[a] $R1 = \Sigma\|\|F_o\|-\|F_c\|\|/\Sigma|F_o|$.

[b] $wR2 = [\Sigma[w(F_o^2-F_c^2)^2]/\Sigma[w(F_o^2)^2]]^{1/2}$

Table II. Selected Bond Lengths (Å) and Angles (deg) of **1**·4CH_2Cl_2, **2**·3.5CH_2Cl_2, **3**·3CH_2Cl_2 and **4**·2CH_2Cl_2

Compound	**1**·4CH_2Cl_2	**2**·3.5CH_2Cl_2	**3**·3CH_2Cl_2	**4**·2CH_2Cl_2
Mo(1)−Mo(2)	2.0920(6)	2.1116(7)	2.1236(8)	2.1449(8)
Mo(3)−Mo(4)	2.1291(6)	2.1140(6)	2.1254(8)	2.1416(8)
$Mo_2\cdots Mo_2$[a]	7.051	6.273	7.070	6.211
Mo(1)−N(1)	2.197(4)	2.147(4)	2.164(4)	2.109(4)
Mo(2)−O(1)	2.121(3)	2.054(3)	2.134(4)	2.026(4)
Mo(3)−N(2)	2.166(4)	2.141(4)	2.175(4)	2.118(5)
Mo(4)−O(2)	2.105(3)	2.058(3)	2.122(4)	2.016(4)
Mo(1)−N(3)	2.166(4)	2.179(4)	2.138(5)	2.167(4)
Mo(1)−N(5)	2.153(4)	2.167(4)	2.130(5)	2.104(5)
Mo(1)−N(7)	2.161(4)	2.154(4)	2.162(5)	2.160(4)
Mo(2)−N(4)	2.129(4)	2.133(4)	2.102(5)	2.119(4)
Mo(2)−N(6)	2.129(4)	2.103(4)	2.117(5)	2.107(5)
Mo(2)−N(8)	2.136(4)	2.106(4)	2.093(5)	2.063(4)
Mo(3)−N(9)	2.121(4)	2.176(4)	2.152(5)	2.140(5)
Mo(3)−N(11)	2.112(4)	2.174(4)	2.131(5)	2.162(4)
Mo(3)−N(13)	2.145(4)	2.136(4)	2.123(5)	2.120(5)
Mo(4)−N(10)	2.123(4)	2.110(4)	2.114(5)	2.114(5)
Mo(4)−N(12)	2.089(4)	2.129(4)	2.093(5)	2.096(5)
Mo(4)−N(14)	2.120(4)	2.111(4)	2.111(5)	2.106(5)
N(1)−C(1)	1.305(6)		1.317(7)	
N(2)−C(2)	1.308(6)		1.302(7)	
N(1)−C(2)		1.324(6)		1.310(7)
N(2)−C(1)		1.323(6)		1.319(7)
O(1)−C(1)	1.282(6)	1.287(5)	1.265(6)	1.283(6)

Table II (continued)

O(2)−C(2)	1.290(5)	1.277(5)	1.274(6)	1.291(6)
C(1)−C(2)	1.528(6)	1.507(6)	1.533(7)	1.516(7)
Mo(1)−Mo(2)−O(1)	95.09(9)	99.38(8)	93.57(10)	98.82(10)
Mo(2)−Mo(1)−N(1)	89.63(10)	98.84(10)	90.25(12)	99.43(12)
Mo(3)−Mo(4)−O(2)	94.04(8)	98.90(9)	93.78(10)	100.11(10)
Mo(4)−Mo(3)−N(2)	89.58(10)	99.92(9)	89.59(12)	98.34(12)

[a] Distance between the midpoints of the two dimolybdenum units.

RESULTS AND DISCUSSION

Syntheses and Structural Results. In prior work, preparations for the neutral α and β isomers were reported. Unfortunately, the synthesis of the β isomer gave relatively low yields and crystals had to be manually separated.[13a] In the present work, efforts have been made to improve the yield and purity of the products, particularly for the β isomer. The yellow α compound is now prepared by reaction of $Mo_2(DAniF)_3(O_2CCH_3)$ and the neutral oxamide in tetrahydrofuran followed by addition of $NaOCH_3$ and stirring over a period of 48 h. Upon removal of the solvent and extraction of the solid with CH_2Cl_2 the product is obtained in high yield (82%) and purity. For the isolation of the pure β isomer the procedure was similar to that for the α isomer but the use of a short reaction time (0.5 h) is essential. The solvent was then removed. This is followed by an extraction with CH_2Cl_2 and then addition of hot ethanol to the dichloromethane extract. To obtain a good yield and a pure product it is important to maintain the temperature of this mixture at ~80 °C for about half an hour. The red β compound precipitates from the hot ethanol/CH_2Cl_2 mixture and some by-products, including a small amount of the soluble α isomer, are removed by filtration. It is interesting that even though both the α and β isomers originate from the same reactants, once formed they do not interconvert in boiling solutions of various solvents such as ethanol, THF, acetonitrile or *o*-dichlorobenzene.

Each of these precursors (α and β) react with ferrocenium hexafluorophosphate $(Cp_2Fe)PF_6$, to produce the oxidized compounds **1**, **2**, **3** and **4**. The reaction stoichiometries must be strictly controlled in order to obtain the pure singly or doubly

oxidized compounds. By carrying out the reactions at low temperature (–78 ˚C), good yields of crystalline material are generally obtained for the four compounds.

The core structure of the complex cation of **1** (α^+) is shown in Figure 8. This mono-charged dimolybdenum pair has an overall structure similar to that of the neutral precursor, with the two [Mo_2] units being orthogonal to each other. Compared to the neutral compound, the most important difference is that in **1** the two dimetal subunits are not structurally identical. In this compound one of the two Mo–Mo bonds is lengthened, relative to that in the precursor, to 2.1291(6) Å, while the other has an Mo–Mo distance (2.0920(6) Å) essentially unchanged from that in the neutral species.[13a] The change in metal–metal bond distance of the first [Mo_2] unit, ca. 0.037 Å, is similar to that observed in other cases where a quadruply bonded Mo_2^{4+} unit is oxidized to an Mo_2^{5+} species, e.g., in the localized compound $\{[Mo_2](CH_3O)_2Zn(OCH_3)_2[Mo_2]\}^{1+}$,[15] in which the difference in bond length between the two dimolybdenum units is 0.035 Å. This indicates that only one of the Mo_2^{4+} species in the precursor has been oxidized to an Mo_2^{5+} unit. Upon oxidation of this unit the formal bond order is lowered from 4.0 to 3.5. Consistently, there are two sets of Mo–ligand bond distances associated with the two different dimetal centers. For the oxamidate group that binds to the Mo_2^{4+} unit the Mo–N and Mo–O bond distances are 2.197(4) and 2.121(3) Å, respectively, which are about the same as those in the precursor,[13a] while the corresponding bonds to the Mo_2^{5+} unit are shortened to 2.166(4) and 2.105(3) Å. The asymmetric molecular structure unambiguously indicates that compound **1** is a mixed-valence complex that belongs to the electronically localized Class I.

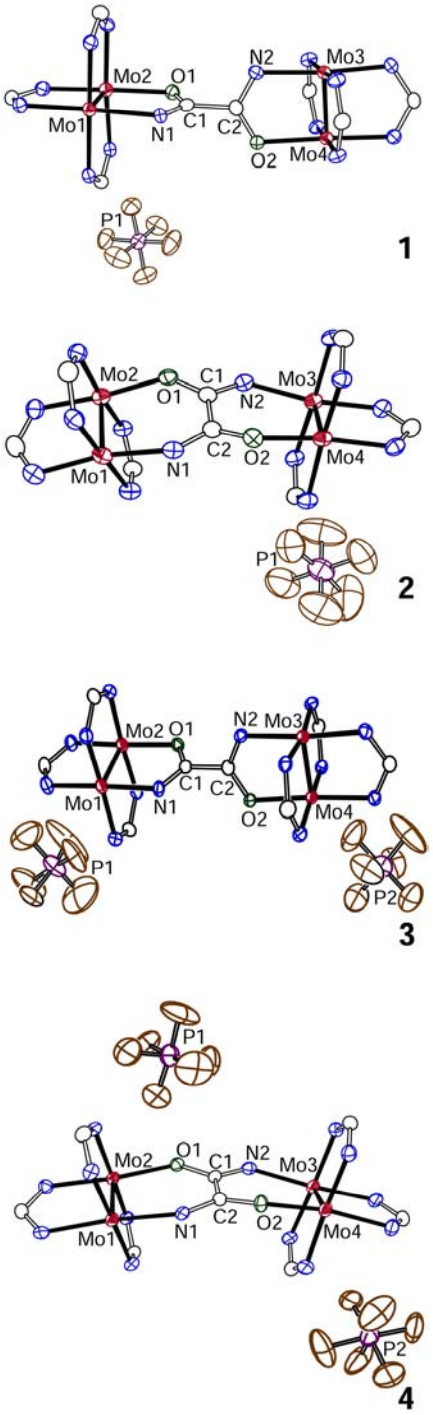

Figure 8. Core structure of **1**–**4** with ellipsoids drawn at the 40% probability level. All *p*-anisyl groups and hydrogen atoms have been omitted for clarity.

Compound **2** is the singly oxidized product having the β form. As shown in Figure 8, the β binding mode in the precursor is retained in the cation of **2**. The oxamidate linker binds each of the two [Mo_2] units with N–C–C–O four-atom binding mode, forming two fused, six-membered, chelating rings. The two Mo_2 units are essentially parallel to each other but the overall structure is slightly bent and twisted, as in the neutral precursor.[13a] This compound has a core structure resembling the singly oxidized dimethyloxamidate–linked analogue,[13b] which has been shown to be a delocalized, mixed-valence complex by various techniques, including X–ray analyses. Contrary to **1** which has two distinct Mo–Mo distances, in the isomer **2** the two crystallographically independent metal–metal bonds are equally lengthened relative to those in the parent compound. The increase in the Mo–Mo bond lengths is from 2.0944(4) Å[13a] to 2.1116(7) and 2.1140(6) Å. The relatively small increase (ca. 0.019 Å) is attributed to the fact that formally only half an electron has been removed from each Mo_2^{4+} unit. In **2**, the metal–ligand bond distances for the two dimolybdenum units are essentially identical but shorter than those in the precursor.[13a] For example, for the two Mo_2 subunits, the Mo–$N_{oxamidate}$ bonds are 2.147(4) and 2.141(4) Å and the Mo–$O_{oxamidate}$ 2.054(3) and 2.058(3) Å, while the neutral β compound has distances of 2.198(3) for the Mo–$N_{oxamidate}$ and 2.093(2) Å for the Mo–$O_{oxamidate}$ bonds.[13a] This MV species is electronically delocalized and it is appropriate to formally assign a half valence to each of the Mo_2 centers, $[Mo_2]^{0.5+}$(di-*p*-anisyloxamidate)$[Mo_2]^{0.5+}$.

The two doubly oxidized compounds **3** and **4** constitute the third α/β isomer pair in this system. The core structures of the dications in each compound are shown in

Figure 8. For **3** (α^{2+}), the two Mo–Mo bond lengths are essentially the same, 2.1248(9) and 2.1243(11) Å, and chemically indistinguishable from that in the oxidized site of its precursor **1** (2.1291(6) Å). In **3**, each of the dimolybdenum units has an Mo_2^{5+} core with a bond order of 3.5 derived from the electronic configuration $\sigma^2\pi^4\delta^1$. Similarly the β isomer (**4**) also has two lengthened Mo–Mo bonds, which are 2.1449(8) and 2.1418(8) Å. It is interesting to note that the metal–metal bonds in **4** are slightly longer than those in **3**, even though the formal oxidation states are the same. The increase in Mo–Mo bond distances is 0.037 Å for the α isomer but 0.049 Å for the β as two electrons are removed. We have been unable to find a straightforward explanation for such difference. However, it appears that the difference is not due to the α/β binding mode because in the two neutral precursors, the metal–metal bond distances are essentially the same.[13a] Along with the difference in metal–metal bond distances, the metal–ligand distances in **4** are shorter, on average, than those in **3** (Table II), implying that the Mo_2 units in **4** are more positively charged than those in **3**. In general, the effect of lowering electron density on the dimetal core should increase the metal–metal bond distance. This is understandable if the metal to ligand back–π–bonding in **4**, the delocalized compound, is greater than that for **3**.

Near-IR Spectroscopy. Different spectroscopic properties for the two isomers were first observed in CH_2Cl_2 solutions of the MV species generated in situ by mixing each of the corresponding neutral precursors with 1 equiv of oxidizing reagent $(Cp_2Fe)PF_6$.[13a] We now show results obtained using crystalline samples of **1** and **2** in KBr pellets. The spectra, recorded in the range of 2000–8000 cm^{-1}, are shown in Figure

9. The β isomer, **2**, exhibits an intense absorption band centered at ca. 4730 cm^{-1} while the spectrum of the α isomer is devoid of absorption bands in the NIR region. This spectrum of **2** measured in a solid sample is very similar to that obtained in CH_2Cl_2 solution, in which the transition was measured at 4700 cm^{-1}.[13a] The bandwidth at half-height, $\Delta\nu_{1/2}$, of 2300 cm^{-1} is significantly smaller than the value of 3300 cm^{-1} calculated for a charge transfer transition of a class II species using the Hush formula, $\Delta\nu_{1/2} = (2310\ \Delta\nu_{max})^{1/2}$.[28] A narrower band suggests that the electronic coupling interaction is stronger than that for a class II species, which is consistent with the structural data. The strong band in the NIR spectrum of this delocalized species may be described as a HOMO–1 → SOMO transition.[13a]

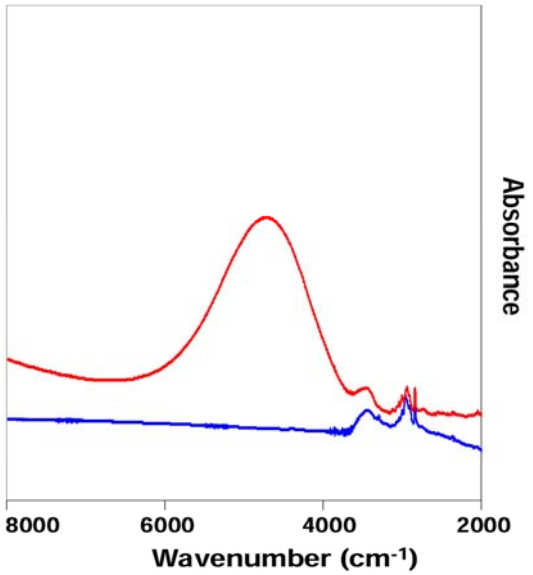

Figure 9. NIR spectra of the crystalline mixed-valence species **1** (in blue) and **2** (in red) in KBr pellets.

Additional support for the latter idea comes from a study employing DFT calculations which showed that in the β form,[13a] the frontier MOs are derived from the combination of the metal δ orbitals with significant involvement of the ligand π orbitals. For the singly oxidized species **2**, the odd electron, resides in a delocalized molecular orbital (SOMO), having electron density equally distributed over the two [Mo_2] units. For the analogous complex β–{[Mo_2](dimethyloxamidate)[Mo_2]}$^+$, it was found that an electronic transition (HOMO–1 → SOMO) at relatively low energy corresponds to the absorption band in the NIR spectrum.[13a] For the α compound (**1**), however, the situation is quite different. DFT calculations on the neutral α precursor[13a] have shown that the molecule has two localized [Mo_2] units that do not interact significantly with each other and thus no intervalence charge transfer band is observed.

EPR Spectra. X–band electron paramagnetic resonance (EPR) spectroscopy has also been employed for the study of **1**–**4**, all of which have formally one or two Mo_2^{5+} units. For the two paramagnetic compounds in α form (**1** and **3**), the EPR spectra were measured at room temperature in CH_2Cl_2 solution. For each compound the spectrum shows one prominent symmetric peak having some hyperfine structure (Figure 10). The spectra for these two species are similar, with little difference in the *g* value. Importantly, the *g* values, 1.950 for **1** and 1.951 for **3**, are significantly smaller than the value expected for a free organic radical, indicating that odd electron resides in a metal-based orbital. For **3**, this result provides further evidence that there are two linked but essentially uncoupled Mo_2^{5+} units forming a diradical. The main signal is attributed to molecules containing only the ^{96}Mo (I = 0) isotope, while the hyperfine structure is due

to molecules with one ^{95,97}Mo (I = 5/2) isotope, which has a natural abundance of about 25%.[29] For both **1** and **3** spectral simulations were done using a localized model with one odd electron residing on an Mo_2 unit. As shown in Table III, by using the parameters g = 1.950 and $A = 21 \times 10^{-4}$ cm^{-1}, similar to those in the parent paddlewheel cation $[Mo_2(DAniF)_4]^+$,[30] the simulated spectra show satisfactory agreement with the experimental results.

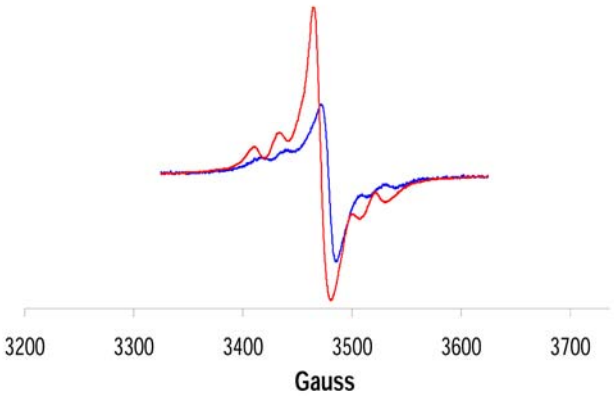

Figure 10. EPR spectra of **1** (in blue) and **3** (in red) in CH_2Cl_2 solution at ambient temperature.

The spectrum for the singly oxidized species **2** in the β form, measured in solution at –60 °C,[31] exhibits a prominent peak (g = 1.947) and several hyperfine lines (Figure 11). However, simulation gives a hyperfine coupling constant $A = 11 \times 10^{-4}$ cm^{-1}, which is about half of that for **1** (Table III). Prior studies on various MV species of the type $\{[Mo_2]L[Mo_2]\}^+$ have shown that electronic delocalization over two Mo_2 units has the effect of lowering the constant A. For example, for the delocalized complex $\{[Mo_2](dioxolenate)[Mo_2]\}^+$,[22] the hyperfine coupling constant A was 12.2×10^{-4} cm^{-1}, while for the weakly coupled compound, $\{[Mo_2](N,N'$-diethylterephthalamidate$)[Mo_2]\}^+$, the A value is 22×10^{-4} cm^{-1}.[32] Chisholm and co-workers have reported that the dimolybdenum pairs linked by oxalate and perfluoroterephthalate, which differ largely in the extent of electronic delocalization, have hyperfine coupling constants of 14.8 G and 27.2 G (14.8×10^{-4} cm^{-1} and 27.2×10^{-4} cm^{-1}, respectively.)[11f]

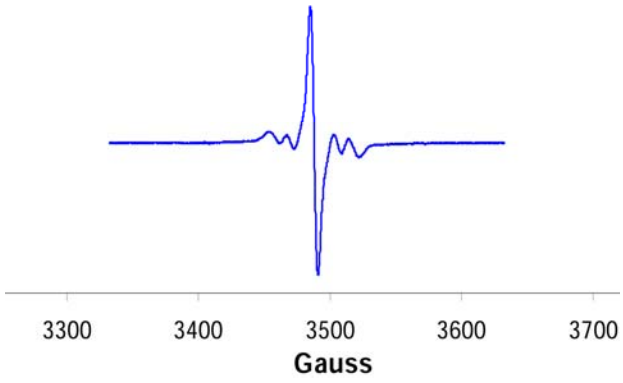

Figure 11. EPR spectrum of **2** at –60 °C in CH_2Cl_2 solution.

Table III. EPR Simulation Parameters of **1**–**4**

compound	**1**	**2**	**3**	**4**
g value	1.950	1.947	1.951	
A ($\times 10^{-4}$ cm^{-1})	21	11	21	diamagnetic

Unlike **1**–**3** which are paramagnetic, complex **4** is diamagnetic as shown by the observation of both sharp signals of the ^{1}H NMR spectrum and because it is EPR silent.[33] Diamagnetism for complexes that have two linked, magnetically equivalent metal complex subunits could result from either metal–metal antiferromagnetic exchange interaction or from pairing of spins by electrons occupying the same delocalized MO. In our previous studies on dimolybdenum pairs, diamagnetic behaviors have been observed for several complexes with different linkers, for example, β–{[Mo_2](dimethyloxamidate)[Mo_2]}$^{2+}$,[13b] {[Mo_2](fluoflavinate)[Mo_2]}$^{2+}$,[21] and {[Mo_2](μ–OR)$_4$[Mo_2]}$^{2+}$.[10h] In all of these compounds the outer electrons are paired up in the same MO.

Magnetic Measurements. Because formally each of the doubly oxidized compounds **3** and **4** has one unpaired electron at each of the two [Mo_2] units, they offer an excellent opportunity for the study the magnetic behavior of a system with two spatially separated odd electrons. For such compounds, the possible interaction patterns include: (1) no coupling; (2) ferromagnetic coupling; and (3) antiferromagnetic coupling. The first case is simply the combination of its parts; it possesses only local spins, each with S = ½. Ferromagnetic coupling would generate a triplet ground state, S = 1, and antiferromagnetic coupling would yield a singlet ground state, S_T = 0. Calculated values of $\chi_m T$ (emu K mol^{-1}) in the limit $T \rightarrow 0$ K, using in each case a spin-only model with g = 2.00, are 0.75, 1, and 0 for each of the three cases, respectively. A variable temperature study of the bulk magnetic susceptibility of **3,** Figure 12, shows a value of $\chi_m T$ of 0.76 emu K mol^{-1} that is essentially independent of T in the range of 50 K to 300 K, while magnetic measurements of **4** give a $\chi_m T$ value close to zero emu K mol^{-1}.[34] This is conclusive evidence that there is no significant spin coupling, either ferromagnetic or antiferromagnetic, in **3** (α^{2+}), and that the two unpaired electrons in **4** (β^{2+}) are antiferromagnetically coupled.

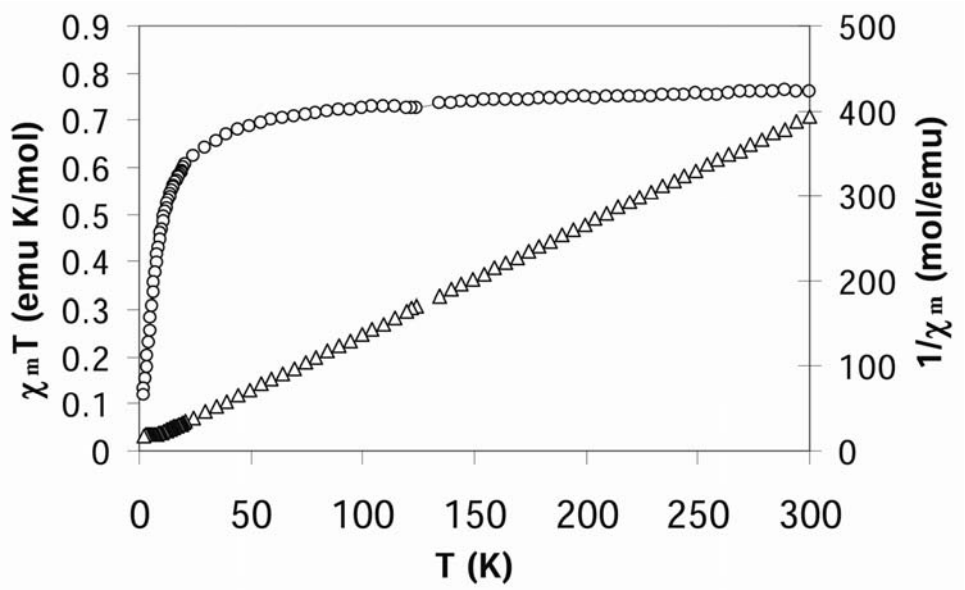

Figure 12. Plots of $\chi_m T$ (o) and $1/\chi_m$ (Δ) vs. temperature for **3**.

CHAPTER III

OXIDATIVE DEPROTONATION IN SINGLE CRYSTALS*

Solvent-free solid-state chemical reactions, while relatively uncommon, are of great interest, especially regarding the development of green chemistry.[35] The single-crystal to single-crystal (SCSC) solid-state transformation is an especially interesting category of such reactions, and it has been studied in a variety of organic reactions.[36] However, few examples of inorganic compounds have been discovered,[37] and most of them involve loss or change of solvent in the coordination sphere or networks, although a few redox reactions have also been reported.[37a,f,k,p]

Coupled deprotonation/electron loss processes, with the net effect of dehydrogenation, occur widely in organic, inorganic, organometallic and biological chemistry.[38] Sometimes the two steps can be examined sequentially, but often they are concerted. When the agent effecting electron removal is elemental oxygen, formation of water is often a part of the process, as in Eq. 2.[39]

$$2H^+ + \tfrac{1}{2}O_2 + 2e \rightarrow H_2O \qquad \text{(eq. 2)}$$

---

* Reproduced in part with permission from: *Inorg. Chem.* **2007**, *46*, 3245, Cotton, F. A.; Li, Z.; Murillo, C. A.; Wang, X.; Yu, R.; Zhao, Q., "Crystal to Crystal Oxidative Deprotonation of a Di(μ-hydroxo) to a Di(μ-oxo) Dimer of Dimolybdenum Units,"

Compounds of the types **VI** and **VII** in Figure 13 were first reported in 1998,[17] where the formamidinate ligands employed were *N*,*N*'-di-*p*-tolylformamidinate. In that case, we found that the $(\mu\text{–}OH)_2$ compound was oxidized by atmospheric oxygen to the $(\mu\text{–}O)_2$ compound. We recently reported[40] the series of transformations shown in Figure 13 where again formation of H_2O according to Eq. 2 appears to accompany the conversion of **VI** to **VII**. In this case the aryl groups in the bridging ArNCHNAr (diarylformamidinate) anions are *m*–$CF_3C_6H_4$. Independently of these two previously reported studies, we have also examined the oxidation of the homologous di(μ–OH) molecule in which the formamidinate ligands are the di-*p*-anisyl analogues. Even though this is the third such system to be studied, several results of non-trivial interest, that deepen our understanding of such reactions, were obtained, and they are presented here. We now report that the dimolybdenum molecular pair $Mo_2(DAniF)_3(\mu\text{-}OH)_2Mo_2(DAniF)_3$ (**5**) undergoes one oxidative conversion to a doubly oxidized product, $Mo_2(DAniF)_3(\mu\text{-}O)_2Mo_2(DAniF)_3$ (**6**), both in solution and as an SCSC process. We also have characterized a probable key intermediate with one OH and one O bridge.

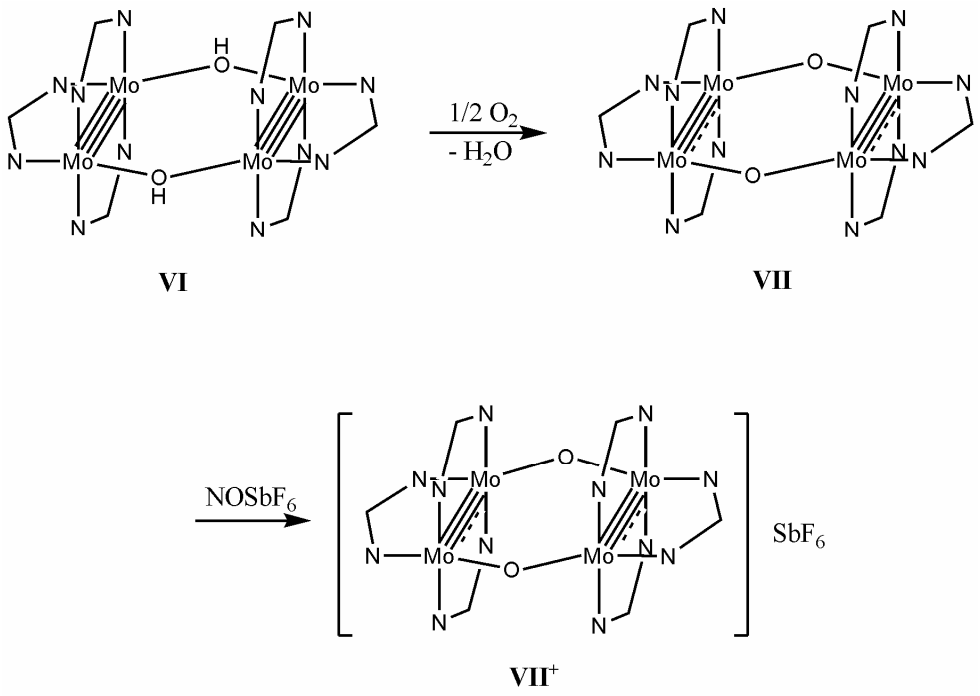

Figure 13: The transformation from a di(μ–OH) complex to a di(μ–O) cation.

EXPERIMENTAL SECTION

Materials and Methods. Solvents were dried and then distilled under N_2 following conventional methods or purified under argon using a Glass Contour solvent purification system. Except where noted, synthetic operations were conducted under N_2 using Schlenk line techniques. The compounds $Mo_2(DAniF)_3(OAc)$[13a] and HDAniF[23] were prepared by following published methods. Solutions of $(OEt_3)BF_4$ (1 M in CH_2Cl_2) and $NaOCH_3$ (0.5 M in methanol) were purchased from Aldrich, and used as received.

Physical Measurements. Elemental analyses were performed by Robertson Microlit Laboratories, Madison, New Jersey. ^{1}H spectra were recorded on a Mercury-300 NMR spectrometer with chemical shifts (δ ppm) referred to residual solvent. Electronic spectra in the UV-vis range 200 to 900 nm were measured on a Shimadzu UV-2501PC spectrophotometer.

Preparation of $Mo_2(DAniF)_3(\mu\text{-}OH)_2Mo_2(DAniF)_3$ (5). A mixture of $Mo_2(DAniF)_3(OAc)$ (0.41 g, 0.40 mmol) in 20 mL of CH_2Cl_2 and 8 mL of 0.5 M NaOMe in methanol was stirred at ambient temperature for 1 h, leading to the formation of yellowish orange supernatant solution with a suspended colorless NaOAc solid. After filtration, the filtrate was mixed with 0.10 mL of degassed H_2O. The mixture was layered carefully with 40 mL of isomeric hexanes. Sometimes two crystal forms (**5**·1.5CH_2Cl_2 and **5**·CH_2Cl_2) were obtained,[41] but usually only **5**·1.5CH_2Cl_2 was observed. The crystalline product was isolated by filtration, washed with 2 × 10 mL of hexanes, and then dried in vacuum. Typical yield: 0.25 g (63%). ^{1}H NMR (in CD_2Cl_2, ppm): 8.88 (s, 4H, N–C*H*–N), 8.19 (s, 2H, N–C*H*–N), 6.34 (d, 4H, aromatic), 6.22 (d, 8H, aromatic),

6.09~6.14 (m, 36H, aromatic), 3.61 (s, 24H, –OC*H*$_3$), 3.60 (s, 12H, –OC*H*$_3$), 2.42 (s, 2H, –O*H*). UV–vis in CH_2Cl_2, λ_{max} (nm) (ε, $M^{-1}cm^{-1}$): 449 (4.1×10^3). Anal. calcd. for $C_{90}H_{92}Mo_4N_{12}O_{14}$ (**5**): C, 55.45; H, 4.76; N, 8.62. Found: C, 55.64; H, 4.65; N, 8.33.

Preparation of $Mo_2(DAniF)_3(\mu\text{-}O)_2Mo_2(DAniF)_3$ (6). Crystals of **6** were obtained directly from crystals of **6**·1.5CH_2Cl_2 after exposure to air for 420 h. The yield is essentially quantitative, but the crystals changed to a paramagnetic, uncharacterized amorphous solid after being stored in air for about two months.

Preparation of $Mo_2(DAniF)_3(\mu\text{-}O)_2Mo_2(DAniF)_3$ (6·2CH_2Cl_2). A solution of **5** (0.24 g, 0.10 mmol) in 10 mL of CH_2Cl_2 was prepared under N_2. Air (10 mL) was then added to the Schlenk flask using a syringe. This mixture was stirred for 4 h, during which time the color of the solution changed from yellow to green. The product was essentially quantitatively precipitated by addition of hexanes. Single crystals of **6**·2CH_2Cl_2 were obtained by diffusion of isomeric hexanes into a dichloromethane solution. Yield: 0.19 g (80%). ^{1}H NMR (in CD_2Cl_2, ppm): 9.31 (s, 2H, N–C*H*–N), 8.03 (s, 4H, N–C*H*–N), 6.40 (d, 8H, aromatic), 6.15~6.27 (m, 40H, aromatic), 3.63 (s, 12H, –OC*H*$_3$), 3.58(s, 24H, –OC*H*$_3$). UV–vis in CH_2Cl_2, λ_{max} (nm) (ε, $M^{-1}cm^{-1}$): 736 (2.0×10^4), 401 (1.9×10^3). Anal. calcd. for $C_{90}H_{90}N_{12}O_{14}Mo_4$ (**6**): C, 55.51; H, 4.66; N, 8.63. Found: C, 55.33; H, 4.45; N, 8.47.

Preparation of $\{[Mo_2(DAniF)_3]_2(\mu\text{-}O)(\mu\text{-}OH)\}BF_4$ (7). To a solution of $[Mo_2(DAniF)_3]_2(\mu{-}O)_2$ (30 mg, 0.015 mmol) in 10 mL of CH_2Cl_2 was added, with stirring, 1.5 mL of 0.01 M solution of HBF_4 in CH_2Cl_2.[42] The reaction mixture was stirred at room temperature for 2 h, and the color changed from green to brown. This

solution was carefully layered with 30 mL of hexanes. Dark brown crystals formed after a period of 7 days. Yield: 20 mg (64%). ^{1}H NMR (in $CDCl_3$, ppm): 9.32 (s, 2H, N–C*H*–N), 8.02 (s, 4H, N–C*H*–N), 6.43 (d, 8H, aromatic), 6.25 (m, 24H, aromatic), 6.15 (d, 16H, aromatic), 3.67 (s, 12H, –OCH_3), 3.62 (s, 24H, –OCH_3), 2.20 (s, 1H, –O*H*). UV–vis in CH_2Cl_2, λ_{max} (nm) (ε, $M^{-1}cm^{-1}$): 550 (sh), 470 (3.8×10^3). Anal. calcd. for $C_{96}H_{105}BF_4Mo_4N_{12}O_{14}$ (**7**·C_6H_{14}): C, 54.35; H, 4.99; N, 7.92. Found: C, 55.24; H, 5.46; N, 8.39.

X-ray Structure Determinations. Single crystals of **5**·1.5CH_2Cl_2, **6**, **6**·2CH_2Cl_2 and **7** suitable for X-ray analyses were each mounted and centered on the tip of a cryoloop attached to a goniometer head. Data were collected at −60 °C on a BRUKER SMART 1000 CCD area detector system. Cell parameters were determined using the program SMART.[24] Data reduction and integration were performed with the software package SAINT,[25] while absorption corrections were applied using the program SADABS.[26] The positions of the heavy atoms were found via direct methods using the program SHELXTL.[27] Subsequent cycles of least-squares refinement followed by difference Fourier syntheses revealed the positions of the remaining non-hydrogen atoms. Hydrogen atoms were added in idealized positions. Non-hydrogen atoms, except some atoms from disordered groups and solvent molecules, were refined with anisotropic displacement parameters. Crystallographic data for **5**·1.5CH_2Cl_2, **6**, **6**·2CH_2Cl_2 and **7** are given in Table IV and selected bond distances and angles in Table V.

Table IV. X-ray Crystallographic Data of **5**–**7**

compound	**5**·1.5CH_2Cl_2[a]	**6**	**6**·2CH_2Cl_2	**7**
formula	$C_{91.5}H_{93}Cl_3Mo_4N_{12}O_{14}$	$C_{90}H_{90}Mo_4N_{12}O_{14}$	$C_{92}H_{94}Cl_4Mo_4N_{12}O_{14}$	$C_{90}H_{91}BF_4Mo_4N_{12}O_{14}$
fw	2074.89	1947.50	2117.35	2035.32
space group	*P*$\bar{1}$ (No. 2)	*P*$\bar{1}$ (No. 2)	*P*$\bar{1}$ (No. 2)	*C*2/c (No. 15)
a (Å)	14.835(2)	14.736(3)	12.973(5)	24.683(3)
b (Å)	17.399(2)	17.278(4)	14.045(5)	14.138(2)
c (Å)	17.809(2)	17.590(4)	14.046(5)	26.693(3)
α (deg)	92.055(2)	91.605(4)	71.250(6)	90
β (deg)	88.116(2)	90.926(4)	73.612(6)	109.503(2)
γ (deg)	93.027(2)	96.177(4)	87.710(6)	90
V ($Å^3$)	4585.1(9)	4450(2)	2321(1)	8781(2)
Z	2	2	1	4
T (K)	213	213	213	213
d_{calcd} (g/cm^3)	1.503	1.453	1.515	1.540
μ (mm^{-1})	0.691	0.619	0.712	0.638
R1[b] (wR2)[c]	0.071 (0.159)	0.162 (0.261)	0.035 (0.072)	0.069 (0.116)

[a] The unit cell for **5**·1.5CH_2Cl_2 was transformed from a unit cell of the same compound with a conventional setting via the transformation matrix (–1 0 0 0 1 0 0 0 –1). The purpose of using an unconventional cell for **5**·1.5CH_2Cl_2 is to facilitate the comparison of the results from time dependent measurements. The β angle changed from 88.116(2) º in **5**·1.5CH_2Cl_2 to an obtuse angle (> 90 º) quickly and reached 90.926(4) º in **6** after 420 h.

[b] $R1 = \Sigma\|F_o|-|F_c\|/\Sigma|F_o|$.

[c] $wR2 = [\Sigma[w(F_o^2-F_c^2)^2]/\Sigma[w(F_o^2)^2]]^{1/2}$.

Table V. Selected Bond Lengths (Å) and Angles (deg) of **5**–**7**

Compound	**5**·1.5CH_2Cl_2	**6**	**6**·2CH_2Cl_2	**7**
Mo(1)–Mo(2)	2.1053(6)	2.151(2)	2.1552(7)	2.1475(5)
Mo(3)–Mo(4)	2.1058(6)	2.151(2)		
Mo_2(1,2)···Mo_2(1A,2A)[a]	4.088	3.720	3.734	3.825
Mo_2(3,4)···Mo_2(3A,4A)	4.083	3.720		
Mo(1)–O(1)	2.146(4)	1.934(8)	1.933(2)	2.073(1)
Mo(2)–O(1)	2.145(4)	1.926(8)	1.935(2)	1.9174(8)[b]
Mo(3)–O(2)	2.130(4)	1.906(8)		
Mo(4)–O(2)	2.135(4)	1.939(8)		
Mo(1)–N(1)	2.170(4)	2.190(9)	2.191(2)	2.150(3)
Mo(1)–N(3)	2.131(4)	2.17(1)	2.174(2)	2.111(3)
Mo(1)–N(5)	2.166(4)	2.17(1)	2.176(2)	2.140(3)
Mo(2)–N(2)	2.152(4)	2.169(9)	2.152(2)	2.158(3)
Mo(2)–N(4)	2.121(4)	2.16(1)	2.191(2)	2.162(3)
Mo(2)–N(6)	2.155(4)	2.152(9)	2.130(2)	2.138(3)
Mo(3)–N(7)	2.156(4)	2.170(9)		
Mo(3)–N(9)	2.139(4)	2.18(1)		
Mo(3)–N(11)	2.149(4)	2.17(1)		
Mo(4)–N(8)	2.153(4)	2.17(1)		
Mo(4)–N(10)	2.122(4)	2.19(1)		
Mo(4)–N(12)	2.141(4)	2.15(1)		
Mo(1)–O(1)– Mo(2A)	144.6(2)	149.1(4)	149.70(9)	143.6(2)[c]
Mo(3)–O(2)– Mo(4A)	146.4(2)	150.8(4)		154.4(2)[d]

[a] distance between the midpoint of the two [Mo_2] units.

[b] Mo(2)–O(2). [c] Mo(1)–O(1)–Mo(1A). [d] Mo(2)–O(2)–Mo(2A).

RESULTS AND DISCUSSION

Syntheses and Structural Results for 5 and 6. Compound **5** was synthesized from the reactions shown in Eqs. 3 and 4. The reaction of $Mo_2(DAniF)_3(OAc)$ and excess NaOMe leads to the formation of $Mo_2(DAniF)_3(OMe)(HOMe)$ (Eq. 3),[13a] which was not isolated, but used *in situ* to react with H_2O (Eq. 4).

$$Mo_2(DAniF)_3(OAc) + NaOMe + MeOH \longrightarrow Mo_2(DAniF)_3(OMe)(HOMe) + NaOAc \quad \text{(eq. 3)}$$

$$2Mo_2(DAniF)_3(OMe)(HOMe) + 2H_2O \longrightarrow [Mo_2(DAniF)_3]_2(\mu\text{-}OH)_2 + 4MeOH \quad \text{(eq. 4)}$$

The yellow crystals of **5**·1.5CH_2Cl_2 used for X-ray work were obtained by placing a layer of isomeric hexanes over a CH_2Cl_2 solution.[41] It crystallized in the space group $P\bar{1}$ with two independent molecules, each residing on an inversion center. The molecular structure of **5** consists of two $Mo_2(DAniF)_3^+$ units which are linked by two hydroxide groups, as shown on the upper section of Figure 14. The bridging oxygen atoms are slightly disordered above and below the plane formed by the dimetal units and μ-O atoms. Similar disorder was observed in other formamidinate analogues.[40] For this crystalline form, the internal conformation of each Mo_2 unit is essentially eclipsed. The largest torsion angle about the Mo–Mo quadruple bond is 1.4(1)°. The crystallographically equivalent Mo–Mo distances of 2.1053(6) and 2.1058(6) Å shown in Table V are typical for a quadruply bonded Mo_2^{4+} unit with a $\sigma^2\pi^4\delta^2$ electronic configuration.[43] The independent Mo–O distances in the range of 2.130(4) to 2.146(4) Å, are close to those in similar molecular pairs with OH bridges.[40] The Mo–O–Mo angles

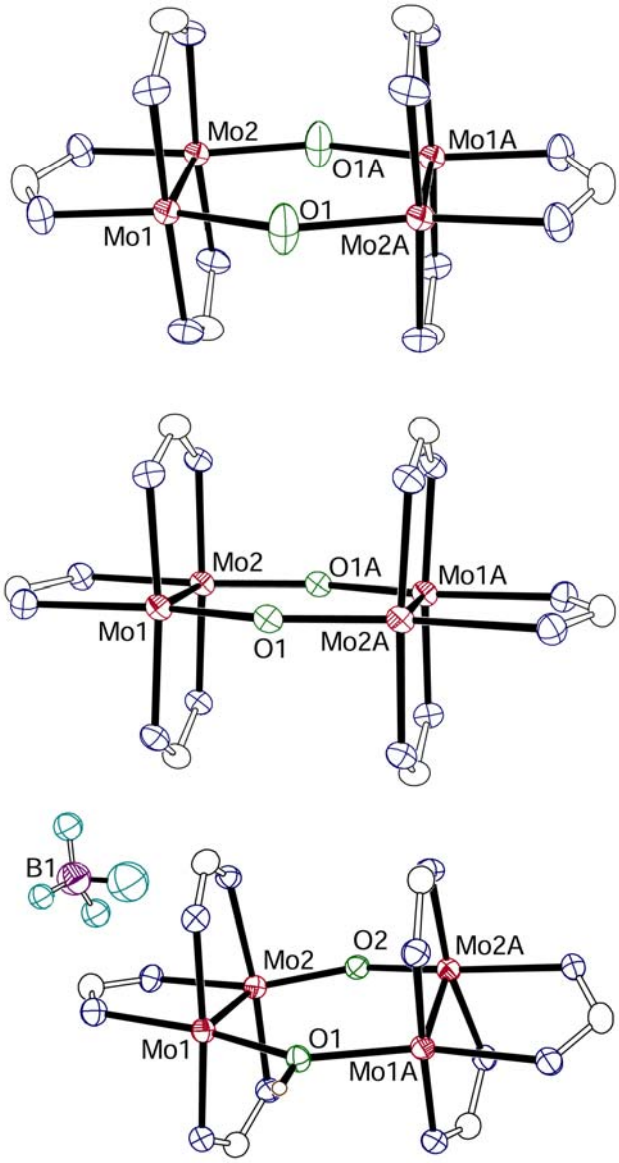

Figure 14. Core structures of compounds **5**·1.5CH_2Cl_2 (top), **6**·2CH_2Cl_2 (middle) and **7** (bottom) drawn with ellipsoids at the 40% probability level. Only one of the crystallographically independent molecules in **5**·1.5CH_2Cl_2 is shown. All *p*-anisyl groups and hydrogen atoms in the methine groups have been omitted for clarity.

are 144.6(2) and 146.4(2)°. The nonbonding distance between the midpoints of the Mo–Mo bonds is about 4.09 Å.

Compound **5** reacts readily with either dry or atmospheric oxygen. Yellow crystals of **5** turn quickly to green on the surface and then to black. Long exposure to air produces a yet unidentified orange-brown, amorphous powder. When diamagnetic crystals of **5** are coated with mineral oil or Paratone oil to slow down diffusion of air into the crystal, and allowed to stand in air, there is a clean SCSC conversion.[44] The variations in metric dimensions that occur during such process over a period of 420 h are shown in Figure 15, and the whole data set is provided in Tables XVII (see Appendix A). The Mo–Mo and Mo–O distances varied smoothly as oxygen was allowed to diffuse into the crystal. During this process the occupancy of the interstitial CH_2Cl_2 molecules significantly decreased,[45,46] as shown in Table XVI of Appendix A.

The total change in each of the metal-to-metal distances (0.045 Å) that occur during the SCSC process is consistent with the final product having two Mo_2^{5+} species. The short Mo─O distances of 1.926[9] Å also support the formulation of the bridging groups as oxo species. This formulation as $Mo_2(DAniF)_3(\mu\text{-}O)_2Mo_2(DAniF)_3$ (**6**) is unambiguous because this compound can also be prepared directly from **5** in solution by reaction with pure dioxygen or oxygen in air and crystallized as the solvate **6**·$2CH_2Cl_2$ (shown at the center of Figure 14) which has similar bond distances (Mo─Mo = 2.1552(7) Å and Mo─O = 1.934[3] Å). What is not unambiguous from the crystallographic data is whether there is an intermediate that formally has an Mo_2^{4+} and an Mo_2^{5+} species with one oxo and one hydroxo bridging group. Careful analyses of the

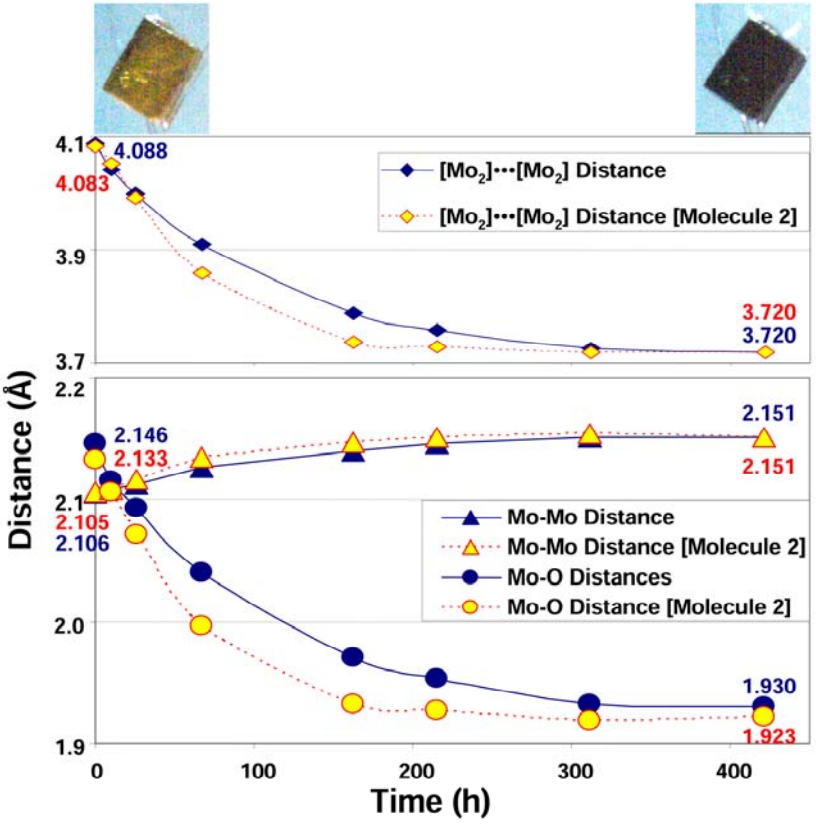

Figure 15. Changes in distances as oxidation from **5**·1.5CH_2Cl_2 to **6** takes place. Data were collected at 213 K. The time was obtained by adding the periods in which the crystal was exposed to air at ambient temperature between collections of data sets. In the upper part the crystals are shown before (upper left) and after (upper right) exposure to air. There are two crystallographically independent molecules in the crystal, each on an inversion center.

data indicates that the data sets corresponding to the partially reacted crystals show only a single diffraction pattern suggesting a one-phase topotactic reaction which could be consistent with the existence of an intermediate with one Mo_2^{5+} unit. It should be noted that such an intermediate would be expected to be paramagnetic. By analogy to other molecular pairs having one $(DAniF)_3Mo_2^{2+}$ unit, such species would be expected to be EPR active.[13b] When EPR spectra were taken using solid samples of **5** exposed to small amounts of air, these were devoid of signals.[47] The lack of signals suggests that during the SCSC transformation **5** is oxidized to **6** without accumulation of intermediates in the crystal.

Solution Behavior. As indicated earlier, compound **6** can be made from **5** in solution by reaction with pure dioxygen or oxygen in air. When this transformation was followed spectroscopically, two very important facts were learned from ^1H NMR spectroscopy: (1) there is no intermediate detectable by NMR; (2) as μ–OH groups disappear from the spectra, they are replaced by H_2O molecules. Figure 16 presents the spectra to support these statements; the spectra in the intermediate range of chemical shifts (Figure 39 in Appendix A) are consistent with these conclusions, but too complicated to allow detailed interpretation. In the 8–10 ppm region it is clearly shown that the set of ligand methine signals for **5** (at 8.9 and 8.2 ppm, 2:1 ratio) disappear and are replaced by those for **6** (at 9.3 ppm and 8.0 ppm, 1:2 ratio). In the 1–3 ppm region the OH signal at 2.4 ppm disappears while the H_2O signal at 1.6 ppm grows. In neither region is there any signal for an intermediate, such as a dimer with one μ–OH and one μ–O bridge. However, a neutral intermediate that has lost one H^+ and one electron (i.e.,

one species with a μ–OH and a μ–O) should give no sharp NMR spectrum since it is paramagnetic, vide supra. On the other hand, if present only in very low concentration it would also not affect the spectra of **5** and **6**.

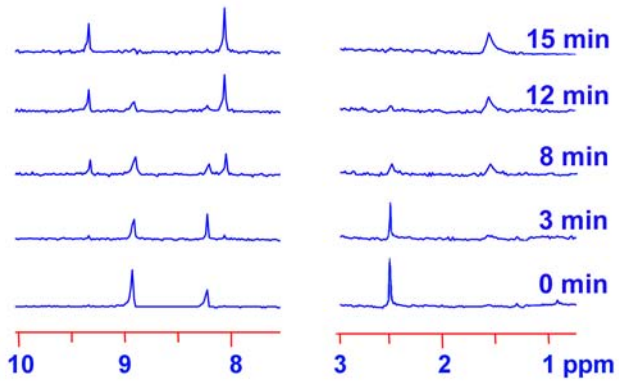

Figure 16. The methine and OH^-/H_2O regions of the ^1H NMR spectra as a CD_2Cl_2 solution of $[Mo_2(DAniF)_3]_2(\mu\text{-}OH)_2$ (**5**) is oxidized by O_2 to $[Mo_2(DAniF)_3]_2(\mu\text{-}O)_2$ (**6**) over a 15-minute period.

The UV-vis spectra of a solution of **5** as it is being oxidized offer definite, though not quantitatively interpretable, evidence that there is a short-lived intermediate in the conversion of **5** to **6**. Figure 17 shows spectra over a 19-minute period during which all of compound **5** in CH_2Cl_2 solution was oxidized to **6**. It must be clearly understood that these spectra do not constitute a kinetic study, because the rate of diffusion of oxygen into the solution was not uniform either in time or in space. In fact, the large change between the 10-minute and the 14-minute spectra is due to the fact that during this time

interval the cap was removed from the sample container and the solution agitated, thus introducing fresh dioxygen.

The important fact shown by these spectra in the 350–500 nm range is that there are more than two chromophores (i.e., not just **5** and **6**) present in the middle period of the overall oxidation process. The simplest explanation would be that there is one transient intermediate that absorbs in the 400–500 nm range. The probable identity of that intermediate (which, from its failure to show up in the ^{1}H NMR spectra, is presumed to be paramagnetic) will be discussed later.

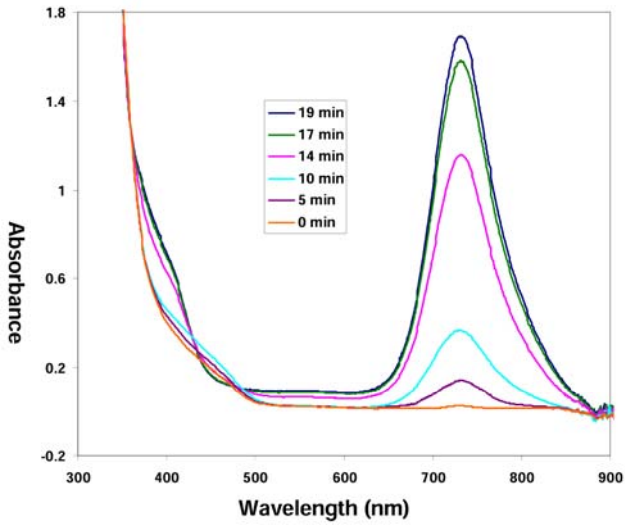

Figure 17. UV-vis spectra in CH_2Cl_2 solution showing the conversion of $[Mo_2(DAniF)_3]_2(\mu\text{-}OH)_2$ to $[Mo_2(DAniF)_3]_2(\mu\text{-}O)_2$. The color code for the time of exposure is given in the inset.

Because the transformation of **5** to **6**, either in solution on in the solid state, requires the loss of four particles — two electrons and two protons — numerous pathways or sequences of steps (although not necessarily four discrete steps) are *á priori* possible. Thus, several different tetramolybdenum intermediates as well as some other intermediates (e.g., $OH^{\cdot}$, $O_2H^{\cdot}$) might occur, and presumably at least one of each type occurs. To be rigorously accurate we do not have firm evidence that H_2O rather than, perhaps, H_2O_2 is the other end product in the SCSC process but we believe this to be by far the most logical presumption,[48] as indicated in the upper part of Figure 13.

Since in the solid state the transformation of **5** to **6** occurs quantitatively and without significant loss of crystallinity,[49] it seems safe to assume that only an intermediate, or intermediates, that have isosteric bridging groups, i.e., two μ–OH, one μ–OH and one μ–O, or two μ–O bridges need be considered. Also, it seems reasonable to assume that in the actual sequence, there will not be two successive proton losses nor two successive electron losses. Thus, consideration may be accorded to only the sequences shown using the core structures in Figure 18.

The intermediate **Y** would be accompanied by either $O_2H^{\cdot}$ or $OH^{\cdot}$.[50] The species **Y** would then be attacked to produce either of the next intermediates, $\mathbf{Z}^+$ (plus O_2H^- or OH^-) or $\mathbf{Z}^-$ (plus O_2H^+ or OH^+). Since the intermediacy of O_2H^+ or OH^+ seems to be hugely unlikely we believe that the intermediate $\mathbf{Z}^-$ can be ruled out. It should also be noted that the sequence **5**→ $\mathbf{X}^+$ → **Y** would entail formation of O_2^- (the well-known superoxide ion) while the sequence **5**→ $\mathbf{X}^-$ → **Y** would generate the intermediate O_2H^+, which seems very much less likely.

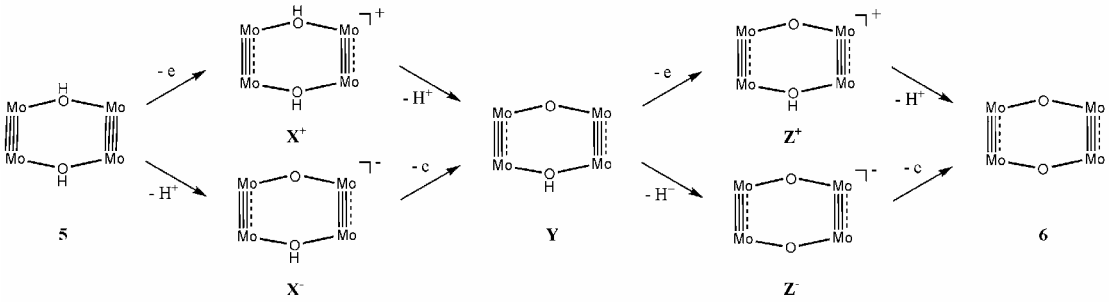

Figure 18: The proposed mechanism for the oxidative deprotonation from a Di(μ–hydroxo) to a Di(μ–oxo) Dimer of Dimolybdenum Units.

If **Y** is accompanied by O_2H^-, the latter might not directly attack **Y** but be converted to $OH^- + O_2$, with OH^- then attacking **Y** to give $\mathbf{Z}^+$ and OH^-.

In any case, we suggest that the most likely sequence of tetramolybdenum intermediates in the conversion of **5** to **6** by O_2 is

$$\mathbf{5} \rightarrow \mathbf{X}^+ \rightarrow \mathbf{Y} \rightarrow \mathbf{Z}^+ \rightarrow \mathbf{6}$$

If the rate-determining step is $\mathbf{5} \rightarrow \mathbf{X}^+$ and this is much slower than the three steps that follow it, detection of $\mathbf{X}^+$, **Y** or $\mathbf{Z}^+$ may be difficult. It is true that $\mathbf{X}^+$ and **Y** should each have an unpaired electron, but they do not accumulate as suggested by the absence of EPR signals.

Additionally the proposed intermediate $\mathbf{Z}^+$ cannot be confirmed *in situ* while the oxidation of **5** to **6** is actually in progress because it is generated from **Y** simultaneously with OH^- with which it immediately reacts to produce **6** and H_2O. However, in the absence of OH^-, $\mathbf{Z}^+$ should be stable, and its existence is strongly supported by the

preparation of $\{[Mo_2(DAniF)_3]_2(\mu\text{–}O)(\mu\text{–}OH)\}BF_4$, **7**, by reaction of **6** with HBF_4 in CH_2Cl_2. This unsymmetrical compound, and presumed intermediate in the deprotonation process, crystallized in the space group *C*2/c with the tetranuclear cation having C_2 symmetry (bottom of Figure 14). The two Mo–Mo distances of 2.1475(5) Å are consistent with a bond order of 3.5 and they are close to those of 2.1552(7) Å in $[Mo_2(DAniF)_3]_2(\mu\text{-}O)_2$, in crystals of **6**·$2CH_2Cl_2$. The two sets of Mo–O distances, however, are distinctly different, with an average Mo–O(1) distance of 2.073(1) Å for the hydroxide bridged group and 1.9174(8)Å for Mo–O(2) in the oxide linker.

Supplemental Information. Full ^{1}H NMR spectra collected at various intervals during the oxidation of $[Mo_2(DAniF)_3]_2(\mu\text{-}OH)_2$ (**5)** to $[Mo_2(DAniF)_3]_2(\mu\text{-}O)_2$ (**6**) (Figure 39), cyclic voltammogram (CV) and differential potential voltammogram (DPV) of $[Mo_2(DAniF)_3]_2(\mu\text{-}O)_2$ (**6**) (Figure 40), and tables of X-ray crystallographic data (Table XVI), selected bond lengths (Å) and angles (deg) data (Table XVII) as a single crystal **5**·$1.5CH_2Cl_2$ was oxidized by air to **6** are provided in Appendix A.

CHAPTER IV

STRONG ELECTRONIC COMMUNICATION BY DIRECT METAL–METAL INTERACTION*

For the singly oxidized complex $\{[Mo_2(cis\text{-}DAniF)_2]_2(\mu\text{-}Cl)_4\}PF_6$ (**8-PF$_6$**), already published in a communication,[51] it was found that upon oxidation of the neutral precursor the separation between the two dimetal units decreased by 0.23 Å. This is contrary to the expectation that an increase in charge would lead to an increase in Coulombic repulsion and a longer $[Mo_2]\cdots[Mo_2]$ separation, $[Mo_2] = Mo_2(cis\text{-}DAniF)_2$. More recently, we observed similar decreases in $[Mo_2]\cdots[Mo_2]$ separations occurring upon oxidation of $[Mo_2(cis\text{-}DAniF)_2]_2(\mu\text{-}OMe)_4$[18] and $[Mo_2(DAniF)_3]_2(\mu\text{-}H)_2$.[30] For these compounds, DFT calculations suggested partial bond formation, directly between the Mo_2 units, as oxidation takes place.

Here we report further studies on **8-PF$_6$** and the syntheses of the Br analogues $[Mo_2(cis\text{-}DAniF)_2]_2(\mu\text{-}Br)_4$ (**9**) and its oxidized product **9-PF$_6$**. We complete the series by oxidizing $[Mo_2(cis\text{-}DAniF)_2]_2(\mu\text{-}I)_4$ (**10**) to **10-PF$_6$**. Structures are provided for the new compounds. Electrochemical data for all isostructural neutral compounds and NIR data for the three mixed-valence species are also presented. DFT calculations support partial formation of long-range Mo to Mo bonds as oxidation occurs. For comparison,

---

* Reproduced in part with permission from *Inorg. Chem.* **2006**, *45*, 9493, Cotton, F. A.; Liu, C. Y.; Murillo, C. A.; Zhao, Q., "Strong Electronic Communication by Direct Metal–Metal Interaction in Molecules with Halide-Bridged Dimolybdenum Pairs,"

DFT calculations are also provided for $[Mo_2Cl_2(PEt_3)_2]_2(\mu\text{-}Cl)_4$,[52] which is known to have a rectangular arrangement of molybdenum atoms with triple and single Mo_2 bonds alternating around the rectangle. The series of compounds $[Mo_2(cis\text{-}DAniF)_2]_2(\mu\text{-}X)_4$, X = Cl, Br, and I, which are the subject of this work, provide a rare opportunity for evaluation of electronic communication in a very similar environment where the size of the halide bridging ligands allows us to tune the direct orbital overlap interaction between dimetal units.

EXPERIMENTAL SECTION

Materials and Methods. Solvents were dried and then distilled under N_2 following conventional methods or purified under argon using a Glass Contour solvent purification system. All synthetic operations were conducted under N_2 using Schlenk line techniques. $[Mo_2(cis\text{-}DAniF)_2(NCCH_3)_4](BF_4)_2$ was prepared by a published method;[53] $[Mo_2(cis\text{-}DAniF)_2]_2(\mu\text{-}Cl)_4$, **8** and $\{[Mo_2(cis\text{-}DAniF)_2]_2(\mu\text{-}Cl)_4\}PF_6$, **8-PF$_6$**, were prepared as reported earlier,[51] the commercially available salts $Bu^n{}_4NX$ (X = Cl, Br, I), were dried overnight at 50 °C under vacuum.

Physical Measurements. Elemental analyses were performed by Robertson Microlit Laboratories, Madison, New Jersey. ^1H NMR spectra were recorded on a Mercury-300 NMR spectrometer with chemical shifts (δ ppm) referenced to $CDCl_3$. Electronic spectra in CH_2Cl_2 were measured in the range of 200 to 800 nm on a Shimadzu UV-2501PC spectrophotometer. The NIR spectra were obtained from a Bruker TEASOR 27 spectrometer. Cyclic voltammograms (CVs) were collected on a

CH Instruments electrochemical analyzer with Pt working and auxiliary electrodes, an Ag/AgCl reference electrode, a scan rate of 100 mV/s (for CVs), and 0.1 M Bu_4NPF_6 (in CH_2Cl_2) as electrolyte. Under these experimental conditions, the $E_{1/2}$ ferrocene/ferrocenium (Fc^+/Fc) couple was measured at 440 mV. EPR spectra were recorded using a Bruker ESP300 spectrometer.

Preparation of $[Mo_2(cis\text{-}DAniF)_2]_2(\mu\text{-}Br)_4$, 9. To a mixture of 0.416 g (0.400 mmol) $[Mo_2(cis\text{-}DAniF)_2(CH_3CN)_4](BF_4)_2$, and an excess of $Bu^n{}_4NBr$ (0.644 g, 2.00 mmol), was added 20 mL of ethanol. A red-brown precipitate formed immediately upon stirring. The mixture was stirred at room temperature for 2 h. The supernatant solution was then decanted and the brown solid was washed twice with 15 mL of ethanol and dried under vacuum. Large dark-red crystals were obtained by slow diffusion of hexanes into a CH_2Cl_2 solution of the product. Yield: 0.25 g (72%). ^1H NMR ($CDCl_3$, 300 MHz): 8.637 (s, 4H, -NC*H*N-), 6.683 (m, 16H, aromatic C-*H*), 6.603 (m, 16H, aromatic C-*H*), 3.678(s, 24H, -OC*H*$_3$); UV–vis, λ_{max} (nm) (ε, $M^{-1}cm^{-1}$): 394 (2.5×10^3), 500 (3.9×10^3). Anal. Calcd for $C_{60}H_{60}Br_4Mo_4N_8O_8$ (**9**): C, 41.79; H, 3.51; N, 6.50. Found: C, 41.87; H, 3.47; N, 6.33.

Preparation of $[Mo_2(cis\text{-}DAniF)_2]_2(\mu\text{-}I)_4$, 10. This compound was prepared similarly to **9** using 0.416 g (0.400 mmol) of $[Mo_2(cis\text{-}DAniF)_2(CH_3CN)_4](BF_4)_2$ and an excess of $Bu^n{}_4NI$ (0.738 g, 2.00 mmol) in 20 mL of ethanol. Yield: 0.36 g (94%). ^1H NMR ($CDCl_3$, 300 MHz, δ, ppm): 8.555 (s, 4H, -NC*H*N-), 6.659 (m, 16H, aromatic C-*H*), 6.595 (m, 16H, aromatic C-*H*), 3.678(s, 24H, -OC*H*$_3$); UV–vis, λ_{max} (nm) (ε, $M^{-1}cm^{-1}$): 403 (3.4×10^3), 508 (3.8×10^3).

Preparation of {[Mo_2(*cis*-DAniF)$_2$]$_2$(μ-Br)$_4$}PF_6, 9-PF_6. Solutions of [Mo_2(*cis*-DAniF)$_2$]$_2$(μ-Br)$_4$, **9** (0.17 g, 0.10 mmol) in 10 mL of CH_2Cl_2, and ferrocenium hexafluorophosphate, (0.036g, 0.11 mmol) in 15 mL of CH_2Cl_2, were prepared separately and cooled down to −78 °C. Transfer of the cold $FcPF_6$ solution through a cannula into the red solution of **9** produced a dark-brown solution. The resultant solution was stirred at low temperature for 30 min and pre-cooled hexanes (50 mL) were then added to produce a dark-brown precipitate. After the solvent was decanted, the solid residue was washed with 20 mL of hexanes and then dried under vacuum. This solid was dissolved in 15 mL of dichloromethane at room temperature, and the solution was layered with 40 mL of hexanes. After about one week, block-shaped crystals were obtained. Yield: 0.16 g (85%). UV–vis, λ_{max} (nm) (ε, $M^{-1}cm^{-1}$): 478 (6.3×10^3), 619 (1.0×10^4). Anal. Calcd for $C_{61}H_{62}Br_4Cl_2F_6Mo_4N_8O_8P$ (**9-PF_6**·CH_2Cl_2): C, 37.49; H, 3.20; N, 5.73. Found: C, 37.75; H, 2.94; N, 5.57.

Preparation of {[Mo_2(*cis*-DAniF)$_2$]$_2$(μ-I)$_4$}PF_6, 10-PF_6. This black compound was synthesized using a procedure similar to that for **9-PF_6**. Small needle-shaped crystals of **10-PF_6**·$2CH_2Cl_2$ were obtained. Yield: 0.16 g (79%). UV–vis, λ_{max} (nm) (ε, $M^{-1}cm^{-1}$): 472 (5.2×10^3), 639 (9.3×10^3). Anal. Calcd for $C_{62}H_{64}I_4Cl_4F_6Mo_4N_8O_8P$ (**10-PF_6**·$2CH_2Cl_2$): C, 33.43; H, 2.90; N, 5.03. Found: C, 33.36; H, 2.56; N, 4.99.

X-ray Structure Determinations. Single crystals suitable for X-ray analysis were mounted and centered on the tips of cryoloops attached to a goniometer head. Data for **9**·$2CH_2Cl_2$, **9-PF_6**·$2CH_2Cl_2$ and **10-PF_6**·$2CH_2Cl_2$ were collected at −60 °C on a BRUKER SMART 1000 CCD area detector system. Cell parameters were determined

using the program SMART.[24] Data reduction and integration were performed with the software package SAINT,[25] while absorption corrections were applied using the program SADABS.[26] The positions of the heavy atoms were found via direct methods using the program SHELXTL.[27] Subsequent cycles of least-squares refinement followed by difference Fourier syntheses revealed the positions of the remaining non-hydrogen atoms. Hydrogen atoms were added in idealized positions. Non-hydrogen atoms were refined with anisotropic displacement parameters. Crystallographic data for **9**·$2CH_2Cl_2$, **9-PF$_6$**·$2CH_2Cl_2$, and **10-PF$_6$**·$2CH_2Cl_2$ are given in Table VI and selected bond distances and angles in Table VII.

Computational Details. Density functional theory (DFT)[54] calculations were performed with the hybrid Becke's[55] three-parameter exchange functional and the Lee-Yang-Parr[56] nonlocal correlation functional (B3LYP) in the Gaussian 03 program.[57] Double-ζ quality basis sets (D95)[58] were used on C, N and H atoms as implemented in Gaussian. For P, Cl, and Br atoms, correlation consistent double-zeta basis sets (CC-PVDZ)[59] were applied, where a double-ζ basis set (LANL2DZ) was applied on I atoms. A small effective core potential (ECP) representing the 1s2s2p3s3p3d core was used for the molybdenum atoms along with its corresponding double-ζ basis set (LANL2DZ).[60] Time-dependent density functional (TD-DFT) calculations[61] were performed to assign the electronic spectra of these compounds. All calculations were performed on either Origin 3800 64-processor SGI or Origin 2000 32-processor SGI supercomputers located at the Texas A&M supercomputing facility.

Table VI. X-ray Crystallographic Data for **9**·$2CH_2Cl_2$, **9-PF_6**·$2CH_2Cl_2$, and **10-PF_6**·$2CH_2Cl_2$

compound	**9**·$2CH_2Cl_2$	**9-PF_6**·$2CH_2Cl_2$	**10-PF_6**·$2CH_2Cl_2$
formula	$C_{62}H_{64}Br_4Cl_4Mo_4N_8O_8$	$C_{62}H_{64}Br_4Cl_4F_6Mo_4N_8O_8P$	$C_{62}H_{64}Cl_4F_6I_4Mo_4N_8O_8P$
fw	1894.41	2039.38	2227.34
space group	$P2_1/n$ (No. 14)	$P\bar{1}$ (No. 2)	$P\bar{1}$ (No. 2)
a (Å)	11.8343(19)	9.895(4)	9.247(2)
b (Å)	12.405(2)	12.165(4)	13.224(3)
c (Å)	23.934(4)	15.609(6)	15.417(3)
α (deg)	90	81.771(6)	89.677(4)
β (deg)	98.568(3)	85.841(6)	79.545(4)
γ (deg)	90	78.464(7)	81.104(4)
V (Å^3)	3474(1)	1820(1)	1831.1(7)
Z	2	1	1
T (K)	213	213	213
d_{calcd} (g/cm^3)	1.811	1.861	2.020
μ (mm^{-1})	3.217	3.110	2.595
R1[a] (wR2[b])	0.042 (0.106)	0.032 (0.089)	0.049 (0.108)

[a] $R1 = \Sigma||F_o|-|F_c||/\Sigma|F_o|$.

[b] $wR2 = [\Sigma[w(F_o^2-F_c^2)^2]/\Sigma[w(F_o^2)^2]]^{1/2}$

Table VII. Selected Bond Distances (Å) and Angles (deg) for **8**, **8-PF$_6$**, **9**, **9-PF$_6$**, **10**, **10-PF$_6$**, and $[Mo_2Cl_2(PEt_3)_2]_2(\mu\text{–}Cl)_4$

Compound	Mo─Mo	$Mo_2\cdots Mo_2$[a]	Mo─X[b]	Mo─N	Mo─X─Mo	ref
8	2.1191(4)	3.601	2.516[2]	2.095[5]	91.42[5]	51
8-PF$_6$	2.1453(3)	3.374	2.490[6]	2.083[3]	85.28[1]	51
9	2.1181(6)	3.697	2.649[2]	2.093[5]	88.50[2]	this work
9-PF$_6$	2.1406(9)	3.488	2.622[2]	2.091[4]	83.38[2]	this work
10	2.117(1)	3.915	2.845[2]	2.100[6]	87.02[2]	17b
10-PF$_6$	2.144(1)	3.632	2.812[2]	2.104[8]	80.50[4]	this work
$[Mo_2Cl_2(PEt_3)_2]_2(\mu\text{-}Cl)_4$	2.211(3)	2.901	2.401[6]		74.50	52

[a] Distance between midpoints of the dimolybdenum bonds.

[b] X = bridging anion.

RESULTS AND DISCUSSION

Syntheses. Compounds **8**, **9** and **10** were previously prepared by cumbersome synthetic methods that involved either reduction of $Mo_2(DAniF)_3Cl_2$ with KC_8 in the presence of $ClSiMe_3$, or reaction of $Mo_2(DAniF)_4$ with $XSiMe_3$ (X = Br, I) over a period of 2 days.[17b] The use of the reaction described by Eq. 5, which follows a procedure reported in a communication for **8**, is far more convenient.[51] This procedure, based on the use of the designed dimolybdenum building block $[Mo_2(cis\text{-}DAniF)_2(CH_3CN)_4]^{2+}$,[53] is general and straightforward for the syntheses of all three compounds as the halides simply displace labile acetonitrile molecules from the dimetal unit and bring the two $[Mo_2]$ units together. However, it is important to use very dry starting materials and solvents to obtain pure products. Because the neutral products have low solubility in polar solvents, e. g., ethanol and acetonitrile, there is an additional driving force for the reaction to proceed.

$$2[Mo_2(cis\text{-}DAniF)_2(CH_3CN)_4](BF_4)_2 + 4Bu^n{}_4NX\ (X = Cl, Br, \text{and } I)$$
$$\rightarrow [Mo_2(cis\text{-}DAniF)_2]_2(\mu\text{–}X)_4 + 4Bu^n{}_4NBF_4 + 8CH_3CN \qquad \text{(eq. 5)}$$

Oxidation of the neutral compounds having X = Br and I with one equiv of $FcPF_6$ produces the singly oxidized species $\{[Mo_2(cis\text{-}DAniF)_2]_2(\mu\text{-}X)_4\}PF_6$, X = Br (**9-PF$_6$**) and I (**10-PF$_6$**).

Structural Results. Compound **9** crystallizes in the monoclinic space group $P2_1/n$ with Z = 2, which requires the molecule to have a crystallographic inversion center. The core of the structure, shown in Figure 19, consists of two [Mo_2] units linked by four Br atoms. The core has idealized D_{2h} symmetry and is similar to those in **8** and **10**.[17b] The crystallographically equivalent Mo−Mo quadruple bond distances, 2.1181(6) Å, are also similar to those of **8** and **10** but about 0.02 Å longer than those in dimolybdenum paddlewheel compounds supported by four three-atom bridging ligands, such as $Mo_2(O_2CCH_3)_4$[62] and $Mo_2(DAniF)_4$.[23] The non-bonding separations between the midpoints of the quadruple bonds for the three compounds are 3.601, 3.697 and 3.915 Å for **8**, **9**, and **10**, respectively, and they increase as the atomic radius of the bridging atom increases from Cl to I via Br (Table VII). These separations are significantly shorter than those in molybdenum-containing pairs (also known as "dimers of dimers"). Among these, the shortest separation is found for L = oxalate (6.94 Å).[12d] The Mo–X distances are 2.516[2], 2.649[2] and 2.845[2] Å for **8**, **9**, and **10**, respectively. The average X−Mo−X angles increase slightly from 81.06[3]° to 82.95[2]° to 83.89[2]° from the Cl to the Br to the I analogue, while the average Mo−X−Mo angles decrease from 91.42[5]° to 88.50[2]° to 87.02[2]° in the same order. These angles are consistent with the increase of atomic radii from Cl to Br, then to I.

The ^{1}H NMR spectra show singlets for both the methine protons (ca. 8.6 ppm) and methoxyl groups (ca. 3.7 ppm). This suggests that the D_{2h} symmetry of the [Mo_2](μ-X)$_4$[Mo_2] molecules persists in solution as all ligand anisyl groups are equivalent.

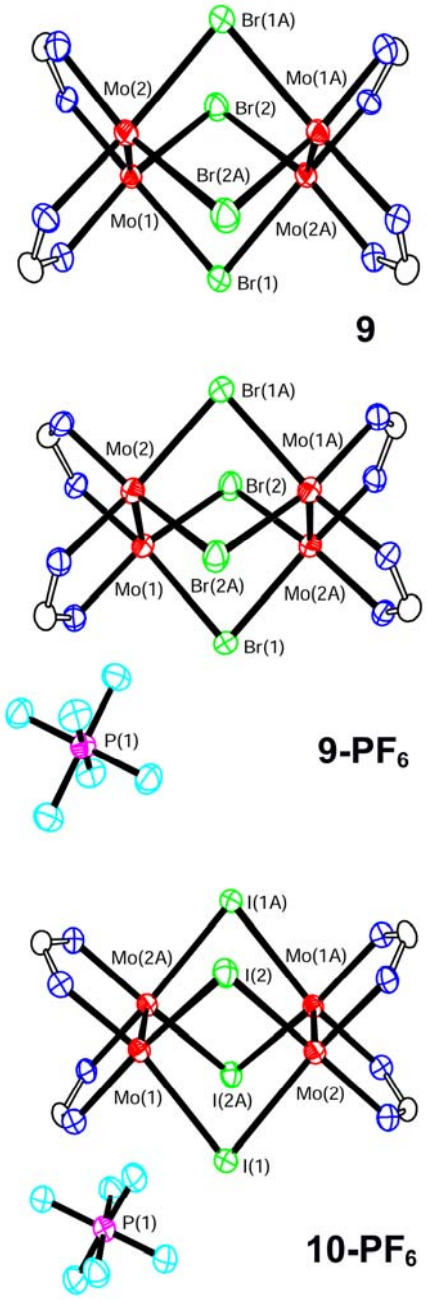

Figure 19. Core structures of **9**·$2CH_2Cl_2$, **9-PF$_6$**·$2CH_2Cl_2$ and **10-PF$_6$**·$2CH_2Cl_2$ drawn with ellipsoids at the 40% probability level. All *p*-anisyl groups and hydrogen atoms have been omitted for clarity.

The mixed-valence complex **9-PF$_6$** crystallizes in triclinic space group $P\bar{1}$ (Figure 19). The cation and anion reside on different inversion centers. Upon removal of one electron, the two Mo–Mo bond distances are lengthened from 2.1181(6) Å in the precursor to 2.1406(9) Å. This lengthening is consistent with an electron being removed from the δ orbitals of the dimetal units and a decrease of 0.25 in overall bond order. The increase of 0.023 Å in the Mo–Mo bond distance in going from **9** to **9-PF$_6$** is similar to those observed in delocalized systems but considerably less than those found in localized mixed-valence complexes of the type $[Mo_2]^+L[Mo_2]^0$.[15b,21,22] The metal─ligand bond distances also appear to be shortened, for example, from 2.649[2] to 2.622[2] Å for Mo–Br and from 2.093[5] to 2.091[4] Å for Mo–N_{DAniF} because of the increase of the oxidation state of the dimetal units, but these changes are very small. Accompanying the increase of the metal─metal bond distance, the separation between the midpoints of the two [Mo_2] units ($Mo_2\cdots Mo_2$) is reduced by about 0.21 Å, from 3.697 to 3.488 Å. The average bridging angles Mo–Br–Mo (83.38[2]°) are smaller than those in the precursor (88.50[2]°). Similar changes on the geometry have been observed for the iodine analogue as one electron is removed from the neutral complex.

Magnetism and NIR Spectra. The X-band EPR spectra for **9-PF$_6$** and **10-PF$_6$** were measured at room temperature in CH_2Cl_2 solution. Only one prominent signal was observed for each complex, which is consistent with a doublet electronic ground state. The *g* values of 1.935 for **9-PF$_6$** and 1.959 for **10-PF$_6$** are significantly different from that for an organic free radical and indicate that the unpaired electron resides in a mainly metal-based orbital. The main peak is due to molecules containing only the ^{96}Mo ($I = 0$)

isotope (about 74% abundance), whereas the small peaks flanking the main signal are due to coupling of four Mo (^{95,97}Mo (I = 5/2) isotopes that have combined natural abundance of about 25%) and four halide atoms. This is again consistent with the electron being delocalized over the two [Mo_2] units.

The NIR spectra of **8-PF_6**, **9-PF_6** and **10-PF_6** were measured in the region from 2000 to 10500 cm^{-1} both in the solid state using KBr pellets (Figure 20 and Table VIII) and in CH_2Cl_2 solutions. In both media, the NIR spectra were essentially the same. Each mixed valence complex shows two intense broad absorption bands centered at ca. 5700 and 7200 cm^{-1}. It is similar to the NIR spectra of the complex $\{[Mo_2(cis\text{-DAniF})_2]_2(\mu\text{-OMe})_4\}^+$ where two broad absorption bands were observed in the NIR region.[18] Such transitions are often referred to as intervalence charge transfer transitions. The spectra of these three mixed-valence species are qualitatively different from those for the [Mo_2]L[Mo_2] systems, for which only one band has been observed in the NIR region.[21,22] Even thought the Hush formula, $\Delta\nu_{1/2} = (2310\nu_{max})^{1/2}$,[28] may not be used to interpret the spectra of these $[Mo_2(cis\text{-DAniF})_2]_2(\mu\text{-X})_4$ compounds, the intense bands are consistent with significant electronic interaction between the two dimolybdenum units.

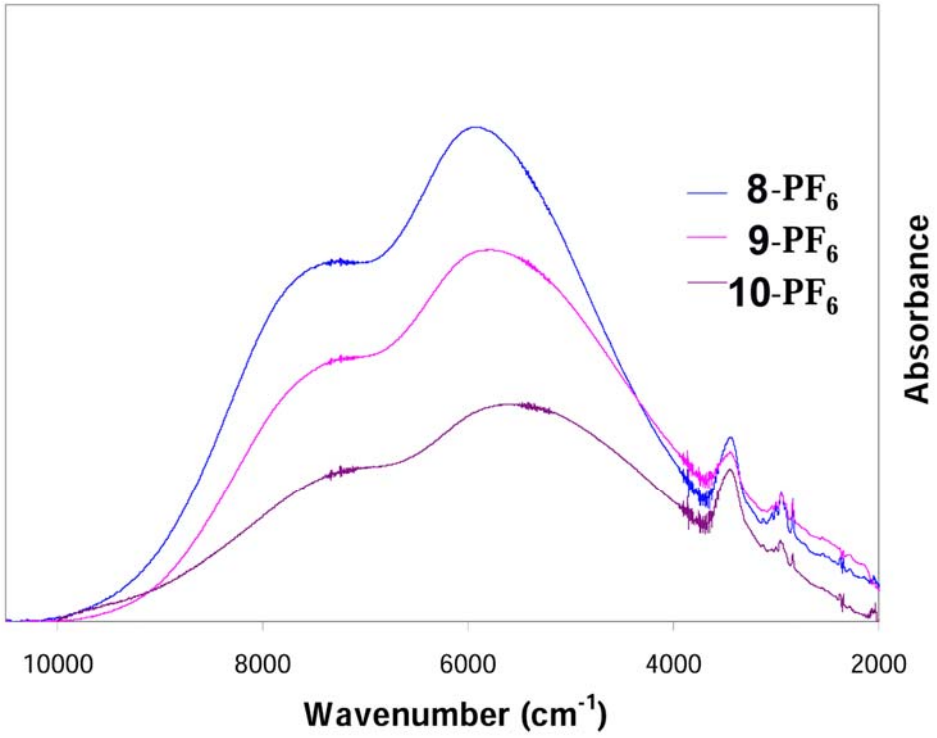

Figure 20. NIR spectra of the crystalline mixed-valence species **8-PF_6**, **9-PF_6**, and **10-PF_6** in KBr pellets.

Table VIII. NIR Data (cm^{-1}) for **8-PF$_6$**, **9-PF$_6$** and **10-PF$_6$**

	High-intensity peak (eV)	HOMO−1(a_g) → SOMO(b_{3u}) Calcd (eV)	Low-intensity peak (eV)	HOMO−1(a_g) → LUMO(b_{2u}) Calcd (eV)
8-PF$_6$	5900(0.73)	6008 (0.745)	7300 (0.90)	6143 (0.762)
9-PF$_6$	5700(0.71)	5763 (0.717)	7200 (0.89)	6068 (0.753)
10-PF$_6$	5600(0.69)	5249 (0.651)	7100 (0.88)	6032 (0.748)

Electrochemistry. The CVs of **9** and **10** are shown in Figure 21, and the electrochemical data for the three compounds are listed in Table IX. These compounds exhibit two well-separated redox couples, corresponding to two one-electron oxidation processes occurring on the two $[Mo_2]$ units. For **8**, **9**, and **10**, the potential separations ($\Delta E_{1/2}$) between the two oxidation processes are 540, 499 and 440 mV, respectively. These very large $\Delta E_{1/2}$ values suggest that there is strong electronic coupling between the two $[Mo_2]$ units. From the values of $\Delta E_{1/2}$, comproportionation constants (K_C) for the equilibrium can be derived.[19] Their magnitudes, ranging from 10^9 to 10^7, are listed in Table IX. Clearly, these singly oxidized species are thermodynamically highly stable, and it is reasonable to make the assumption that the stability is due to delocalization of the charge.

It has been established in many other cases that back bonding from the metal centers to the linker, e. g., d_{xz}, $d_{yz} \rightarrow \pi^*$ for linked mononuclear compounds[6] and $\delta \rightarrow \pi^*$ for systems with dimetal units,[12] is the major pathway by which electronic communication between the two metal centers occurs. Similar back bonding is not expected for the $[Mo_2]_2(\mu\text{-}X_4)$ species because of the nature of the linkers, nor is the geometric relationship of the dimolybdenum building blocks to each other conducive to strong coupling via the linkers. Therefore the explanation for the strong electronic coupling observed in these species must be different.

It appears that the short metal to metal separations promote strong electrostatic interactions; hence, it is one of the major factors that enhance the electronic coupling over the two $[Mo_2]$ units. It is noted also that some lobes of the δ orbitals from the two

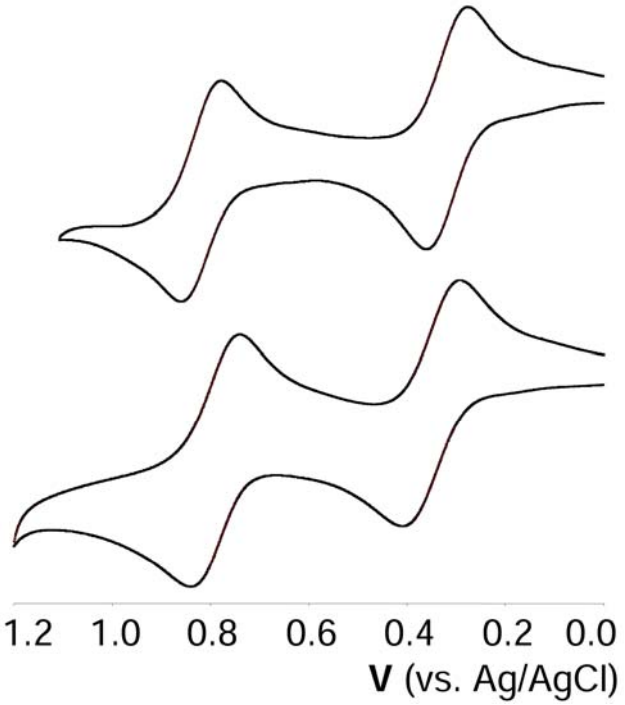

Figure 21. Cyclic voltammograms for **9** (upper) and **10** (lower) in CH_2Cl_2 solution.

Table IX. Oxidation Potentials and Comproportionation Constants for **8**, **9**, and **10** Along with Separations between Dimetal Units

	$Mo_2{\cdots}Mo_2$ (Å)	$E_{1/2}(1)$ (mV)	$E_{1/2}(2)$ (mV)	$\Delta E_{1/2}$ (mV)	K_C	ref
8	3.601	260	800	540	1.3×10^9	51
9	3.697	314	813	499	2.7×10^8	this work
10	3.915	350	790	440	2.7×10^7	this work

[Mo_2] units are pointing directly toward each other, as shown in Figure 22. Given the short Mo_2···Mo_2 distances (3.6 ~ 3.9 Å) and the D_{2h} molecular symmetry, it appears that electron delocalization may occur via a direct metal to metal σ interaction. Electron delocalization in this complex system is supported by the X-ray structural analysis of the mixed-valence species **8-PF$_6$**,[51] **9-PF$_6$** and **10-PF$_6$**.

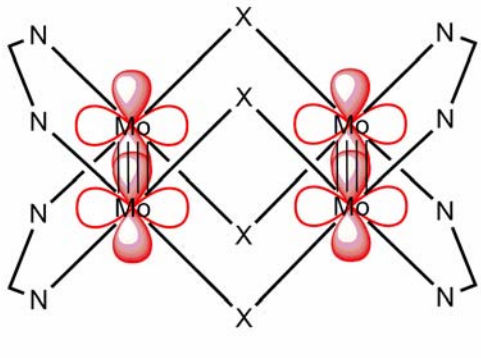

Figure 22. Interaction between the δ orbitals from the two dimolybdenum units.

For this series of compounds, the coupling effect decreases as the atomic number of the bridging atom X increases. Figure 23 shows that the $\Delta E_{1/2}$ values are nearly linearly related to the distances between [Mo_2] units (d in Å), and the $\Delta E_{1/2}$ values decrease as d increases with an increase in the atomic radius of X. The trend in the $\Delta E_{1/2}$ values appears reasonable regardless of whether an electrostatic interaction or a direct metal to metal σ interaction between two [Mo_2] units or both are responsible for the

electronic coupling. Also, the bridging atom (X) has an influence on the first redox process, $E_{1/2}^{(+1/0)}$, and these $E_{1/2}(1)$ values are nearly a linear function of the electronegativity of the halogen atom, as shown in Figure 24.

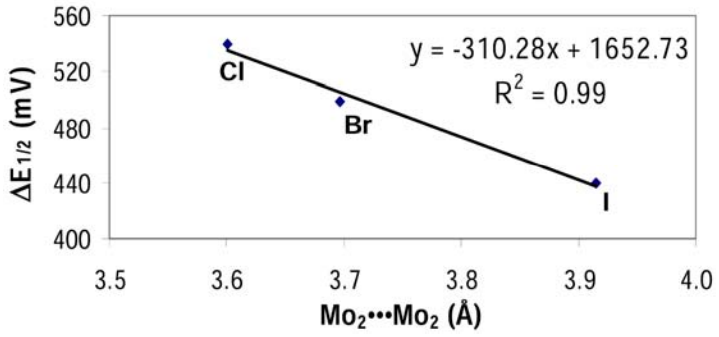

Figure 23. $\Delta E_{½}$ values versus the distances between the midpoints of the $[Mo_2]$ units, $Mo_2 \cdots Mo_2$, in $[Mo_2(cis\text{-}DAniF)_2]_2X_4$ (X = Cl, Br, and I).

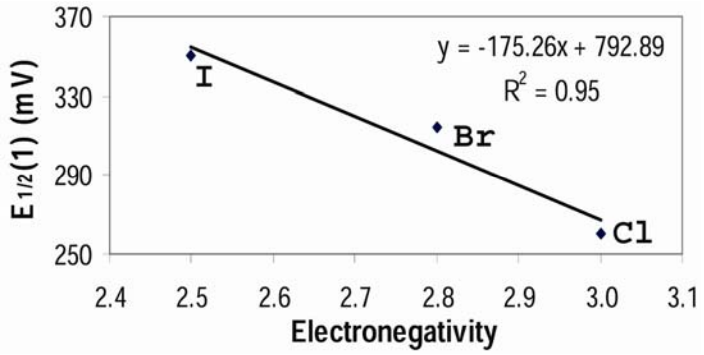

Figure 24. The $E_{½}(1)$ values (mV) as a function of electronegativity of the μ-X atoms: Cl, Br, and I.

Electronic Structures and DFT Calculations. A series of DFT calculations and fragment analysis were carried out to better understand the electronic interaction between the [Mo_2] units. Geometry optimizations for the neutral and singly oxidized species were done using the parameters from the crystal structures as starting points. The models, with all anisyl groups replaced by hydrogen atoms, were simplified to [Mo_2(*cis*-NHCHNH)$_2$]$_2$(μ-X)$_4$ (X = Cl, Br, I) having D_{2h} symmetry.

The general agreement between the calculated and the experimental geometric data shown in Tables X and VII suggests that such a simplification is reasonable. The overestimation of the Mo–Mo distances (ca. 0.04 Å) is reasonable because of the use of hydrogen atoms in the theoretical study instead of the basic *p*-anisyl groups. All changes in bond distances and angles resulting from the oxidation are in good agreement with those from X-ray crystallography. After one electron was removed in the halide bridged complexes, the calculated distances between the midpoints of the two [Mo_2] units decreased by about 0.21 Å ~ 0.27 Å; these changes are comparable with the experimental decreases which are ca. 0.21 Å ~ 0.28 Å.

Analysis of the frontier orbitals from the calculations (Figures 25 and 26) indicate that direct σ interaction through space occurs between the δ orbitals in the dimetal units. The two filled δ orbitals interact with each other and generate two molecular orbitals, one bonding (a_g, δ+δ) and one antibonding (b_{3u}, δ−δ) over the four molybdenum atoms. The combination of the two δ* orbitals gives two more molecular orbitals, which again include one bonding (b_{2u}, δ*+δ*) and one antibonding (b_{1g}, δ*−δ*). The orbitals from the molybdenum atoms make the largest contribution to these two sets

Table X. Calculated Bond Lengths (Å) and Angles (deg) for Models of **8**, **9**, **10** and $[Mo_2Cl_2(PMe_3)_2]_2(\mu\text{-}Cl)_4$

	Charge	Mo−Mo	$Mo_2\cdots Mo_2$	Mo−X[a]	Mo−X−Mo
8	0	2.160	3.706	2.594	91.17
	+1	2.181	3.503	2.556	86.52
9	0	2.161	3.864	2.765	88.66
	+1	2.182	3.632	2.721	83.72
10	0	2.163	4.054	2.975	85.89
	+1	2.184	3.780	2.921	80.63
$[Mo_2Cl_2(PMe_3)_2]_2(\mu\text{-}Cl)_4$	0	2.240	2.918	2.453	72.98

[a] X = bridging anion.

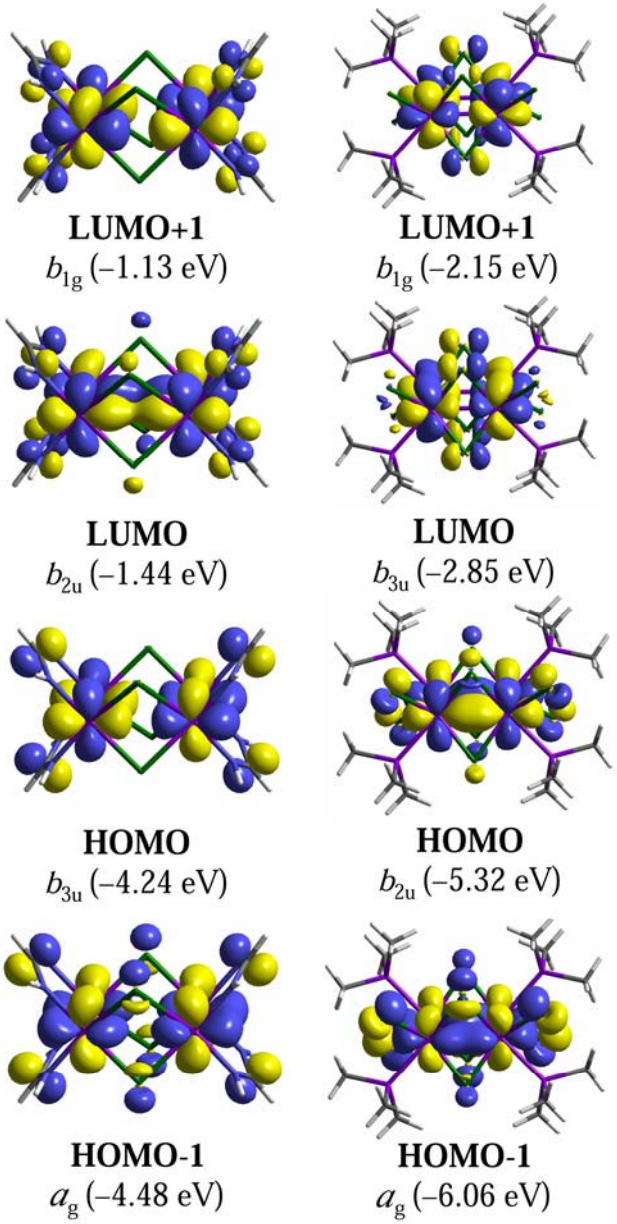

Figure 25. Selected frontier orbitals for the models $[Mo_2(cis\text{-}NHCHNH)_2]_2Cl_4$ (left) and $[Mo_2Cl_2(PMe_3)_2]_2(\mu\text{-}Cl)_4$ (right) using an isosurface value of 0.03.

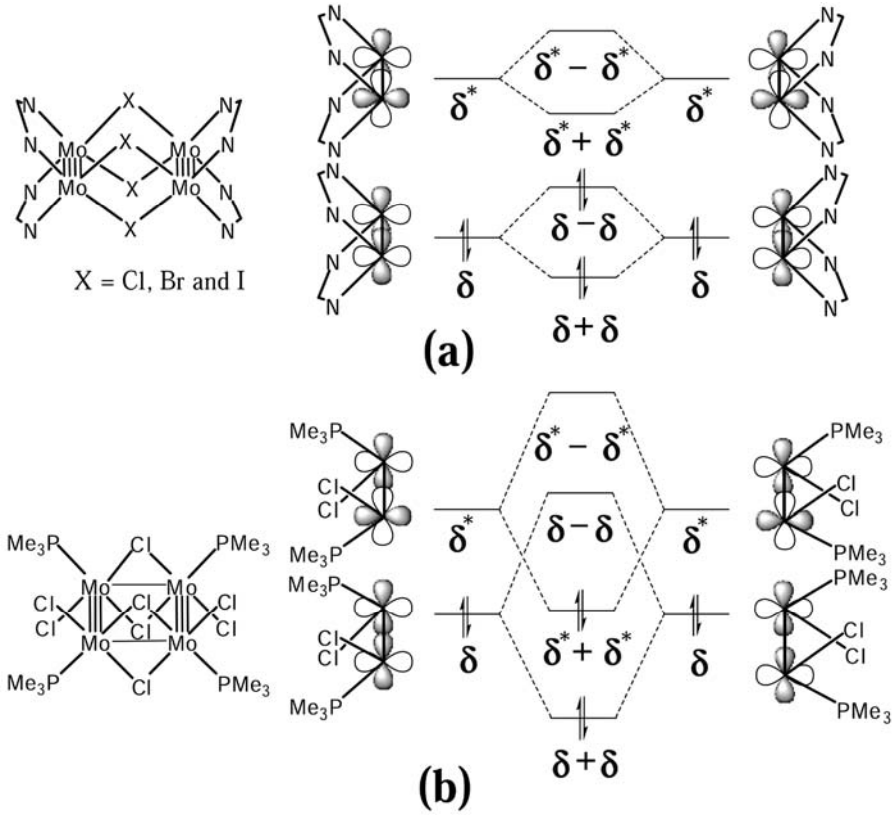

Figure 26. Orbital interaction diagram for $[Mo_2(cis\text{-}NHCHNH)_2]_2X_4$ (X = Cl, Br, I) (upper) and $[Mo_2Cl_2(PMe_3)_2]_2(\mu\text{-}Cl)_4$ (lower). The two dimetal units are shown in the left and right columns, respectively.

of MOs (ca. 70% ~ 87%). The frontier orbitals for [*cis*-$Mo_2(NHCHNH)_2]_2(\mu\text{-}Cl)_4$ are shown in Figure 25a, in which the in-phase combination of the δ orbitals (a_g, δ+δ), is the HOMO−1, whereas the HOMO is the out-of-phase combination of the δ orbitals (b_{3u}, δ–δ). There would be no bonding between the two [Mo_2] units, with each dimolybdenum unit remaining quadruply bonded. The energy difference, ΔE, between δ–δ and δ+δ orbitals, is a measure of the electronic interaction between the two dimetal units.[30] The calculations (Table XI) show that the ΔE values are 0.21, 0.23, and 0.25 eV for **10**, **9**, and **8**, respectively. This indicates that the electronic coupling between the two dimetal units increases as the two dimetal units approach each other, as would be expected from the shortening of the $Mo_2\cdots Mo_2$ distances.

To obtain the detailed relationship between the ΔE values and the $Mo_2\cdots Mo_2$ distance, a fragment analysis and comparative study were carried out. The calculations were done at the DFT level using a model that brought together two $[Mo_2(HNCHNH)_2]^{2+}$ components devoid of linking atoms but having the same relative orientation than that in $[Mo_2(NHCHNH)_2]_2(\mu\text{-}Cl)_4$. When the $Mo_2\cdots Mo_2$ distance was varied, the ΔE values changed. The calculation indicates that when the $Mo_2\cdots Mo_2$ distance is equal to or larger than 9 Å (green region in Figure 27), there is no direct interaction between the two dimetal units; the two δ orbitals have the same energy and the ΔE values are essentially zero. When the two [Mo_2] units approach each other (red region), the direct σ interaction affects the energy of the two δ orbitals. The two δ orbitals form a set of molecular orbitals δ+δ and δ–δ, where the two δ* orbitals form δ*+δ* and δ*–δ* MOs. The ΔE (Y axis, $E_{\delta-\delta} - E_{\delta+\delta}$)

Table XI. Comparison of ΔE (eV) with Calculated Distances between [Mo_2] Units

	$Mo_2\cdots Mo_2$ (exp)	$Mo_2\cdots Mo_2$ (calcd)	ΔE (eV)[a]	$\Delta E_{1/2}$ (mV)	ref
$Mo_4Cl_8(PMe_3)_4$	2.901(2)[52]	2.918	3.21	NA	this work
[*cis*-$Mo_2(DAniF)_2]_2(OCH_3)_4$	3.245	3.333	0.34	554	18
8	3.601	3.706	0.25	540	this work
9	3.697	3.864	0.23	499	this work
10	3.915	4.054	0.21	440	this work

[a] $\Delta E = E_{\delta-\delta} - E_{\delta+\delta}$

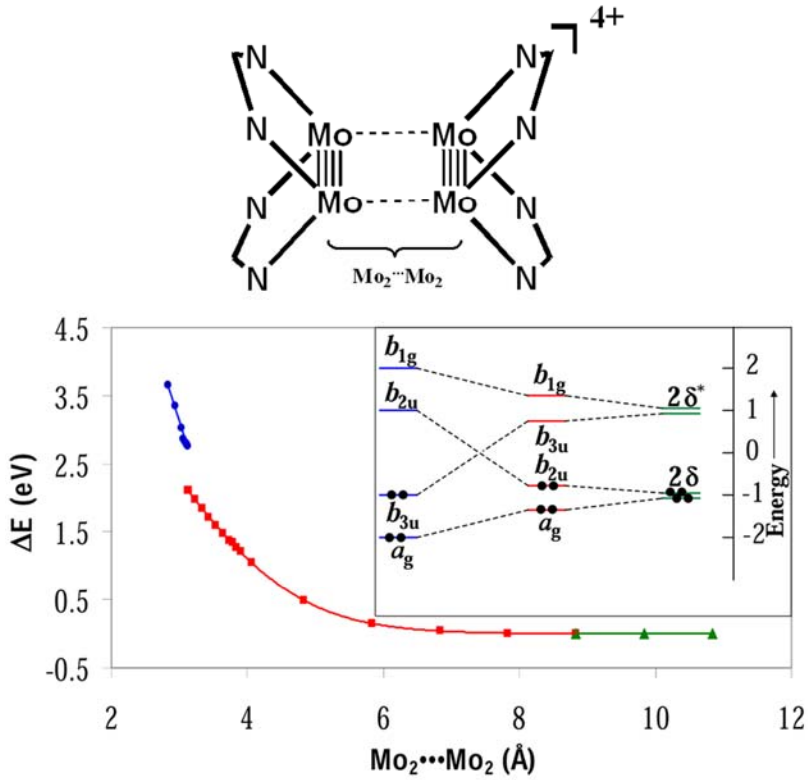

Figure 27. Comparison of the calculated ΔE ($E_{\delta-\delta}$–$E_{\delta+\delta}$) values versus the distance between the midpoints of the [Mo_2] units. In the inset an orbital correlation diagram is given. Color code: green = two widely separated δ orbitals from two dimetal units; red = the two δ orbitals close enough for significant interactions to occur, blue = tetrametal analogue of cyclobutadiyne. The electron configurations correspond to the ground state for each state.

values slowly increase at first and then rise quickly until the $Mo_2\cdots Mo_2$ distance (X axis) reaches 3.12 Å. In that state, there is direct σ interaction between the two [Mo_2] units and the strength of the interaction increases even more rapidly as the $Mo_2\cdots Mo_2$ distance decreases. As the two dimetal units approach each other, the energy difference between the orbitals of δ–δ and δ*+δ* will be smaller because of the increase in the ΔE values. At some point, the order of these two orbitals will be switched. The calculations show that when the $Mo_2\cdots Mo_2$ distance is less than 3.12 Å (blue region), the δ*+δ* orbital becomes the HOMO and δ–δ is the LUMO. There is no longer a δ bond in each [Mo_2] unit because there is equal electron density in the δ and δ* orbitals. Simultaneously two σ single bonds form between the two [Mo_2] units resulting in a rectangle with two single bonds and two triple bonds. This route resembles the 2+2 cycloaddition in the process of dimerization of ethylene to cyclobutane in which breaking of two $p\pi$ orbitals takes place and two new σ single bonds are formed.[63]

One example of this type of rectangle is $[Mo_2Cl_2(PEt_3)_2]_2(\mu\text{-}Cl)_4$[52] in which the short Mo─Mo bonds, not supported by bridging ligands, are 2.211(3) Å and the long bonds each bridged by two Cl atoms are 2.901(2) Å. Note that this distance is less than the calculated crossover state (3.12 Å). DFT calculations were performed on this molecule using the simplified model $[Mo_2Cl_2(PMe_3)_2]_2(\mu\text{-}Cl)_4$. The frontier orbitals analysis (Figure 25b) shows that the HOMO is indeed the in-phase combination of the δ* orbitals ($b_{2u,}$ δ*+δ*), whereas the LUMO is the antibonding combination of the δ orbitals ($b_{3u,}$ δ–δ), and this complex is a tetrametal analogue of cyclobutadiyne as initially proposed.[52] The frontier MOs also show that none of the single bonds or the

triple bonds can be viewed as isolated, and that the four electrons on the HOMO and HOMO−1 are delocalized over the four molybdenum atoms.

For the singly oxidized cation $\{[Mo_2(cis\text{-}NHCHNH)_2]_2(\mu\text{-}Cl)_4\}^+$, the electronic structure (Figure 28) is similar to that of the precursor where the four metal-based frontier MOs are comprised mainly of the δ and δ* orbitals from the two dimetal units. This is consistent with the EPR spectra of the mixed-valence complexes which show that the electron is in an orbital that has mainly metal character because of the low *g* values (1.912 for Cl,[51] 1.935 for Br and 1.959 for I). Upon a one-electron oxidation of the neutral precursor, removal of the electron from this metal-based orbital results in the lengthening of bond distances within the multiply bonded Mo–Mo units. Simultaneously, because of the antibonding character (δ–δ) between the two adjacent $[Mo_2]$ units, shortening of the $Mo_2\cdots Mo_2$ distances occurs between adjacent units.

The DFT calculations on the three singly oxidized species show that the spin density of the SOMO (Figure 29) is delocalized over the two dimolybdenum units in each case. Because the model used requires these two units to be equivalent, these results do not, in themselves, constitute evidence for delocalization. They were not done with that objective in mind, but rather to support the belief that direct σ interaction provides an efficient route for the electronic communication between the redox centers.

Time-dependent (TD–DFT) calculations were also carried out on the halide bridged complexes using the optimized geometry of the models $[Mo_2(cis\text{-}NHCHNH)_2]_2(\mu\text{-}X)_4$ (X = Cl, Br, I). Such calculations have been useful in understanding the electronic spectra of compounds having two $[Mo_2]$ units linked by dicarboxylate

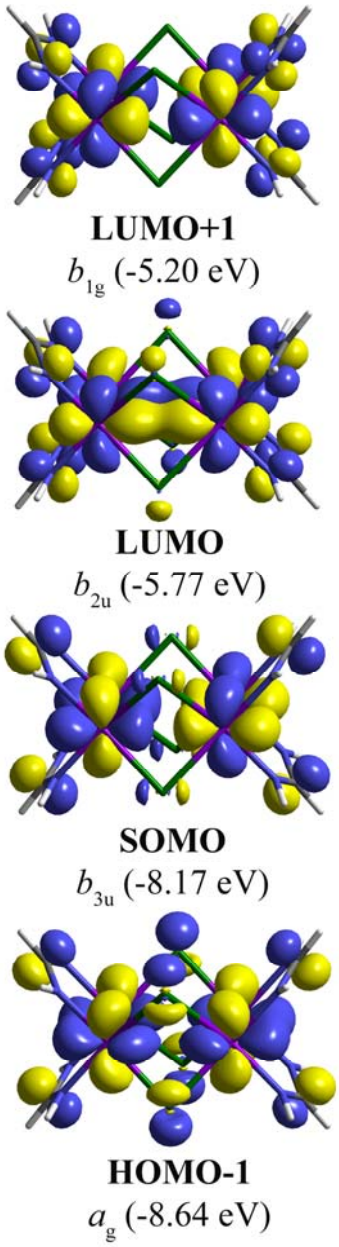

Figure 28. Selected alfa frontier orbital for $\{[Mo_2(NHCHNH)_2]_2Cl_4\}^+$, **8-PF$_6$**, drawn with an isosurface value of 0.03.

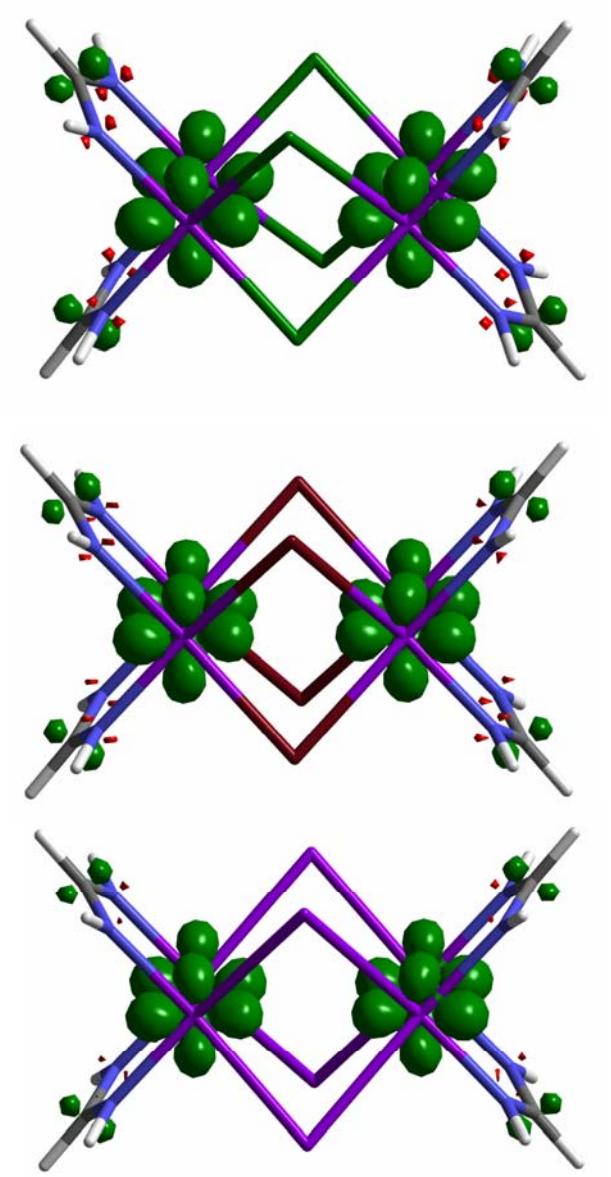

Figure 29. Spin density diagram of the SOMO for **8-PF$_6$** (top), **9-PF$_6$** (center) and **10-PF$_6$** (bottom) with an isosurface value of 0.006.

groups.[12c] As mentioned earlier, the three neutral species each show two weak absorption bands in the UV–Vis range. The one, observed at 495 nm for **8** is calculated at 552 nm for the two symmetry allowed δ → δ* type transitions that are close in energy, namely HOMO to LUMO+1 (δ−δ → δ*−δ*) and HOMO−1 to LUMO (δ+δ → δ*+δ*). The higher energy one, observed at ca. 390 nm and calculated at 452 nm, is a δ → π* transition (HOMO → LUMO+2), where the LUMO+2 is the in-phase combination of the two π* orbital from Mo_2 units. For **9** and **10**, similar transitions were calculated.

For the mixed-valence species **8-PF$_6$**, the band at 600 nm is assigned to a LMCT band from the ligand based orbital HOMO−4 → SOMO which is calculated at 628 nm while the band at 434 nm corresponds to the SOMO → LUMO+1 (δ−δ → δ*−δ*) transition. Similar transitions were calculated for **9-PF$_6$** and **10-PF$_6$**. Two absorptions are predicted in the NIR range, and these bands appear experimentally in the electronic spectra at ca. 5700 and 7200 cm^{-1} as shown in Figure 20. The more intense band centered at ca. 5700 cm^{-1} is the HOMO−1 → SOMO transition. The one centered at ca. 7200 cm^{-1} is tentatively assigned to HOMO−1 → LUMO (δ+δ → δ*+δ*) based upon the calculated orbital energies and their symmetry given in Table VIII. For these two transitions in $\{[Mo_2(cis\text{-}NHCHNH)_2]_2(\mu\text{-}X)_4\}^+$ cations, the calculations show that the energies (eV) decrease from 0.745 and 0.762 in **8**$^+$, to 0.717 and 0.753 in **9**$^+$, then to 0.651 and 0.748 eV in **10**$^+$, which follow the experimental trend.

CHAPTER V

FLUORIDE-BRIDGED CYCLIC DIMOLYBDENUM TRIADS*

Supramolecular chemistry based on extended ligand coordination to metal ions is an active research area.[64] The diverse binding modes of metal units and the vast array of organic and/or inorganic fragments that can be used as ligands has resulted in countless well-defined discrete molecules and infinite networks with various sizes, shapes, topologies and dimensions.[65] In addition to fundamental interest, studies in this field are expected to lead to the development, through molecular design, of new functional materials that may be used in applications such as chemical storage,[66] sensors[67] and catalysis.[68]

In our recent studies on dimetal-containing supramolecular compounds, much attention has been devoted to linkers capable of linking multiple, covalently-bonded dimetal units (e.g., Mo_2^{4+}, Rh_2^{4+} and Ru_2^{4+}).[69] By careful selection of the linker, compounds with a great variety of conformations and binding patterns have been obtained.[10] This diversity has allowed better understanding of the impact of the linker on the electronic interaction between dimetal units. For instance, a tetrahedral inorganic linker, e.g., $M(OCH_3)_4^{2-}$ (M = Zn or Co), brings together two [Mo_2] units perpendicular to each other, which severely limits electron delocalization over the two dimetal centers

*Reproduced in part with permission from *Inorg. Chem.* **2006**, *45*, 9480, Cotton, F. A.; Liu, C. Y.; Murillo, C. A.; Zhao, Q. "An Isomeric Pair of Fluoride-Bridged Cyclic Dimolybdenum Triads", Copyright 2007 American Chemical Society.

because of the lack of metal-ligand π orbital interaction.[15] When single atoms such as H^- serve as bridges, the distances between the two dimetal centers may be greatly reduced so that strong electronic interaction attributable to direct metal–metal orbital interactions is observed.[30]

Previous Chapter has shown that assemblies of dimolybdenum units, $[Mo_2(cis\text{-}DAniF)_2]^{2+}$, with the halogen atoms Cl^-, Br^- and I^-, produce quadruply-bridged tetranuclear compounds of the general formula $[Mo_2(cis\text{-}DAniF)_2]_2(\mu\text{-}X)_4$. However, in considering the possibility of using the first member of the halogen family, F^-, in the same way it must be kept in mind that it differs in many ways from other halogens because of its small size and high electronegativity.[70] In many organometallic fluorides, fluorine functions as the structure directing element capable of connecting from two to four non-metal or metal atoms.[71] In these compounds, the compositions and molecular structures are highly diversified ranging from discrete small molecules to supramolecular arrays. When a fluorine atom bridges two single metal atoms, linear or bent binding patterns may be expected. While the linear bridges support cyclic tetramers M_4F_4 (M = Mo, Ru, Yb, Al, Ti, etc.),[72] the bent bridging mode occurs in cyclic M_3F_3 trinuclear species (M = Al, Sc, Sm, etc.).[73] A valid generalization, however, is that the fluorine atom is far more inclined than the other halogen atoms to form linear or nearly linear bridges.

In the present work, fluoride anions, F^-, have been found to cause the assembly of dimolybdenum units $[Mo_2(cis\text{-}DAniF)_2]^{2+}$, represented for simplicity as $[Mo_2]$, to form cyclic triads. The compounds that have been synthesized and crystallographically

characterized include α-[Mo_2(*cis*-DAniF)$_2$]$_3$(μ-F)$_6$ (**11**), β-{[Mo_2(*cis*-DAniF)$_2$]$_3$(μ-F)$_6$}(BPh_4) (**12** or β^+), and β-[Mo_2(DAniF)$_2$]$_3$(μ-F)$_6$ (**13**). Compounds **11** and **13** are geometric isomers that do not interconvert even in boiling THF or toluene, nor photochemically. The idealized symmetries for the two isomers are C_{2v} and D_{3h} for the α and β species, respectively (Figure 30).

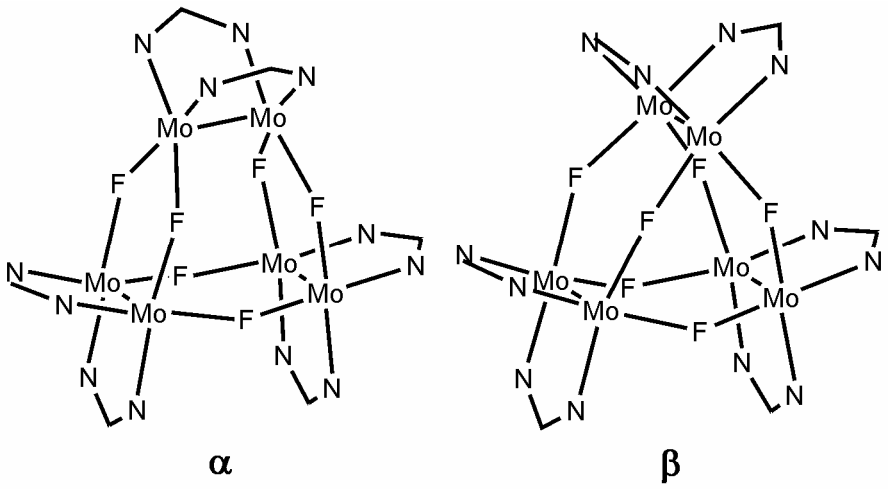

Figure 30. Core structure of the fluoride-bridged isomeric triads.

EXPERIMENTAL SECTION

Materials and Methods. Solvents were purified under argon using a Glass Contour solvent purification system or distilled over appropriate drying agents under nitrogen. All synthetic operations were conducted under N_2 using Schlenk line techniques. The starting material, $[Mo_2(cis\text{-}DAniF)_2(NCCH_3)_4](BF_4)_2$, was prepared according to a published method.[53] Commercially available chemicals were used as received except for potassium fluoride which was heated at 350 °C under vacuum overnight before use. Ferrocenium tetraphenylborate, $[FeCp_2]BPh_4$, was prepared by mixing a solution of ferrocenium chloride in ethanol and a solution with an excess of $NaBPh_4$ in the same solvent. A grayish blue precipitate formed immediately. After stirring for 0.5 h, the solid was filtrated and washed with a small amount of ethanol, and then dried under vacuum. Because this compound appeared to be light sensitive, it was prepared immediately prior to use and stored in a dark vial.

Characterization Measurements. Elemental analyses were performed by Robertson Microlit Laboratories, Madison, New Jersey. Electronic spectra were measured on a Shimadzu UV-2501PC spectrometer in CH_2Cl_2 solution. NMR spectra were recorded on a Mercury 300 spectrometer with chemical shifts (δ) referenced to the protonated residue in $CDCl_3$ for ^1H NMR and to CCl_3F in CD_2Cl_2 for ^{19}F NMR. Cyclic voltammograms and differential pulse voltammograms were recorded on a BAS 100 electrochemical analyzer with Pt working and auxiliary electrodes, Ag/AgCl reference electrode, scan rate of 100 mV/sec, and 0.1 M Bu_4NPF_6 as electrolyte. Under these

electrochemical conditions, the $E_{1/2}$ for the ferrocene/ferrocenium couple (Fc/Fc^{+}) was measured at 440 mV.

X-ray Structure Determinations. Single crystals suitable for X-ray analyses were obtained by diffusion of hexanes into CH_2Cl_2 solutions of the corresponding compound. Each crystal was mounted on the tip of a cryoloop attached to the goniometer head. Data for **11**·$2CH_2Cl_2$, **12**·$2CH_2Cl_2$, and **13**·$2CH_2Cl_2$·C_6H_{14} were collected at −60 ºC on a BRUKER SMART 1000 CCD area detector system. Cell parameters were determined using the program SMART.[24] Data reduction and integration were performed with the software package SAINT[25] and absorption corrections were applied by using SADABS.[26] Using the program package SHELXTL,[27] the structures were solved by direct methods and refined. Non-hydrogen atoms, except for those of disordered parts and solvent molecules, were refined with anisotropic displacement parameters. Hydrogen atoms were placed in calculated positions. Crystallographic data are presented in Table XII and selected bond distances and angles are listed in Table XIII.

Table XII. X-ray Crystallographic Data for **11**·$2CH_2Cl_2$, **12**·$2CH_2Cl_2$ and **13**·$2CH_2Cl_2$·C_6H_{14}

	11·$2CH_2Cl_2$	**12**·$2CH_2Cl_2$	**13**·$2CH_2Cl_2$·C_6H_{14}
empirical formula	$C_{92}H_9Cl_4F_6Mo_6N_{12}O_{12}$	$C_{116}H_{114}BCl_4F_6Mo_6N_{12}O_{12}$	$C_{98}H_{108}Cl_4F_6Mo_6N_{12}O_{12}$
fw	2391.23	2710.44	2477.40
space group	$P\bar{1}$	$P2_1/c$	$P2_1/c$
a, Å	14.146(2)	19.923(3)	24.15(1)
b, Å	14.286(2)	28.670(4)	16.360(6)
c, Å	26.043(4)	20.496(3)	26.45(1)
α, deg	76.605(3)	90	90
β, deg	76.147(3)	98.590(3)	90.387(7)
γ, deg	70.266(3)	90	90
V Å^3	4744(1)	11576(3)	10449(7)
Z	2	4	4
λ, Å	0.71073	0.71073	0.71073
d_{calcd}, g/cm^3	1.674	1.555	1.575
μ, mm^{-1}	0.960	0.797	0.874
R1[a] (wR2[b])	0.0525 (0.1018)	0.0761 (0.1057)	0.1194 (0.2074)

[a] $R1 = \Sigma||F_o|-|F_c||/\Sigma|F_o|$.

[b] $wR2 = [\Sigma[w(F_o^2-F_c^2)^2]/\Sigma[w(F_o^2)^2]]^{1/2}$

Table XIII. Selected Bond Lengths (Å) and Angles (deg) for **11**·$2CH_2Cl_2$, **12**·$2CH_2Cl_2$ and **13**·$2CH_2Cl_2$·C_6H_{14}

	11·$2CH_2Cl_2$	**12**·$2CH_2Cl_2$	**13**·$2CH_2Cl_2$·C_6H_{14}
Mo(1)−Mo(2)	2.1055(6)	2.1585(6)	2.118(2)
Mo(3)−Mo(4)	2.1082(6)	2.1355(6)	2.119(2)
Mo(5)−Mo(6)	2.1159(5)	2.1369(6)	2.119(2)
Mo(1)−F(1)	2.095(2)	2.032(3)	2.085(8)
Mo(1)−F(5)	2.108(2)	2.043(3)	2.099(7)
Mo(2)−F(2)	2.098(2)	2.086(3)	2.119(8)
Mo(2)−F(6)	2.104(2)	2.044(3)	2.116(7)
Mo(3)−F(1)	2.104(2)	2.049(3)	2.107(8)
Mo(3)−F(3)	2.107(2)	2.093(3)	2.127(7)
Mo(4)−F(2)	2.099(2)	2.102(3)	2.116(8)
Mo(4)−F(4)	2.112(2)	2.083(3)	2.101(7)
Mo(5)−F(3)	2.112(2)	2.089(3)	2.095(7)
Mo(5)−F(4)	2.117(2)		
Mo(5)−F(5)		2.064(3)	2.101(8)
Mo(6)−F(4)		2.083(3)	2.125(7)
Mo(6)−F(5)	2.119(2)		
Mo(6)−F(6)	2.119(2)	2.069(3)	2.109(7)
F(1)−Mo(1)−F(5)	82.59(9)	84.3(1)	82.8(3)
F(2)−Mo(2)−F(6)	83.42(9)	83.9(1)	83.3(3)
F(1)−Mo(3)−F(3)	82.28(9)	85.0(1)	82.4(3)
F(2)−Mo(4)−F(4)	83.09(9)	81.9(1)	81.4(3)
F(3)−Mo(5)−F(4)	83.10(9)		
F(3)−Mo(5)−F(5)		83.2(1)	82.4(3)

Table XIII (continued)

F(6)−Mo(6)−F(5)	82.72(9)		
F(6)−Mo(6)−F(4)		85.1(1)	83.1(3)
Mo(1)−F(1)−Mo(3)	148.3(1)	142.9(1)	141.4(4)
Mo(2)−F(2)−Mo(4)	146.0(1)	144.1(1)	141.5(4)
Mo(3)−F(3)−Mo(5)	128.6(1)	140.8(1)	141.5(4)
Mo(4)−F(4)−Mo(5)	128.0(1)		
Mo(4)−F(4)−Mo(6)		143.0(1)	141.5(4)
Mo(1)−F(5)−Mo(5)		143.7(1)	141.4(4)
Mo(1)−F(5)−Mo(6)	128.2(1)		
Mo(2)−F(6)−Mo(6)	128.8(1)	142.8(1)	140.2(4)

Preparation of α-[Mo_2(*cis*-DAniF)$_2$]$_3$(μ-F)$_6$, 11, method A. To a flask containing [Mo_2(*cis*-DAniF)$_2$($NCCH_3$)$_4$](BF_4)$_2$ (0.624 g, 0.600 mmol) and an excess amount of tris(dimethylamino)sulfur(trimethylsilyl)difluoride (0.600 g, 2.14 mmol), was added 20 mL of acetonitrile. The resultant solution was stirred at room temperature for 4 h, yielding a light yellow solid. The supernatant solution was decanted and the solid was washed with acetonitrile (2 × 10 mL) and then dried under vacuum. Yield: 0.300 g (74%). This material was used for the preparation of **12** without further purification. A yellow crystalline product was obtained by diffusion of hexanes into a dichloromethane solution of the product. ^{1}H NMR (δ, ppm in $CDCl_3$): 8.79 (s, 2H, ─NC*H*N─), 8.65 (s, 2H, ─NC*H*N─), 8.19 (s, 2H, ─NC*H*N─), 6.73 (m, 8H, aromatic), 6.52 (m, 8H, aromatic), 6.42-6.27 (m, 32H, aromatic), 3.68 (s, 12H, ─OCH_3), 3.64 (s, 12H, ─OCH_3), 3.63 (s, 12H, ─OCH_3). ^{19}F NMR (δ, ppm in CD_2Cl_2): −242.9(s, 4F), −244.9 (s, 2F). UV–Vis (λ_{max}, nm) (ε, $M^{-1}cm^{-1}$): 404 (5.6×10^3), 479 (2.8×10^3). Anal. Calcd for $C_{91}H_{92}Cl_2F_6Mo_6N_{12}O_{12}$ (**11**·CH_2Cl_2): C, 47.39; H, 4.02; N, 7.29. Found: C, 47.24; H, 4.02; N, 7.36.

Preparation of α-[Mo_2(*cis*-DAniF)$_2$]$_3$(μ-F)$_6$, 11, method B. [Mo_2(*cis*-DAniF)$_2$($NCCH_3$)$_4$](BF_4)$_2$ (0.416 g, 0.400 mmol) and KF (0.322 g, 4.00 mmol) were mixed in 20 mL of acetonitrile. The mixture was stirred at ca. 60 ~ 70 ° C for 5 h, producing a yellow precipitate. The supernatant solution was decanted. The solid was washed with acetonitrile (2 × 10 mL) and dried under vacuum. The crude product was dissolved in ca. 15 mL of dichloromethane. The solution was allowed to pass though a

Celite-packed frit. The filtrate was layered with 40 mL of hexanes. Yield of yellow crystals: 0.05 g (18%).

Preparation of {β-[Mo_2(*cis*-DAniF)$_2$]$_3$(μ-F)$_6$}(BPh_4), 12. A yellow solution of **11** (0.140 g, 0.063 mmol) in 10 mL of CH_2Cl_2 and a blue solution having 1 equiv of $[FeCp_2]BPh_4$ (0.032 g, 0.063 mmol) in 15 mL of CH_2Cl_2 were prepared separately and cooled to −78 °C. The two solutions were mixed by transferring the oxidizing reagent to the dimolybdenum complex at low temperature using a cannula, to produce a dark brown solution. After the resultant solution was stirred at −78 °C for 30 min, a copious amount of pre-cooled hexanes was added by a syringe to produce a dark brown precipitate. The supernatant solvent was then decanted and the solid residue was washed with 20 mL of hexanes. The solid was dissolved in dichloromethane and the solution was layered with hexanes to obtain a dark crystalline product. Yield: 0.104 g (63 % based on **12**·CH_2Cl_2). UV–Vis (λ_{max}, nm) (ε, $M^{-1}cm^{-1}$): 478 (3.1×10^3), 619 (1.1×10^3). Anal. Calcd for $C_{115}H_{112}BCl_2F_6Mo_6N_{12}O_{12}$ (**12**·CH_2Cl_2): C, 52.61; H, 4.30; N, 6.40. Found: C, 52.29; H, 3.92; N, 6.32.

Preparation of β-[Mo_2(*cis*-DAniF)$_2$]$_3$(μ-F)$_6$, 13. To a flask containing dark brown {β-[Mo_2(*cis*-DAniF)$_2$]$_3$(μ-F)$_6$}PF_6 [74] (0.237 g, 0.100 mmol) and a large excess of Al dust (1.50 g, 55.6 mmol) was added 20 mL of acetonitrile. The mixture was stirred at room temperature for about 5 h, yielding a yellow solid. After decanting the supernatant brown solution, the solid mixture was washed with a small amount of acetonitrile. The residue was extracted with 10 mL of CH_2Cl_2, followed by filtration via a Celite-packed column to remove the Al dust. After the volume of the filtrate was reduced under

vacuum to *ca.* 5 mL, a mixture of isomeric hexanes (40 mL) was added by syringe to produce a light yellow precipitate. This solid was collected by filtration and dried under vacuum. Yield: 0.152 g (68 %). Crystalline material for analysis was obtained by diffusion of hexanes into a dichloromethane solution. ^{1}H NMR (δ, ppm in $CDCl_3$): 8.78 (s, 6H, ─NC*H*N─), 6.59 (d, 24H, aromatic), 6.38 (d, 24H, aromatic), 3.63 (s, 36H, ─OC*H*$_3$). ^{19}F NMR (δ, ppm in CD_2Cl_2): −249.4(s, 6F). UV–Vis (λ_{max}, nm) (ε, $M^{-1}cm^{-1}$): 409 (5.4×10^3), 476 (1.8×10^3). Anal. Calcd for $C_{91}H_{92}Cl_2F_6Mo_6N_{12}O_{12}$ (**13**·CH_2Cl_2): C, 47.39; H, 4.02; N, 7.29. Found: C, 47.87; H, 4.08; N, 7.22.

Study of the α→α$^+$→β$^+$→β Conversion Process. A yellow solution of **11** (α) in 10 mL of CH_2Cl_2 and a blue solution having 1 equiv of $[FeCp_2]PF_6$ in 15 mL of CH_2Cl_2 were prepared separately and cooled to −78 °C. The two solutions were mixed by transferring via cannula that of the oxidizing agent into that having the dimolybdenum complex at low temperature. The brown solution of α$^+$ was stirred at −78 °C for 30 min to assure that the reaction had gone to completion. The solution was then transferred to a flask which contained 2 equiv of the reducing agent (Bu^n_4N)BH_4. The color of the solution changed immediately to yellowish brown. This solution was stirred at −78 °C for 0.5 h and the solvent was then removed under vacuum. Both ^{1}H and ^{19}F NMR spectra of the residue showed that the reduced product is the α species. A similar procedure was repeated using resting temperatures of −20 and 0 °C for 20 and 1.0 h, respectively (vide infra).

RESULTS AND DISCUSSION

Structural Considerations. Compound **11** crystallizes in the triclinic space group $P\bar{1}$ with the molecule residing on a general position ($Z = 2$). The molecule consists of three dimolybdenum units, $[Mo_2(cis\text{-}DAniF)_2]^{2+}$, bridged by six fluoride anions as shown by the core structure at the top of Figure 31. The molecular structure of **11** is a significant departure from precedent, in that the structures of other compounds containing $[Mo_2]$ units bridged by halide anions were all "dimer of dimers" structures with two parallel Mo_2^{4+} units, and had the general formula $[Mo_2(cis\text{-}DAniF)_2]_2(\mu\text{-}X)_4$ (X = Cl^-, Br^- and I^-) in Chapter IV. There is also a report of two triply bonded Mo_2^{6+} units coupled by four F^- anions in $[Mo_2(OBu^t)_4]_2(\mu\text{-}F)_4$ in which the dimetal units are orthogonal to each other.[75] In **11**, the three dimetal units are oriented in two orthogonal directions. Two of them are structurally equivalent and parallel to each other, but mutually perpendicular to the third one. The six fluorine atoms bridging six molybdenum atoms give rise to five-membered rings, Mo—F—Mo—Mo—F, on two sides of the molecule and a six-membered ring, Mo—Mo—F—Mo—Mo—F, on the other. There is an idealized two-fold axis that passes through the center of the six-membered ring and the midpoint of the Mo(5)–Mo(6) bond. In addition, there are two idealized mirror planes perpendicular to each other that intersect at the C_2 axis, and the overall structure has idealized C_{2v} symmetry. This structural motif is designated the α form.

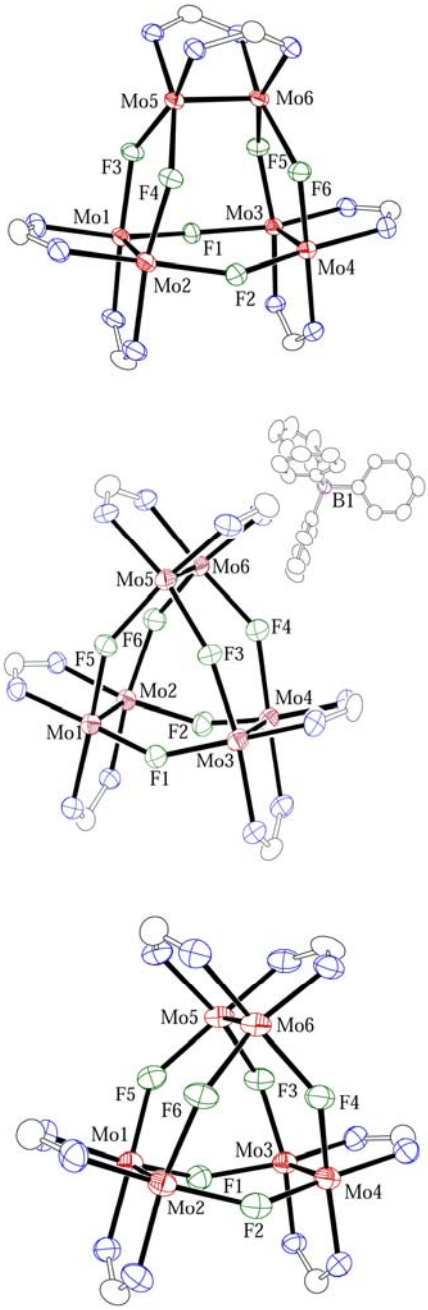

Figure 31. Core structures of **11**·$2CH_2Cl_2$ (top), **12**·$2CH_2Cl_2$ (center) and **13**·$2CH_2Cl_2$·C_6H_{14} (bottom) drawn with ellipsoids at the 40% probability level. All *p*-anisyl groups and hydrogen atoms have been omitted for clarity.

In the α form the bond distances for the two parallel dimetal units are essentially the same (2.1055(6), 2.1082(6) Å), while the third one, 2.1159(5) Å, is but slightly (0.009 Å) longer. The separations between midpoints of the [Mo_2] units are all ca. 4.0 Å despite the difference in binding modes. As expected, there are two sets of Mo–F–Mo angles. Such angles between the two parallel [Mo_2] units, about 147°, are significantly larger than those that connect to the perpendicular Mo_2^{4+} unit, which are about 128°. In $[Mo_2(OBu^t)_4]_2(\mu\text{-}F)_4$, in which fluoride anions bridge two perpendicular Mo_2^{6+} units, the Mo–F–Mo angles are 123 ~ 125°.[75] It should be noted that in the fluorine-bridged clusters, the Mo–F–Mo angles are considerably larger than the Mo–X–Mo angles found in the halide-bridged dimolybdenum dimers in Chapter IV, which range from 87 to 91°. This is in agreement with the well known fact that when the small fluorine atoms serve as bridges, they tend toward a more linear binding mode which increases the distance and reduces the repulsion between metal atoms.

The molecular structure of **11** evidently persists in solution as shown by the ^1H NMR spectrum. The six methine protons, one from each of the DAniF ligands, are present as three singlets (8.19 ~ 8.79 ppm) in a ratio of 1:1:1, in agreement with the idealized C_{2v} symmetry of the molecule. There are also three singlets at 3.68, 3.64 and 3.63 ppm, respectively, in a ratio of 1:1:1, which account for the 24 protons of the methoxy groups on the ligands of the two parallel [Mo_2] units in two orientations and the 12 hydrogen atoms from the third unit. Although the two DAniF ligands that support each of the two parallel Mo_2^{4+} units are not in the same chemical environment, these signals are not resolved under our experimental conditions. The ^{19}F NMR spectrum

presents two resonances in the ratio of 2:1, at –243 and –245 ppm as expected for a solution structure that is the same as that in the solid state.

Compound **12** was prepared by oxidation of **11** using 1 equiv of the oxidizing reagent $[FeCp_2]BPh_4$ which gives high quality single crystals.[76] The molecule of **12** resides on a general position of the monoclinic $P2_1/c$ space group. As shown at the center of Figure 31, the structure of the cation in **12** differs from that of the precursor **11** in that it is a triangle with three geometrically identical $[Mo_2(cis\text{-}DAniF)_2]^{2+}$ units as the vertices. All three dimolybdenum units are parallel to each other, and to an idealized C_3 axis that passes through the center of the triangle. Addition of a plane and three C_2 axes perpendicular to the C_3 axis gives an idealized D_{3h} symmetry for the molecule. This structural motif of the molecule will henceforth be designated the β form. Clearly a structural rearrangement of the cyclic triad from the α (C_{2v}) to the β (D_{3h}) form occurs during or quickly following the removal of one electron from **11**.

The neutral compound **13**, an isomer of **11**, was obtained by reduction of **12**. As shown at the bottom of Figure 31, it has a β structural motif, like its precursor **12**. Thus, **13** is a geometric isomer of **11** that possesses idealized D_{3h} symmetry instead of C_{2v} symmetry. In **13**, the three Mo─Mo bond distances, ca. 2.12 Å, fall in the range of Mo–Mo quadruply bonded units having two bridging ligands.[43] The six Mo─F─Mo angles are all about 141°, similar to those found in **12**. The center to center separation between two $[Mo_2]$ units is about 4.0 Å.

The D_{3h} symmetry of **13** is retained in solution as confirmed by the ^1H and ^{19}F NMR spectra. In the ^1H NMR spectrum, there is only one resonance for the methine

protons, a singlet at 8.78 ppm, and a singlet at 3.63 for the methoxy groups. For the six equivalent bridging fluorine atoms, the ^{19}F resonance occurs as a singlet at −249 ppm.

Syntheses. With the use of the designed building block $[Mo_2(cis\text{-}DAniF)_2(NCCH_3)_4]^{2+}$, which has been used frequently in this laboratory as a corner piece for the construction of various cyclic $[Mo_2]$-containing supramolecules,[69] the preparation of **11**, $\alpha\text{-}[Mo_2(cis\text{-}DAniF)_2]_3(\mu\text{–}F)_6$, proceeds in a straightforward and convenient manner. Acetonitrile serves well as the solvent because the low solubility of the neutral product in this polar solvent provides an additional driving force to the reaction. Alcohol solvents such as methanol or ethanol should be avoided because the alkoxide anions are capable of bridging $[Mo_2]$ units, forming compounds such as $[Mo_2(cis\text{-}DAniF)_2]_2(\mu\text{-}OR)_4$.[18] As fluoride sources, either organic compounds such as tris(dimethylamino)sulfur(trimethylsilyl)difluoride or inorganic salts such as KF can be used. However, the former provided substantially higher yields than those obtained from reactions using KF. To achieve high yield and purity, it is essential that all the solvents and reagents be rigorously dry. If trace amounts of H_2O are present, the hydroxide anion may partially replace some bridging fluorine atoms. Water is also known to promote a side reaction that leads to the formation of the paddlewheel compound $Mo_2(DAniF)_4$. Unlike reactions with the other halides, Cl^-, Br^- and I^-, that give $[Mo_2(cis\text{-}DAniF)_2]_2(\mu\text{–}X)_4$ compounds, direct assembly of dimolybdenum units with fluoride sources yields exclusively the cyclic triad **11**. The reason for this difference in behavior is that the fluorine atoms are far more inclined than the other halogen atoms to form linear or nearly linear bridges.[70b]

The isolation of products from chemical oxidation of compounds having two or more linked dimolybdenum units has not frequently been accomplished, even for compounds that show reversible electrochemical redox processes. For example, dicarboxylate-linked Mo_2 compounds have not yet given isolable products upon addition of oxidizing reagents. In some cases the compound $Mo_2(DAniF)_4$ has been isolated, although how it forms is not known. In other cases, however, we have successfully oxidized at low temperature a series of dimolybdenum pairs by using a mild oxidizing reagent, such as ferrocenium hexafluorophosphate.[18] By employing similar reaction conditions, oxidation of the neutral compound **11** afforded **12** in good yield. Compound **12** is the first mixed-valent supramolecular complex with three $[Mo_2]$ units. Electrochemical measurements of **11**, shown in Figure 32, suggested that the ferrocenium cation, $FeCp_2^+$, with a potential of 0.45 V (vs Ag/AgCl in CH_2Cl_2) would be capable of oxidizing two dimolybdenum centers. Thus, to obtain a pure singly oxidized compound, it was critical to precisely control the stoichiometry of the reactants. As mentioned earlier, compound **12** differs from **11** not only in oxidation state but also in molecular geometry, and under the preparative conditions, oxidation of **11** with an α structure does not allow the isolation of an α^+ product.

Reduction of **12** with aluminum metal in acetonitrile produced a yellow precipitate which was identified as another neutral compound, **13**, which was shown to be an isomer of **11** with a β structure. It should be noted that the method applicable for the preparation of a given isomer produces none of the other. Direct assembly generates only **11** and no **13**, while reduction of **12** gives only **13** but no **11**.

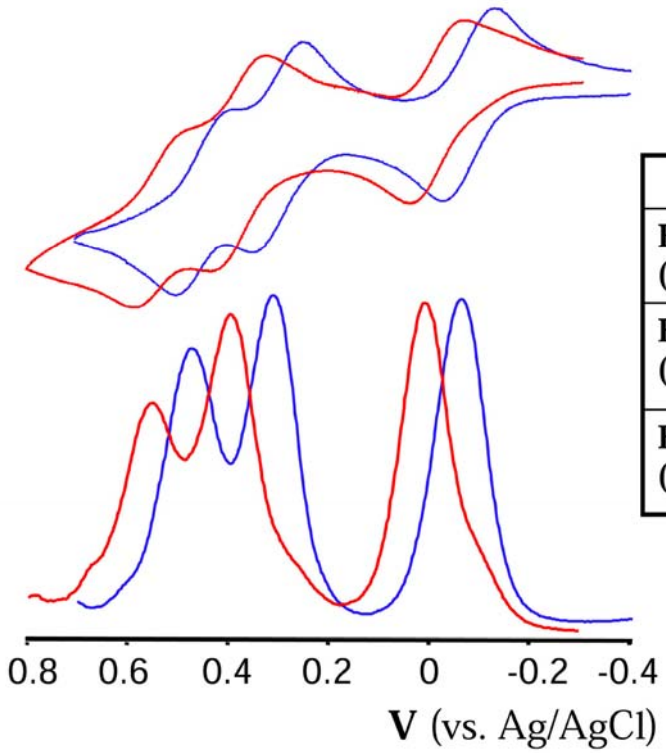

	11(α)	13(β)
$E_{1/2}^{+1/0}$ (mV)	−11	−116
$E_{1/2}^{+2/+1}$ (mV)	378	290
$E_{1/2}^{+3/+2}$ (mV)	540	430

Figure 32. Cyclic voltammograms (CVs) and differential pulse voltammograms (DPVs) of **11** and **13** in CH_2Cl_2. Experimental values (vs Ag/AgCl) are shown in the inset.

α – β Geometry Transformation. As mentioned earlier, the two neutral isomeric compounds, **11** and **13** in α and β forms, respectively, must be synthesized in different ways. Direct assembly from the molybdenum building block and a source of F^- anions gives exclusively the α isomer while the β isomer, **13**, was isolated by reduction of the monocation in **12**, which has the same geometric form, and may be denoted β^+. Formation of molecule **11** is kinetically favored over **13** in the initial preparative reaction, while neither **11** nor **13** is structurally labile. The molecular identity for each of them is retained both in the solid state and in solution. No interconversion was observed under refluxing THF, CH_2Cl_2 or toluene for about six hours. Addition of $Bu^n_4NPF_6$ to the refluxing solutions had no effect. No interconversion was observed either after 3 h upon irradiation of a toluene solution with a UV lamp having a wavelength of 350 nm.

In view of these facts, the key question to be answered is: Does the β^+ ion arise in a way that is concerted with the oxidation of the neutral α molecule, or is there an α^+ ion that is first formed as a discrete though short-lived intermediate? An answer to this question has been obtained by a series of experiments designed to provide semiquantitative estimates of the lifetime of an α^+ intermediate, if one existed. The first such experiment was carried out at −78 ºC which is the temperature used in the synthesis of **12**. After a solution of **11** was treated at that temperature with one equivalent of $[FeCp_2]PF_6$, the oxidized solution was allowed to stand at −78 ºC for 5 h and then reduced with an excess of $(Bu^n_4N)BH_4$. Both ^1H and ^{19}F NMR spectra showed that **11**, with its α form structure was regenerated without a trace of the β isomer, **13**. In a second experiment, after oxidation of **11** at −78 ºC the solution was allowed to warm to −20 ºC

and remain at that temperature for 20 h before the reduction was carried out, about 20% α^+ had converted to β^+ as shown by the ratio of the signals in the NMR spectra of α and β forms. At 0 °C, all of the α^+ rearranged to β^+ after 1 h. These reactions show that the $\alpha \rightarrow \alpha^+$ and $\beta^+ \rightarrow \beta$ processes take place readily and fast even at −78 °C, while $\alpha^+ \rightarrow \beta^+$ is temperature and time dependent, as shown in Figure 33.

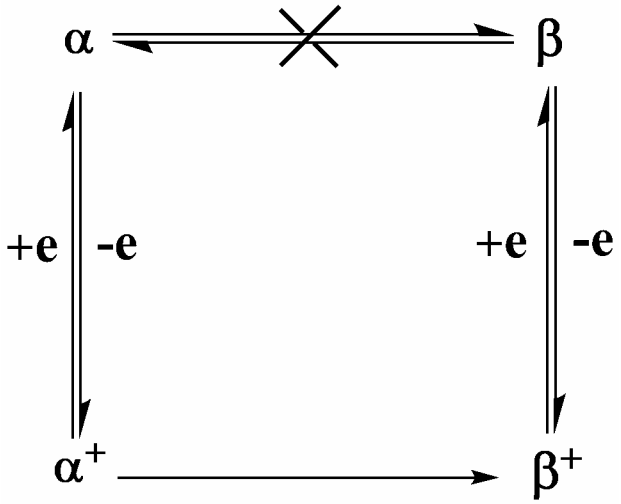

Figure 33. Cycle of the transformation between the isomer pair.

CHAPTER VI

A METAL HYDRIDE WITH QUADRUPLY BONDED DIMOLYBDENUM UNITS

The chemistry of transition metal hydrides can be traced back to 1931 with the discovery of $H_2Fe(CO)_4$ by Hieber and coworkers.[77] Many related metal carbonyl hydrides have since been synthesized including $HCo(CO)_4$.[78] These two complexes have been of great importance in catalytic processes, such as the industrial hydroformylation, hydrogenation and hydrodesulfurization processes.[79] Nowadays, interest in transition metal hydrides has been focused in the study of catalytic processes in organometallic chemistry and by the chemical industry because many are highly selective and efficient catalysts[80] and as materials for energy storage[81] and have promising uses in the so-called hydrogen economy.[82] Additionally, they have important uses in organic chemistry as powerful reducing agents.[83] Hydrides have also been invoked in metalloenzymes, especially hydrogenases, and this represents a very active area of research.[84]

Hydrogen, the simplest element in the periodic table, binds transition metals in a geat variety of modes (Figure 34)[70] which include terminal,[85] doubly bridging,[85] triply bridging (capping),[86] as a η^2-H_2 ligand to form sideways-bound dihydrogen complexes (nonclassical arrangement),[87] and agnostic M···H—C interactions to form a 3c-2e bond,[70] etc. A recent study in this laboratory reported that reductive substitution reactions of $Mo_2(DArF)_3Cl_2$, DArF = *N*,*N*′-diarylformamidinate (Ar = *p*-tolyl and *p*-anisyl), with $NaHBEt_3$ produces very stable tetranuclear complexes, $[Mo_2(DArF)_3]_2(\mu$-

$H)_2$, in which two quadruply bonded $Mo_2(DArF)_3$ units are linked by two hydride units forming a $\overset{\lceil}{\text{Mo}}\text{—Mo—H—Mo—Mo—}\overset{\rceil}{\text{H}}$ ring.[16] Here we describe the assembly of a molecule in which two $[Mo_2(cis\text{-}DAniF)_2]^{2+}$ units are linked by four hydride anions having a distorted tetrahedral Mo_4 skeleton consisting of four $\overset{\lceil}{\text{Mo}}\text{—H—Mo—Mo—}\overset{\rceil}{\text{H}}$ five-member rings. The two quadruply bonded dimolybdenum units are essentially orthogonal. The separation between the midpoints of the metal−metal bonds of only 2.718 Å represents the shortest Mo_2•••Mo_2 distance known for complexes with multiple dimolybdenum units.

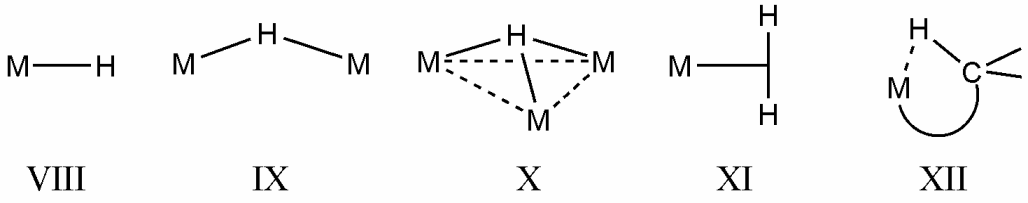

VIII IX X XI XII

Figure 34. Variety of binding modes of transition metal hydrides.

EXPERIMENTAL SECTION

Materials and Methods. Solvents were dried and then distilled under N_2 following conventional methods or purified under argon using a Glass Contour solvent purification system. The synthesis was conducted under N_2 using Schlenk line techniques. $[Mo_2(cis\text{-}DAniF)_2(NCCH_3)_4](BF_4)_2$[53] and HDAniF[23] were prepared following published methods.

Physical Measurements. Elemental analyses were performed by Robertson Microlit Laboratories, Madison, New Jersey. ^{1}H NMR spectra were recorded at 25 °C on a Mercury-300 NMR spectrometer with chemical shifts (δ ppm) referenced to solvent residence. Electronic spectra in the UV−vis range were measured in the range of 200 to 800 nm on a Shimadzu UV−2501PC spectrophotometer. Cyclic voltammograms were recorded on a CH Instruments Model-CH1620A electrochemical analyzer with Pt working and auxiliary electrodes, Ag/AgCl reference electrode, scan rate of 100 mV/sec, and 0.1 M Bu_4NPF_6 as electrolyte.

Preparation of $[Mo_2(DAniF)_2]_2(\mu\text{-}H)_4$, 14. To a suspension of $[Mo_2(cis\text{-}DAniF)_2(NCCH_3)_4](BF_4)_2$ (0.14 g, 0.13 mmol) and $Bu^n{}_4NBH_4$ (0.08 g, 0.31 mmol), 20 mL ether was added. The red dimolybdenum compound remained at the bottom of the flask because its solubility in ether is very small. After the mixture was stirred for about 16 h, the solid turned yellowish brown. After the solvent was decanted, the yellow-brown product was washed by 2 × 15 mL ether and dried under vacuum. Crystallization from a 1:3 mixture of toluene:hexane produced small dark-red, block-shaped and star-shaped crystals, both of which had the same unit cell parameters and ^{1}H NMR spectra.

Yield of crystals: 62 mg (34%). ^{1}H NMR (in benzene, ppm): 8.90 (s, 4H,-NC*H*N-), 6.85 (d, 16H, aromatic), 6.54 (d, 16H, aromatic), 6.23 (s, 4H, Mo*H*Mo), 3.14 (s, 24H, -OCH_3). ^{1}H NMR (in acetone, ppm): 8.81 (s, 4H,-NC*H*N-), 6.80 (d, 16H, aromatic), 6.72 (d, 16H, aromatic), 5.38 (s, 4H, Mo*H*Mo), 3.78 (s, 24H, -OCH_3). ^{1}H NMR (in a 1:1 mixture of acetone:benzene , ppm): 8.69 (s, 4H,-NC*H*N-), 6.62 (d, 16H, aromatic), 6.46 (d, 16H, aromatic), 5.67 (s, 4H, Mo*H*Mo), 3.35 (s, 24H, -OCH_3). Uv-vis in benzene, λ_{max} (nm) (ε, $M^{-1}cm^{-1}$): 525 (5.4×10^3). Anal. calcd. for $C_{60}H_{64}Mo_4N_8O_8$ (**14**): C, 51.15; H, 4.58; N, 7.95. Found: C, 51.41; H, 4.72; N, 7.67.

X−ray Structure Determinations. A single crystal suitable for X-ray analysis was mounted and centered on the tip of a cryoloop. The crystal was then attached to a goniometer head. Data for **14** were collected at −60 °C on a BRUKER SMART 1000 CCD area detector system. Cell parameters were determined using the program SMART.[24] Data reduction and integration were performed with the software package SAINT,[25] while absorption corrections were applied using the program SADABS.[26] The positions of the heavy atoms were found via direct methods using the program SHELXTL.[27] Subsequent cycles of least-squares refinement followed by difference Fourier syntheses revealed the positions of the remaining non-hydrogen atoms. The bridging hydride species were clearly defined in the electron density maps, and the positions were refined without constraints. All other Hydrogen atoms were added in idealized positions. Non-hydrogen atoms were refined with anisotropic displacement parameters. Crystallographic data for **14** are given in Table XIV and selected bond distances and angles in Table XV.

Table XIV. X−ray Crystallographic Data of **14**

compound	**14**
empirical formula	$C_{60}H_{64}Mo_4N_8O_8$
fw	1408.95
space group	*C*2/c (No.15)
a (Å)	27.206(5)
b (Å)	16.046(3)
c (Å)	17.643(3)
α (deg)	90
β (deg)	129.913(2)
γ (deg)	90
V (Å^3)	5907.6(18)
Z	4
T (K)	213
d_{calcd} (g/cm^3)	1.584
μ (mm^{-1})	0.890
R1[a] (wR2[b])	0.029 (0.069)

[a] $R1 = \Sigma||F_o|-|F_c||/\Sigma|F_o|$.

[b] $wR2 = [\Sigma[w(F_o^2-F_c^2)^2]/\Sigma[w(F_o^2)^2]]^{1/2}$

Table XV. Selected Bond Lengths (Å) and Angles (deg) of **14** from X-ray Crystallography and Simplified Mode of **14** from DFT Calculations

compound	**14**	**14** (calcd)
Mo1–Mo1A	2.0864(6)	2.128
Mo2–Mo2A	2.0859(6)	2.129
Mo_2•••Mo_2[a]	2.718	2.778
Mo1•••Mo2	3.0781(6)	3.160
Mo1•••Mo2A	3.1063(6)	3.159
Mo1–H1	2.03(4)	1.934
Mo1A–H2	2.14(3)	1.943
Mo2–H1	1.90(4)	1.951
Mo2A–H2A	2.15(3)	1.934
Mo1–H1– Mo2	102.9(4)	109.16
Mo1A–H2–Mo2	92.7(4)	108.83
Mo1–Mo1A–Mo2A–Mo2	80.62(2)	82.66

[a] distance between the midpoint of the two [Mo_2] units.

Computational Details. Density functional theory (DFT)[54] calculations were performed with the hybrid Becke's[55] three-parameter exchange functional and the Lee-Yang-Parr[56] nonlocal correlation functional (B3LYP) in the Gaussian 03 program.[57] Double-ζ quality basis sets (D95)[58] were used on C, N and H atoms as implemented in Gaussian. A small effective core potential (ECP) representing the 1s2s2p3s3p3d core was used for the molybdenum atoms along with its corresponding double-ζ basis set (LANL2DZ).[60] Time-dependent density functional (TD-DFT) calculations[61] were performed to aid in the assignment of the electronic spectrum. All calculations were performed on Origin 3800 64-processor SGI supercomputers located at the Texas A&M supercomputing facility.

RESULTS AND DISCUSSION

Syntheses. The first approach to the synthesis of **14** was to use a procedure similar to that used for cuboidal clusters of the type $[Mo_2(cis\text{-}DAniF)_2]_2(\mu\text{-}X)_4$, $X = Cl^-$, Br^- and I^-, discussed in Chapter IV, which are made in acetonitrile or ethanol according to the Eq. 6:

$$2[Mo_2(cis\text{-}DAniF)_2(NCCH_3)_4](BF_4)_2 + 4Bu^t{}_4NX \rightarrow [Mo_2(cis\text{-}DAniF)_2]_2(\mu\text{-}X)_4 + 4Bu^t{}_4NBF_4 \qquad \text{(eq. 6)}$$

However, unlike reactions with the halides that produces the product in the polar solvents, reaction of the building block $[Mo_2(cis\text{-}DAniF)_2(NCCH_3)_4]^{2+}$ with a variety of hydride sources, such as KH, LiH, $NaBH_4$ and $NaAlEt_3H$, does not give the hydride analogue. The only the combination of hydride source and solvent that was found to

produce the target compound was that of $Bu^n_4NBH_4$ and ether. The low solubility of the neutral product in ether appears to provide an additional driving force to the reaction. As the pink building block slowly dissolved in ether, a brown precipitate was produced simultaneously. A long stirring period is essential for the reaction to go to completion. The use of alcohols such as methanol or ethanol as solvent should be avoided because the alkoxide anions are capable of bridging $[Mo_2]$ units, forming alkoxide bridged compounds.[18] To obtain analytically pure samples in satisfactory yield, it is essential to rigorously dry all solvents and reagents. If trace amounts of H_2O are present, the hydroxide groups partially replace the bridging hydride atoms. Water is also known to promote a side reaction that leads to the formation of the paddlewheel compound $Mo_2(DAniF)_4$ as discussed in Chapter V.

Unlike the stable complexes $[Mo_2(DArF)_3]_2(\mu\text{-}H)_2$, in which two hydride groups link two dimolybdenum units, compound **14** is extremely air and moisture sensitive. This compound also reacts with chlorinated solvents such as CH_2Cl_2 giving $[Mo_2(DAniF)_2]_2(\mu\text{-}Cl)_4$, as shown by the isolation of red block-shaped crystals from solutions of **14** in mixtures of CH_2Cl_2/hexane that were analyzed by X-ray crystallography.

Structural Results. Compound **14** crystallizes in the monoclinic space group *C*2/c with the molecule residing on a special position ($Z = 4$). The molecule consists of two dimolybdenum units, $[Mo_2(cis\text{-}DAniF)_2]^{2+}$, bridged only by four hydride groups as shown by the structure of the core in Figure 35. Unlike the structures of the cuboidal $[Mo_2(cis\text{-}DAniF)_2]_2(\mu\text{-}X)_4$ compounds which have essentially parallel Mo_2 units, as

discussed in Chapter IV, the two dimetal units in **14** are essentially perpendicular to each other with a torsion angle of 80.62(2)˚. The four hydride anions linking the molybdenum atoms give rise to two five-membered rings, Mo—H—Mo—Mo—H. If the supporting DAniF ligands are ignored, the Mo_4H_4 core can be described by an elongated tetrahedron (shown in red in Figure 36) in which the H atoms are at the midpoint of four long edges and the Mo_2 units are in the two short edges. The hydride groups are unprotected by the DAniF groups in contrast to those in the $[Mo_2(DArF)_3]_2(\mu\text{-}H)_2$ compounds where the two hydrides are wrapped by six formamidinate ligands. Because of this the likelihood of the hydrides being attacked by other molecules is greatly enhanced in **14** its reactivity is much greater than that of $[Mo_2(DArF)_3]_2(\mu\text{-}H)_2$.

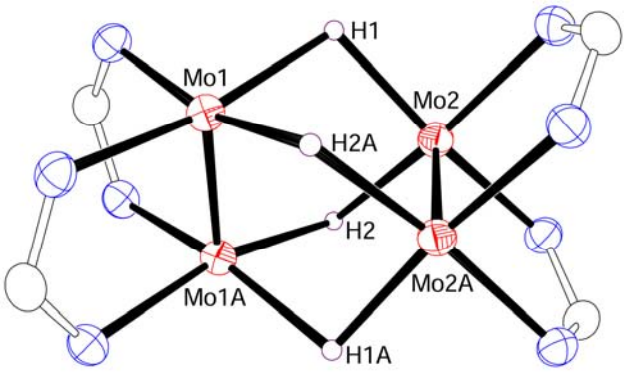

Figure 35. Core structure of **14** with ellipsoids drawn at the 40% probability level. All *p*-anisyl groups and hydrogen atoms in the methine groups have been omitted for clarity.

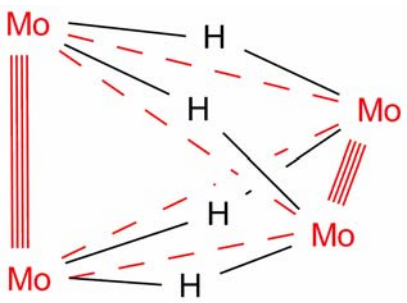

Figure 36. Drawing of the elongated tetrahedron core of **14**.

The metal–metal bond distances for the two crystallographically independent dimolybdenum units are essentially the same (2.0864(6), 2.0859(6) Å in Table XV), falling in the range of Mo–Mo quadruply bonded compounds having two bridging ligands.[43] The $\delta \rightarrow \delta^*$ transition is observed at 525 nm in the UV-vis spectrum. The separation between the midpoints of the [Mo_2] units is only 2.718 Å, which gives the shortest $Mo_2 \cdots Mo_2$ distance known for complexes with multiple dimolybdenum units. The Mo─H distances[88] of around 1.90 ~ 2.15 Å are slightly longer than those distances (ca. 1.85 Å) in the terminal Mo─H[89] and other hydride bridged complexes.[16,90] The bent Mo─H─Mo angles are in the range of 93 ~ 103°, smaller than those found in hydride bridged complexes.[16,90]

The molecular structure of **14** is a significant departure from those of the halide bridged "dimer of dimers" structures with two parallel quadruply bonded Mo_2^{4+} units in

Chapter IV, but resembles the structure of $[Mo_2(OBu^t)_4]_2(\mu\text{-}F)_4$, that has two triply bonded Mo_2^{6+} units are coupled by four F^- anions, in that the dimetal units are orthogonal to each other.[75] In **14**, there is a two-fold axis that passes through the two midpoints of the Mo–Mo bonds (Mo1–Mo1A and Mo2–Mo2A) and two idealized mirror planes perpendicular to each other that intersect at the C_2 axis. In addition, there are two idealized two-fold axis that pass through the midpoints of each two separated long edges of the distorted tetrahedral core, namely Mo1–Mo2 and Mo1A–Mo2A, Mo1A–Mo2 and Mo1–Mo2A, respectively, and the overall structure has idealized D_{2d} symmetry. In the idealized structure the sets of DAniF ligands and hydride anions are each equivalent.

The ^{1}H NMR spectrum of **14** in C_6D_6 shows the presence of a highly symmetrical species in solution and is consistent with the solid state structure. The signal for the four methine protons, one from each of the DAniF ligands, appears as a singlet (8.90 ppm in C_6D_6). In this solvent there is also only one singlet at 3.14 ppm in benzene, which accounts for the 24 protons of the methoxy groups. The signals for the aromatic groups also support this assignment. Finally, the solvent dependent singlets at 6.23 ppm (benzene), 5.38 ppm (acetone) and 5.67 (1:1 acetone:benzene), all integrate as four hydrogen atoms and have been assigned to the hydride linkers.

Electrochemistry and DFT Calculations. The cyclic voltammogram (CV) of **14** measured in THF exhibits only one redox couple at a potential of 0.20 V vs. Ag/AgCl. Although the shape of the wave resembles those for reversible processes, the intensity rapidly decreases indicating that this corresponds to an irreversible process

which is likely due to oxidation of the hydride groups. Oxidation of **14** using Ferrocenium BF_4 salt in acetone produced gas bulbs, which should be the H_2 evolution as the hydride groups of compound **14** were oxidized.

A series of DFT calculations were carried out to better understand the electronic interaction between the [Mo_2] units. Geometry optimization on **14** was done using the parameters from the crystal structure as starting point. The model, with all anisyl groups replaced by hydrogen atoms, was simplified to $[Mo_2(cis\text{-}NHCHNH)_2]_2(\mu\text{-}H)_4$ (**XIII** in Figure 37) without imposing symmetry constraints. The general agreement between the calculated and the experimental geometric data shown in Table XV suggests that such a simplification is reasonable. The overestimation of the Mo–Mo distances (ca. 0.04 Å) is reasonable and consistent with previous studies because of the use of hydrogen atoms instead of the basic *p*-anisyl groups for the calculations.[12c]

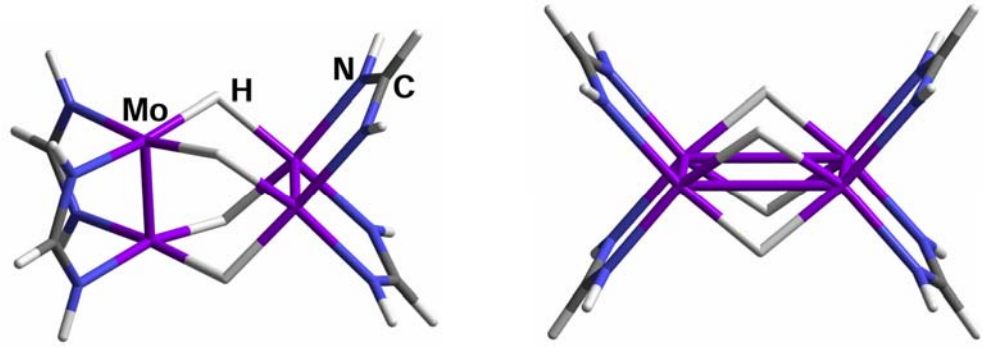

XIII XIV

Figure 37. Simplified modes of **14** and its proposed cuboidal isomer for DFT calculations.

Geometry optimization was also performed on the possible isomer **XIV** (Figure 37) having two parallel [Mo_2] units to resemble the halide-containing [Mo_2(*cis*-DAniF)$_2$]$_2$(μ-X)$_4$ species in Chapter IV. This isomer, which was not observed experimentally, does have an energy that is higher by 3.8 Kcal/mol than that of the model of **14**. Even though the calculated energy difference is relatively small, the results are consistent with the experiment results. It should be noted, however, that the existence of the second isomer can not be ruled out under different experimental conditions. It is possible that **14** is the kinetic product favored by its insolubility in the reaction media.

An analysis of the frontier orbitals from the calculations (Figure 38) indicates that there is only very small interaction between the δ orbitals in the dimetal units, which is due to the electrostatic repulsion. The two molecular orbitals, one bonding (a_g, δ+δ) and one antibonding (b_{3u}, δ−δ) over the four molybdenum atoms, are slightly different in energy. The two δ* orbitals as the LUMO and LUMO+1 are degenerated, which again indicates that the electronic interaction between the two dimetal units are considerably small. The electronic communication is limited here because of the short of both the conjugation through the linker and the symmetry allowed orbital overlap through space.

Time-dependent (TD–DFT) calculations were also carried out on the hydride bridged complex using the optimized geometry of the model [Mo_2(*cis*-NHCHNH)$_2$]$_2$(μ-H)$_4$. Such calculations have been useful in understanding the electronic spectra of compounds having two [Mo_2] units linked by dicarboxylate groups.[12c] The neutral species **1** show one weak absorption band in the UV–Vis range. The band, observed at 525 nm, is calculated at 561 nm for the symmetry allowed δ → δ* type transition.

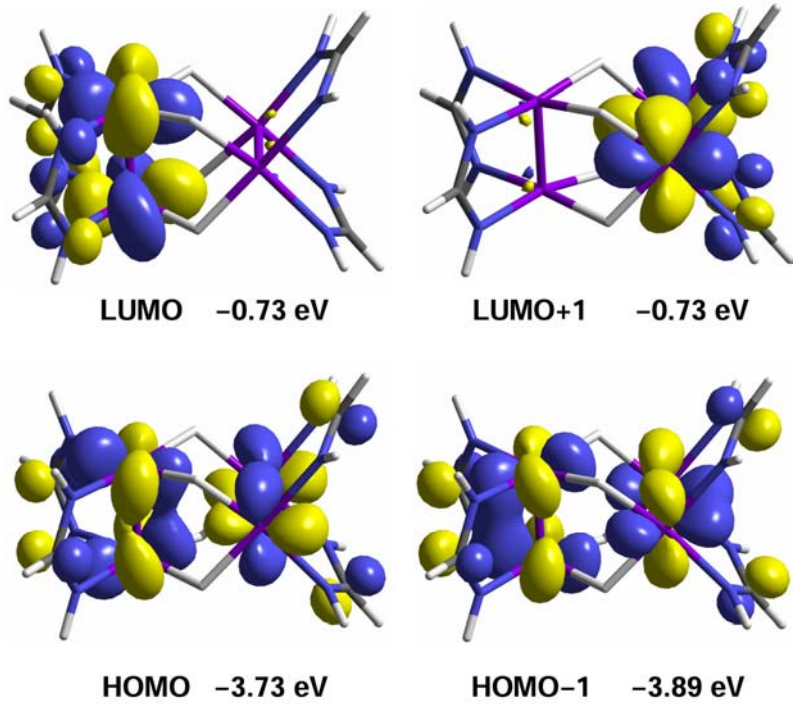

Figure 38. The 0.04 surface contour diagrams for the frontier orbitals for model of **14** calculated using DFT.

CHAPTER VII

CONCLUSIONS

Earlier work in this laboratory had shown that two linkage isomers containing dimolybdenum units with bridged oxamidate dianions have large differences in electronic communication with K_c's values being about 10^6 times larger for the β form which has two six-membered rings formed by the 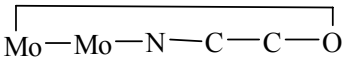 groups than for the α form.[13a] Unfortunately the neutral compounds (especially that in the β form) had been obtained in low yields and isolation of the pure products was difficult. This hampered further study of this interesting system. Chapter II shows the syntheses that give higher yields of the α and β products with good purity, as well as the structures, NIR and EPR spectra of the α^+, α^{2+}, β^+ and β^{2+} species. The results unambiguously show that the α^+ species is electronically localized while the β^+ species is delocalized. We also confirm that while the α^{2+} species is a diradical, the β^{2+} species is essentially diamagnetic. Using these isomers, we demonstrate how important the conformation of the linker is in mediating electronic communication between metal containing units.

In Chapter III, a dimolybdenum molecular pair, $Mo_2(DAniF)_3(\mu{-}OH)_2Mo_2(DAniF)_3$ (**5**), was synthesized and studied by X-ray crystallography. The oxidative conversion of single crystals of **5** to $Mo_2(DAniF)_3(\mu{-}O)_2Mo_2(DAniF)_3$, **6**, has been observed, and studied crystallographically in detail. These observations provide an interesting case of SCSC

transformations and give a rare insight into the deprotonation process effected by dioxygen.

The overall reaction sequence, in schematic form (Eq. 7) is:

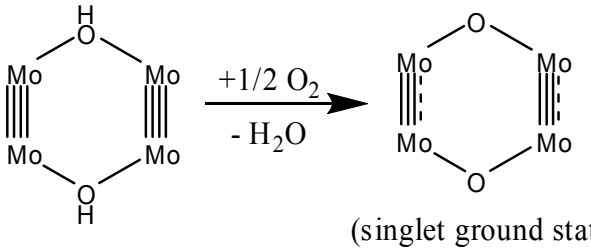

(singlet ground state) (eq. 7)

Chapter IV has shown that upon oxidation of the compounds $[Mo_2(cis\text{-}DAniF)_2]_2(\mu\text{-}X)_4$, X = Cl, Br, I to species containing the corresponding $\{[Mo_2(cis\text{-}DAniF)_2]_2(\mu\text{-}X)_4\}^+$ cations, the separation between dimetal units ($[Mo_2]\cdots[Mo_2]$) decreases in spite of the increase in electrostatic charge. The decrease is caused by an increase in electronic communication which is principally due to a direct overlap between the δ orbitals from the adjacent dimetal units which leads to partial bond formation. In these compounds the $\Delta E_{1/2}$ values decrease as $Mo_2\cdots Mo_2$ increases with an increase in the atomic radius of X.

In Chapter V, a pair of isomeric cyclic triads containing three quadruply-bonded $[Mo_2]$ units, $[Mo_2(cis\text{-}DAniF)_2]^{2+}$ bridged by six fluoride anions, has been synthesized and crystallographically characterized. For the α isomer, the three $[Mo_2]$ units are oriented in two orthogonal directions. Two of them are structurally equivalent and parallel to each other, but oriented perpendicular to the third one. The β isomer is a triangle with three geometrically identical $[Mo_2]$ units, parallel to each other, as the

vertices. Thus the β isomer possesses idealized D_{3h} symmetry while the α isomer only has C_{2v} symmetry. These two isomers do not interconvert in boiling THF or toluene or under irradiation with ultraviolet light but oxidation of the α isomer first generates an α^+ species that changes to β^+. The two isomers have very similar electrochemical behavior, both showing three reversible one-electron redox processes for the $[Mo_2]$ centers, and similar potential separations ($\Delta E_{1/2}$). The first and second redox couples are well separated (ca. 390 ~ 410 mV), while the second and third ones are separated by only about 150 mV.

Chapter VI discussed that the hydride anions, H^-, have been found to cause the assembly of dimolybdenum units $[Mo_2(cis\text{-}DAniF)_2]^{2+}$, represented for simplicity as $[Mo_2]$, to form a tetranuclear complex $[Mo_2(cis\text{-}DAniF)_2]_2(\mu\text{-}H)_4$ (**14**) with a Mo_4H_4 core that may be described as an elongated tetrahedron in which the four H atoms are along the four long edges and the Mo_2 units along the short edges. The two quadruply bonded dimolybdenum units, separated by only 2.718 Å, are essentially orthogonal. It gives the shortest $[Mo_2]\cdots[Mo_2]$ distance known so far for complexes with multiple dimolybdenum units. DFT calculations indicate that there is a cuboidal isomer 3.8 Kcal/mol above that of **14** but such isomer is not observed.

REFERENCES

(1) (a) Ward, M. D. *Chem. Soc. Rev.* **1995**, *34*, 121. (b) Astruc, D. *Acc. Chem. Res.* **1997**, *30*, 383. (c) McCleverty, J. A.; Ward, M. D. *Acc. Chem. Res.* **1998**, *31*, 842. (d) Li, Z.; Beatty, A. M.; Fehlner, T. P. *Inorg. Chem.* **2003**, *42*, 5707. (e) Biancardo, M.; Schwab, P. F.; Argazzi, R.; Bignozzi, C. A. *Inorg. Chem.* **2003**, *42*, 3966.

(2) Prassides, K. Ed. *Mixed-valency Systems. Applications in Chemistry, Physics and Biology*; Kluwer Academic Publishers: Dordrecht, The Netherlands, **1991**.

(3) (a) Blondin, G.; Gired, J.-J. *Chem. Rev.* **1990**, *90*, 1359 and references therein. (b) Gamelin, D. R.; Bominaar, E. L.; Kirk, M. L.; Wieghardt, K.; Solomon, E. I. *J. Am. Chem. Soc.* **1996**, *118*, 8085 and references therein.

(4) (a) Creutz, C. *Prog. Inorg. Chem*. **1983**, *30*, 1. (b) Richardson, D. E.; Taube, H. *Coord. Chem. Rev.* **1984**, *60*, 107. (c) Demadis, K. D.; Hartshorn, C. M.; Meyer, T. J. *Chem. Rev*. **2001**, *101*, 2655 (d) Kaim, W.; Klein, A.; Glöckle, M. *Acc. Chem. Res*. **2000**, *33*, 755.

(5) (a) Creutz, C.; Taube, H. *J. Am. Chem. Soc.* **1969**, *91*, 3988. (b) Creutz, C.; Taube, H. *J. Am. Chem. Soc.* **1973**, *95*, 1086.

(6) (a) Dogan, A.; Sarkar, B.; Klein, A.; Lissner, F.; Schleid, T.; Fiedler, J.; Zalis, S.; Jain, V. K.; Kaim, W. *Inorg. Chem*. **2004**, *43*, 5973. (b) Rigaut, S.; Olivier, C.; Costuas, K.; Choua, S.; Fadhel, O.; Massue, J.; Turek, P.; Saillard, J.-Y.; Dixneuf, P. H.; Touchard, D. *J. Am. Chem. Soc.* **2006**, *128*, 5859. (c)

D'Alessandro, D. M.; Dinolfo, P. H.; Davies, M. S.; Hupp, J. T.; Keene, F. R. *Inorg. Chem*. **2006**, *45*, 3261.

(7) Robin, M. B.; Day, P. *Adv. Inorg. Chem. Radiochem*. **1967**, *10*, 357.

(8) Hush, N. S. *Prog. Inorg. Chem*. **1967**, *8*, 391.

(9) (a) Stebler, A.; Ammeter, J. H.; Füerholz, U.; Ludi, A. *Inorg. Chem*. **1984**, *23*, 2764. (b) Bunker, B. C.; Drago, R. S.; Hendrickson, D. N.; Richman, R. M.; Kessel, S. L. *J. Am. Chem. Soc*. **1978**, *100*, 3805. (c) Fürholz, U.; Bürgi, H.-B.; Wagner, F. E.; Stebler, A.; Ammeter, J. H.; Krausz, E.; Clark, R. J. H.; Stead, M. J.; Ludi, A. *J. Am. Chem. Soc.* **1984**, *106*, 121. (d) Fürholz, U.; Joss, S.; Bürgi, H.-B.; Ludi, A. *Inorg. Chem*. 1**985**, *24*, 943.

(10) Cotton, F. A.; Murillo, C. A.; Walton, R. A. Eds. *Multiple Bonds between Metal Atoms, 3rd ed.*; Springer Science and Business Media, Inc. New York, **2005**.

(11) (a) Chisholm, M. H.; Patmore, N. J. *Acc. Chem. Res.* **2007**, *39*, 19. (b) Burdzinski, G. T.; Ramnauth, R.; Chisholm, M. H.; Gustafson, T. L. *J. Am. Chem. Soc.* **2006**, *128*, 6776. (c) Chisholm, M. H.; Feil, F.; Hadad, C. M.; Patmore, N. J. *J. Am. Chem. Soc.* **2005**, *127*, 18150. (d) Barybin, M. V.; Chisholm, M. H.; Dalal, N. S.; Holovics, T. H.; Patmore, N. J.; Robinson, R. E.; Zipse, D. J. *J. Am. Chem. Soc.* **2005**, *127*, 15182. (e) Bursten, B. E.; Chisholm, M. H.; D'Acchioli, J. S. *Inorg. Chem.* **2005**, *44*, 5571. (f) Chisholm, M. H.; Pate, B. D.; Wilson, P. J.; Zaleski, J. M. *Chem. Commun*. **2002**, 1084. (g) Cayton, R. H.; Chisholm, M. H.; Huffman, J. C.; Lobkovsky, E. B. *J. Am. Chem. Soc.* **1991**, *113*, 8709.

(12) (a) Cotton, F. A.; Donahue, J. P.; Lin, C.; Murillo, C. A. *Inorg. Chem.* **2001**, *40*, 1234. (b) Cotton, F. A.; Donahue, J. P.; Murillo, C. A. *J. Am. Chem. Soc*. **2003**, *125*, 5436. (c) Cotton, F. A.; Donahue, P. J.; Murillo, C. A.; Pérez, L. M. *J. Am. Chem. Soc*. **2003**, *125*, 5486.

(13) (a) Cotton, F. A.; Liu, C. Y.; Murillo, C. A.; Villagrán, D.; Wang, X. *J. Am. Chem. Soc*. **2003**, *125*, 13564. (b) Cotton, F. A.; Liu, C. Y.; Murillo, C. A.; Villagrán, D.; Wang, X. *J. Am. Chem. Soc*. **2004**, *126*, 14822.

(14) Cotton, F. A.; Donahue, J. P.; Murillo, C. A. *Inorg. Chem*. **2001**, *40*, 2229.

(15) (a) Cotton, F. A.; Liu, C. Y.; Murillo, C. A.; Wang, X. *Inorg. Chem*. **2003**, *42*, 4619. (b) Cotton, F. A.; Dalal, N. S.; Liu, C. Y.; Murillo, C. A.; North J. M.; Wang, X. *J. Am. Chem. Soc.* **2003**, *125*, 12945.

(16) Cotton, F. A.; Daniels, L. M.; Jordan IV, G. T.; Lin, C.; Murillo, C. A. *J. Am. Chem. Soc*. **1998**, *120*, 3398.

(17) (a) Cotton, F. A.; Daniels, L. M.; Jordan IV, G. T.; Lin, C.; Murillo, C. A. *Inorg. Chem. Commun*. **1998**, 109. (b) Cotton, F. A.; Daniels, L. M.; Guimet, I.; Henning, R. W.; Jordan IV, G. T.; Lin, C.; Schultz, A. J.; Murillo, C. A. *J. Am. Chem. Soc*. **1998**, *120*, 12531.

(18) Cotton, F. A.; Li, Z.; Liu, C. Y.; Murillo, C. A.; Zhao, Q. *Inorg. Chem*. **2006**, *45*, 6387.

(19) Richardson, D. E.; Taube, H. *Inorg. Chem*. **1981**, *20*, 1278.

(20) (a) Cotton, F. A.; Hillard, E. A.; Murillo, C. A. *Inorg. Chem*. **2002**, *41*, 1639. (b) Cotton, F. A.; Daniels, L. M.; Murillo, C. A.; Wilkinson, C. C. *J. Am. Chem. Soc*. **2002**, *124*, 9249.

(21) Cotton, F. A.; Li, Z.; Liu, C. Y.; Murillo, C. A.; Villagrán, D. *Inorg. Chem*. **2006**, *45*, 767.

(22) Cotton, F. A.; Murillo, C. A.; Villagrán, D.; Yu, R. *J. Am. Chem. Soc.* **2006**, *128*, 3281.

(23) Lin, C.; Protasiewicz, J. D.; Ren, T. *Inorg. Chem.* **1996**, *35*, 6422.

(24) SMART V 5.05 Software for the CCD Detector System; Bruker Analytical X-ray System, Inc.: Madison, WI, 1998.

(25) SAINT. Data Reduction Software. V 6.36A; Bruker Analytical X-ray System, Inc.: Madison, WI, 2002.

(26) SADABS. Bruker/Siemens Area Detector Absorption and Other Corrections. V2.03; Bruker Analytical X-ray System, Inc.: Madison, WI, 2002.

(27) Sheldrick, G. M., SHELXTL. V 6.12; Bruker Analytical X-ray Systems, Inc.: Madison, WI, 2000.

(28) The Hush formula is appropriate for systems with two dimetal units linked by *one* linker. See: Hush, N. S. *Coord. Chem. Rev.* **1985**, *64*, 135.

(29) For an early example of the use of Mo isotopes for establishing mixed valence, see Bruns, W.; Kaim, W.; Waldör, E.; Krejčik, M. *J. Chem. Soc., Chem. Commun*. **1993**, 1868.

(30) Cotton, F. A.; Donahue, J. P.; Huang, P.; Murillo, C. A.; Villagrán, D.; Wang, X. *Z. Anorg. Allg. Chem.* **2005**, *631*, 2606.

(31) The EPR spectrum of **2** at room temperature gives the same *g* value and hyperfine structure.

(32) Cotton, F. A.; Li, Z.; Liu, C. Y.; Murillo, C. A. *Inorg. Chem*. **2006**, *45*, 9765.

(33) To obtain a clean ^{1}H NMR spectrum of **4** (β^{2+}) with sharp signals it is important to add a small amount of iodine to oxidize a trace of **2** (β^{+}) present as an impurity in solution. The EPR spectra of **4** (β^{2+}) also showed a small amount of **2** (β^{+}). Its EPR signal also disappeared upon addition of a small amount of iodine. These observations are consistent with **4** (β^{2+}) being diamagnetic.

(34) This value is typically less than 0.10 emu K mol^{-1}, and independent of *T*. Such background value is due to the existence of a small amount of contamination from the singly oxidized β^{+} species. See ref. 33.

(35) (a) Poliakoff, M.; Fizpatrick, J. M.; Farren, T. R. A.; Anastas, P. T. *Science* **2002**, *297*, 807. (b) Anastas, P. T.; Kirchtoff, M. M. *Acc. Chem. Res.* **2002**, *35*, 686. (c) Cheng, K.; Foxman, B. M.; Gersten, S. W. *Mol. Cryst. Liq. Cryst*. **1979**, *52*, 77.

(36) (a) Toda, F. *Acc. Chem. Res.* **1995**, *28*, 480. (b) Tanaka, A.; Toda, F. *Chem. Rev.* **2000**, *100*, 1025. (c) Ohmori, O.; Kawano, M.; Fujita, M. *J. Am. Chem. Soc.* **2004**, *126*, 16292.(d) Turowska-Tyrk, I.; Trzop, E.; Scheffer, J. R.; Chen, S. *Acta. Cryst.* **2006**, *B62*, 128. (e) Garcia-Garibay, M. A. *Acc. Chem. Res.* **2003**, *36*, 491.

(37) (a) Iorganidis, L.; Kanatzidis, M. G. *J. Am. Chem. Soc.* **2000**, *122*, 8319. (b) Chui, S. S.-Y.; Lo, S. M.-F.; Charmant, J. P. H.; Orpen, A. G.; Williams, I. D. *Science* **1999**, *283*, 1148. (c) Suh, M. P.; Ko, G. W.; *J. Am. Chem. Soc.* **2002**, *124*, 10976. (d) Rather, B.; Zaworotko, M. J. *Chem. Commun.* **2003**, 830. (e) Lee, E. Y.; Suh, M. P. *Angew. Chem. Int. Ed.* **2004**, *43*, 2798. (f) Choi, H. J.; Suh, M. P. *J. Am. Chem. Soc.* **2004**, *126*, 15844. (g) Takamizawa, S.; Nakata, E.; Saito, T. *Angew. Chem. Int. Ed.* **2004**, *43*, 1368. (h) Halder, G. J.; Kepert, C. J. *J. Am. Chem. Soc.* **2005**, *127*, 7891. (i) Dieters, E.; Bulach, V.; Hosseini, M. W. *Chem. Commun.* **2005**, 3906. (j) Takaoka, K.; Kawano, M.; Tominaga, M.; Fujita, M. *Angew. Chem. Int. Ed.* **2005**, *44*, 2151. (k) Armentano, D.; Munno, G. D.; Mastropietro, T. F.; Julve, M.; Lloret, F. *J. Am. Chem. Soc.* **2005**, *127*, 10778. (l) Kondo, M.; Murata, M.; Nishihara, H.; Nishibori, E.; Aoyagi, S.; Yoshida, M.; Kinoshita, Y.; Sakata, M. *Angew. Chem. Int. Ed.* **2006**, *45*, 5461. (m) Di, L.; Foxman, B. M. *Chem. Mater.* **1992**, *4*, 258. (n) Vela, M. J.; Buchholz, V.; Enkelmann, V.; Snider, B. B.; Foxman, B. M. *Chem. Commun*. **2000**, 2225. (o) Sandor, R. B.; Foxman, B. M. *Tetrahedron* **2000**, *56*, 6805. (p) Iordanidis, L.; Kanatzidis, M. *Angew. Chem. Int. Ed.* **2000**, *39*, 1927. (q) Brezesinski, T.; Groenewolt, M.; Antonietti, M.; Smarsly, B. *Angew. Chem. Int. Ed.* **2006**, *45*, 781. (r) Papaefstathiou, G. S.; Zhong, Z.; Geng, L.; MacGillivray, L. R. *J. Am. Chem. Soc*. **2004**, *126*, 9158.

(38) (a) Ghisla S.; Thorpe, C. *Eur. J. Biochem.* **2004**, *271*, 494. (b) Reetz, M. T.; Eibach F. *Angew. Chem. Int. Ed. Engl.* **1978**, *17*, 278. (c) Bietti, M.; Capone, A. *J. Org. Chem.* **2006**, *71*, 5260.

(39) Some important processes for which this equation also applies are the C─H hydroxylation by cytochrome P450 (e.g., Schöneboom, S.; Cohen, S.; Lin, H.; Shaik, S.; Thiel, W. *J. Am. Chem. Soc*. **2004**, *126*, 4017 and Bathelt, C. M.; Zurek, J.; Mulholland, A. J.; Harvey, J. N. *J. Am. Chem. Soc*. **2005**, *127*, 12900.) and proton-coupled electron transfer from phenols, flavonols and other antioxidants (e.g., Sjödin, M.; Irebo, T.; Utas, J. E.; Lind, J.; Merényi, G.; Åkermark, B.; Hammarström. L. *J. Am. Chem. Soc*. **2006**, *128*, 13076 and Fukumoto, L. R.; Mazza, G. *J. Agric. Food Chem*. **2000**, *48*, 3597.)

(40) Cotton, F. A.; Murillo, C. A.; Yu, R.; Zhao, Q. *Inorg. Chem.* **2006**, *45*, 9046.

(41) On rare occasions two different types of crystals were isolated from the same flask, both in the space group *P*ī, but differing in the number of interstitial CH_2Cl_2 molecules (**5**·1.5CH_2Cl_2 and **5**·CH_2Cl_2). In both cases the molecules of **5** are chemically the same. Crystal data for **5**·CH2Cl2: triclinic, *P*ī, *a* = 13.511(4), *b* = 13.808(4), *c* = 14.241(4) Å, α = 95.594(4), β = 109.780(5), γ = 107.869(5)º, *V* = 2318(1) Å3, *Z* = 1, Mo(1)–Mo(2) = 2.1058(7) Å. Crystals of **5**·CH_2Cl_2 transform on exposure to air to **6**·CH_2Cl_2 also in a SCSC fashion. Crystal data for **6**·CH_2Cl_2: triclinic, *P*ī, *a* = 13.486(3), *b* = 13.741(3), *c* = 14.255(3) Å, α = 95.435(4), β = 109.579(4), γ = 108.355(4)º, *V* = 2302.1(9) Å3, *Z* = 1, Mo(1)–Mo(2) = 2.1540(6) Å.

(42) The solution of HBF_4 in CH_2Cl_2 was made from a 0.5 mL of a 1 M solution of $(OEt_3)BF_4$ in CH_2Cl_2 which was diluted with CH_2Cl_2 to a volume of 50 mL. A trace of water was used to generate HBF_4.

(43) Cotton, F. A.; Daniels, L. M.; Hillard, E. A.; Murillo, C. A. *Inorg. Chem.* **2002**, *41*, 2466.

(44) For comparison, yellow crystals of $[Mo_2(Dm CF_3F)_3]_2(\mu\text{-}OH)_2$ (D*m*CF_3F = *N*,*N*′-di-*m*-trifluoromethylphenylformamidinate) lost crystallinity immediately upon exposure to air. See ref. 40.

(45) In the limit of oxidation (when no CH_2Cl_2 was used in the refinement), calculations using PLATON/SQUEEZE show that the total potential solvent accessible void in **6** is 246 $Å^3$ and the electron count/cell is 32, which is much less than that expected (144 electrons/cell) for the three CH_2Cl_2 molecules that were present at the beginning of the process.

(46) Because of the loss of interstitial CH_2Cl_2 molecules the mosaicity of the crystal of **6** increased and the R values are higher than those for **6**·1.5CH_2Cl_2. However, the bond distances for **6** are quite similar to those for the molecules in crystals of **6**·2CH_2Cl_2 that were obtained from solution.

(47) Excess oxygen turned the color of the solid (an also solutions) to red. Because this mixture did not provide good crystalline samples, it has not yet been identified. In solution exposed to excess oxygen the NMR and EPR spectra showed that the mixture contained paramagnetic species.

(48) During refinement of crystal data for **6**, there was indication that an interstitial water molecule was present in the crystal.

(49) There is only a small loss of crystallinity due to loss of interstitial solvent as crystals were cooled on a stream of N_2.

(50) For a recent study of the reduction of O_2 to $O_2H^{\cdot}$, see: Geletii, Y. V.; Hill, C. L.; Atalla, R. H.; Weinstock, I. A. *J. Am. Chem. Soc*. **2006**, *128*, 17033.

(51) Cotton, F. A.; Liu, C. Y.; Murillo, C. A.; Wang, X. *Chem. Commun*. **2003**, 2190.

(52) (a) McGinnis, R. N.; Ryan, T. R.; McCarley, R. E. *J. Am. Chem. Soc.* **1978**, *100*, 7900. (b) Cotton, F. A.; Shang, M. *J. Cluster Sci.* **1991**, *2*, 121.

(53) Chisholm, M. H.; Cotton, F. A.; Daniels, L. M.; Folting, K.; Huffman, J. C.; Iyer, S. S.; Lin, C.; Macintosh, A. M.; Murillo, C. A. *J. Chem. Soc., Dalton Trans.* **1999**, 1387.

(54) (a) Hohenberg, P.; Kohn, W. *Phys. Rev.* **1964**, *136*, B864. (b) Parr, R. G.; Yang, W. *Density-Functional Theory of Atoms and Molecules*, Oxford University Press: Oxford, 1989.

(55) (a) Becke, A. D. *Phys. Rev. A* **1988**, *38*, 3098. (b) Becke, A. D. *J. Chem. Phys.* **1993**, *98*, 1372. (c) Becke, A. D. *J. Chem. Phys.* **1993**, *98*, 5648.

(56) Lee, C. T.; Yang, W. T.; Parr, R. G. *Phys. Rev. B* **1998**, *37*, 785.

(57) *Gaussian 03, Revision C.02*, Frisch, M. J.; Trucks, G. W.; Schlegel, H. B.; Scuseria, G. E.; Robb, M. A.; Cheeseman, J. R.; Montgomery, Jr., J. A.; Vreven, T.; Kudin, K. N.; Burant, J. C.; Millam, J. M.; Iyengar, S. S.; Tomasi, J.; Barone, V.; Mennucci, B.; Cossi, M.; Scalmani, G.; Rega, N.; Petersson, G. A.;

Nakatsuji, H.; Hada, M.; Ehara, M.; Toyota, K.; Fukuda, R.; Hasegawa, J.; Ishida, M.; Nakajima, T.; Honda, Y.; Kitao, O.; Nakai, H.; Klene, M.; Li, X.; Knox, J. E.; Hratchian, H. P.; Cross, J. B.; Bakken, V.; Adamo, C.; Jaramillo, J.; Gomperts, R.; Stratmann, R. E.; Yazyev, O.; Austin, A. J.; Cammi, R.; Pomelli, C.; Ochterski, J. W.; Ayala, P. Y.; Morokuma, K.; Voth, G. A.; Salvador, P.; Dannenberg, J. J.; Zakrzewski, V. G.; Dapprich, S.; Daniels, A. D.; Strain, M. C.; Farkas, O.; Malick, D. K.; Rabuck, A. D.; Raghavachari, K.; Foresman, J. B.; Ortiz, J. V.; Cui, Q.; Baboul, A. G.; Clifford, S.; Cioslowski, J.; Stefanov, B. B.; Liu, G.; Liashenko, A.; Piskorz, P.; Komaromi, I.; Martin, R. L.; Fox, D. J.; Keith, T.; Al-Laham, M. A.; Peng, C. Y.; Nanayakkara, A.; Challacombe, M.; Gill, P. M. W.; Johnson, B.; Chen, W.; Wong, M. W.; Gonzalez, C.; and Pople, J. A.; Gaussian, Inc.: Wallingford CT, 2004.

(58) (a) Dunning, T. H.; Hay, P. J. In *Modern Theoretical Chemistry. 3. Methods of Electronic Structure Theory*, Schaefer III, H. F., Ed. Plenum Press: New York, 1977; pp.1-28. (b) Woon, D. E.; Dunning, T. H. *J. Chem. Phys.* **1993**, *98*, 1358.

(59) (a) Dunning, T. H. *J. Chem. Phys.* **1989**, *90*, 1007. (b) Woon, D. E.; Dunning, T. H. *J. Chem. Phys.* **1993**, *98*, 1358. (c) Wilson, A. K.; Woon, D. E.; Peterson, K. A.; Dunning, T. H. *J. Chem. Phys.* **1999**, *110*, 7667.

(60) (a) Wadt, W. R.; Hay, P. J. *J. Chem. Phys.* **1985**, *82*, 284. (b) Hay, P. J.; Wadt, W. R. *J. Chem. Phys.* **1985**, *82*, 299.

(61) Casida, M. E.; Jamorski, C.; Casida, K. C.; Salahub, D. R. *J. Chem. Phys.* **1998**, *108*, 4439.

(62) Cotton, F. A.; Mester, Z. C.; Webb, T. R. *Acta Crystallogr.* **1974**, *B30*, 2768.

(63) Cotton, F. A. *Chemical Applications of Group Theory*, 3rd ed. John Wiley and Sons: New York, 1990.

(64) See for example: (a) Fujita, M.; Tominaga, M.; Hori, A.; Therrien, B. *Acc. Chem. Res.* **2005**, *38*, 371. (b) Fujita, M. *Chem. Soc. Rev.* **1998**, *27*, 417. (c) Fujita, M. *Acc. Chem. Res*. **1999**, *32*, 53. (d) Ruben, M.; Rojo, J.; Romero-Salguero, F. J.; Uppadine, L. H.; Lehn, J.-M. A*ngew. Chem. Int. Ed.* **2004**, *43*, 3644. (e) Mirkin, C. A.; Holliday, B. J. *Angew. Chem. Int. Ed.* **2001**, *40*, 2022.

(65) (a) Caulder, D.; Raymond, K. N. *Acc. Chem. Res*. **1999**, *32*, 975. (b) Klausmeyer, K. K.; Wilson, S. R.; Rauchfuss, T. B. *J. Am. Chem. Soc.* **1999**, *121*, 2705. (c) Evans, O. R.; Lin, W. *Acc. Chem. Res.* **2002**, *35*, 511. (d) Giananeschi, N. C.; Masar III, M. S.; Mirkin, C. A. *Acc. Chem. Res*. **2005**, *38*, 825.

(66) (a) Janiak, C. *Angew. Chem. Int. Ed. Engl.* **1997**, *36*, 1431. (b) Sudik, A. C.; Millward, A. R.; Ockwig, N. W.; Cote, A. P.; Kim, J.; Yaghi, O. M. *J. Am. Chem. Soc.* **2005**, *127*, 7110. (c) Rowsell, J. L. C.; Yaghi, O. M. *Angew. Chem. Int. Ed*. **2005**, *44*, 4670.

(67) (a) Maspoch, D.; Ruiz-Molina, D.; Wurst, K.; Domingo, N.; Cavallini, M.; Biscarini, F.; Tejada, J.; Rovira, C.; Veciana, J. *Nat. Mater.* **2003**, *2*, 190. (b) Halder, G. J.; Kepert, C. J.; Moubaraki, B.; Murray, K. S.; Cashion, J. D. *Science* **2002**, *298*, 1762.

(68) (a) Wu, C.-D.; Hu, A.; Zhang, L.; Lin, W. *J. Am. Chem. Soc.* **2005**, *127*, 8940. (b) Janiak, C. *Dalton Trans.* **2003**, 2781.

(69) (a) Cotton, F. A.; Lin, C.; Murillo, C. A. *Acc. Chem. Res.* **2001**, *34*, 759. (b) Cotton, F. A.; Lin, C.; Murillo, C. A. *Proc. Natl. Acad. Sci. U.S.A.* **2002**, *99*, 4810.

(70) (a) Politzer, P.; Timberlake, J. W. *J. Org. Chem*. **1972**, *37*, 3557. (b) Cotton, F. A.; Wilkinson, G.; Murillo, C. A.; Bochmann, M. *Advanced Inorganic Chemistry*, 6th ed. John Wiley & Sons: New York, 1999.

(71) Roesky, H. W.; Haiduc, I. *J. Chem. Soc., Dalton Trans.* **1999**, 2249.

(72) (a) Edwards, A. J.; Peacock, R. D.; Small, R. W. H. *J. Chem. Soc*. **1962**, 4486. (b) Holloway, J. H.; Peacock, R. D.; Small, R. W. H. *J. Chem. Soc*. **1964**, 644. (c) Peacock, R. D.; Marshall, C. J.; Russell, D. R.; Wilson, I. L. *J. Chem. Soc.*, *Chem. Commun*. **1970**, 1643. (d) Burns, C. J.; Berg, D. J.; Andersen, R. A. *J. Chem. Soc., Chem. Commun*. **1987**, 272. (e) Gundersen, G.; Haugen, T.; Haaland, A. *J. Chem. Soc., Chem. Commun*. **1972**, 708. (f) Weidlein, J.; Krieg. V. *J. Organomet. Chem*. **1968**, *11*, 9. (g) Yu, P.; Montero, M. L.; Barnes, C. E.; Roesky, H. W.; Usón, I. *Inorg. Chem*. **1998**, *37*, 2595. (h) Troyanov, S. I.; Varga, V.; Mach, K. *J. Organomet. Chem*. **1991**, *402*, 201. (i) Palacios, F.; Royo, P.; Serrano, J. L.; Balcázar, J. L.; Fonseca, I.; Florencio, F. *J. Organomet. Chem*. **1989**, *375*, 51.

(73) (a) Waezsada, S. D.; Liu, F. Q.; Murphy, E. F.; Roesky, H. W.; Teichert, M.; Usón, I.; Schmidt, H. G.; Albers, T.; Parisini, E.; Noltemeyer, M. *Organometallics* **1997**, *16*, 1260. (b) Bottomley, F.; Paez, D. E.; White, P. S. *J.*

Organomet. Chem. **1985**, *291*, 35. (c) Schumann, H.; Keitsch, M. R.; Winterfeld, J.; Demtschuk, J. *J. Organomet. Chem*. **1996**, *525*, 279.

(74) The compound {β-[Mo_2(*cis*-DAniF)$_2$]$_3$(μ-F)$_6$}PF_6 was made similarly to **12** but using [$FeCp_2$]PF_6 instead of [$FeCp_2$]BPh_4. The structure of {β-[Mo_2(*cis*-DAniF)$_2$]$_3$(μ-F)$_6$}PF_6 is similar to that of **12**. Anal. Calcd for $C_{90}H_{90}F_{12}Mo_6N_{12}O_{12}P$: C, 45.68; H, 3.83; N, 7.10. Found: C, 45.87; H, 4.02; N, 7.36.

(75) Chisholm, M. H.; Huffman, J. C.; Kelly, R. L. *J. Am. Chem. Soc.* **1979**, *101*, 7100.

(76) Although the compounds with counter ions such as BF_4^- and PF_6^- may be synthesized using the corresponding ferrocenium salt, the quality of their crystals is not as good.

(77) (a) Hieber, W.; Leutert, F. *Naturwissenschaften* **1931**, *19*, 360. (b) Hieber, W.; Leutert, F. *Z. Anorg. Allg. Chem.* **1932**, *204*, 145. (c) Hieber, W.; Leutert, F. *Ber. Dtsch. Chem. Ges.* **1931**, *64*, 2832. (d) Hieber, W.; Vetter, H. *Z. Anorg. Allg. Chem.* **1933**, *212*, 145. (e) Hieber, W.; Mühlbauer, F.; Ehmann, E. A. *Ber. Dtsch. Chem. Ges.* **1932**, *65*, 1090.

(78) (a) Hieber, W.; Schulten, H. *Z. Anorg. Allg. Chem.* **1937**, *232*, 17. (b) Hieber, W.; Schulten, H. *Z. Anorg. Allg. Chem.* **1937**, *232*, 29.

(79) (a) Cornils, B.; Herrmann, W. A.; Rasch, M. *Angew. Chem. Int. Ed. Engl.* **1994**, *33*, 2144. (b) Cornils, B.; Herrmann, W. A.; Rasch, M. *Angew. Chem. Int. Ed. Engl.* **1994**, *33*, 2348.

(80) (a) Cornils, B.; Herrmann, W. A. In *Applied Homogenous Catalysis with Organometallic Compounds*, VCH, Weinheim, 1996. (b) Labinger, J. A. in A. Dedieu (Ed.), *Transition Metal Hydrides*. VCH, Weinheim, 1992; p. 361. (c) Dong, Z.-R.; Li, Y.-Y.; Chen, J.-S.; Li, B.-Z.; Xing, Y.; Gao, J.-X. *Org. Lett.* **2005**, *7*, 1043.

(81) (a) Khaselev, O.; Turner, J. A. *Science* **1998**, *280*, 425. (b) Turner, J. A. *Science* **1999**, *285*, 687.

(82) (a) Nocera, D. *Science* **2007**, *315*, 789. (b) Gregoire-Padró, C. E. *Energy & Fuels* **1998**, *12,* 1. (c) Thomas, J. M.; Raja, R.; Johnson, B. F. G.; Hermans, S.; Jones, M. D.; Khimyak, T. *Ind. Eng. Chem. Res.* **2003**, *42*, 1563. (d) Berry, G. D.; Aceves, S. M. *Energy & Fuels* **1998**, *12*, 49.

(83) Connelly, N. G.; Geiger, W. E. *Chem. Rev.* **1996**, *96*, 877.

(84) (a) Peters, J. W.; Lanzilotta, W. N.; Lemon, B. J.; Seefeldt, L. C. *Science* **1998**, *282*, 1853. (b) Ogo, S.; Kabe, R.; Uehara, K.; Kure, B.; Nishimura, T.; Menon, S. C.; Harada, R.; Fukuzumi, S.; Higuchi, Y.; Ohhara, T.; Tamada, T.; Kuroki, R. *Science* **2007**, *316*, 585.

(85) (a) Pearson, R. G. *Chem. Rev.* **1985**, *85*, 41. (b) Cotton, F. A. In *Basic Inorganic Chemistry*, *3rd Edition*, Wiley, New York, 1994.

(86) (a) Ohashi, M.; Matsubara, K.; Iizuka, T.; Suzuki, H. *Angew. Chem. Int. Ed.* **2003**, *42*, 937. (b) Bau, R.; Ho, N. N.; Schneider, J. J.; Mason, S. A.; McIntyre, G. J. *Inorg. Chem.* **2004**, *43*, 555.

(87) (a) Kubas, G. J.; Ryan, R. R.; Swanson, B. I.; Vergamini, P. J.; Wasserman, H. J. *J. Am. Chem. Soc.* **1984**, *106*, 451. (b) Kubas, G. J.; Ryan, R. R. *Polyhedron* **1986**, *5*, 473.

(88) It should be noted that positions of hydrogen atoms are not accurately determined by X-ray crystallography.

(89) Cugny, J.; Schmalle, H. W.; Fox, T.; Blacque, O.; Alfonso, M.; Berke, H. *Eur. J. Inorg. Chem.* **2006**, 540.

(90) (a) Alvarez, M. A.; García, M. E.; Ramos, A.; Ruiz, M. A. *Organometallics* **2002**, *21*, 5515. (b) Petersen, J. L.; Dahl, L. F.; Williams, J. M. *J. Am. Chem. Soc.* **1974**, *96*, 6610.

APPENDIX A

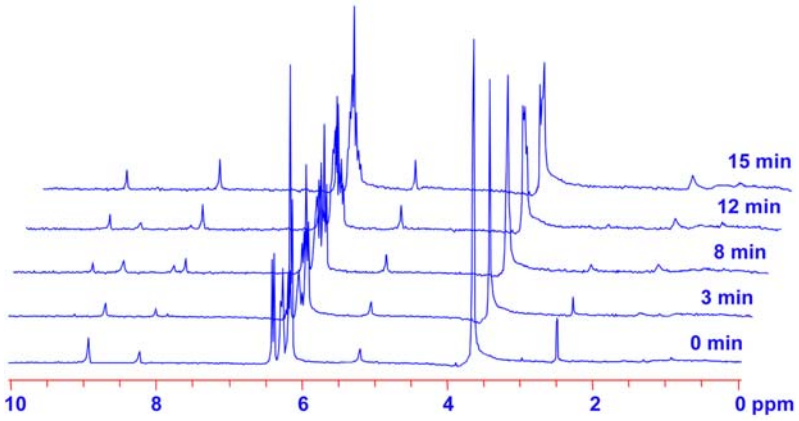

Figure 39. ^{1}H NMR spectra in the range 0–10 ppm of a CD_2Cl_2 solution of $[Mo_2(DAniF)_3]_2(\mu\text{-}OH)_2$ (**5**) as it is oxidized by O_2 to $[Mo_2(DAniF)_3]_2(\mu\text{-}O)_2$ (**6**) over a 15-minute period.

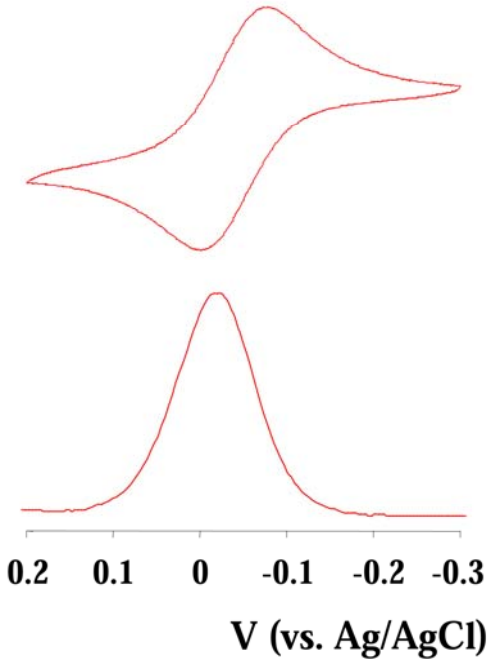

Figure 40. Cyclic voltammogram (CV) and differential potential voltammogram (DPV) of $[Mo_2(DAniF)_3]_2(\mu\text{-}O)_2$ (**6**) in CH_2Cl_2. Potentials are referenced to Ag/AgCl. The CV and DPV were collected on a CH Instruments electrochemical analyzer with Pt working and auxiliary electrodes, an Ag/AgCl reference electrode, a scan rate of 100 mV/s (for CVs), and 0.1 M Bu_4NPF_6 (in CH_2Cl_2) as electrolyte. Under these experimental conditions, the $E_{1/2}$ ferrocenium/ferrocene (Fc^+/Fc) couple was measured at 440 mV.

Table XVI. X-ray Crystallographic Data for the Transformation of a Single Crystal **5**·1.5CH_2Cl_2 to **6** upon Exposure to Air

compound	**5**·1.5CH_2Cl_2							**6**
cumulative time of exposure to air (h)	0	10	26	67	163	215	312	420
CH_2Cl_2 occupancy [a]	1.5	0.457(9)	0.253(7)	0.184(9)	0	0	0	0
void volume ($Å^3$) [b]	14	170	163	156	152	283	273	246
electron count/cell [b]	0	7	4	6	7	25	22	32
formula	$C_{91.5}H_{93}Cl_3Mo_4N_{12}O_{14}$	$C_{90.46}H_{90.92}Cl_{0.92}Mo_4N_{12}O_{14}$	$C_{90.25}H_{90.50}Cl_{0.50}Mo_4N_{12}O_{14}$	$C_{90.18}H_{90.36}Cl_{0.36}Mo_4N_{12}O_{14}$	$C_{90}H_{90}Mo_4N_{12}O_{14}$	$C_{90}H_{90}Mo_4N_{12}O_{14}$	$C_{90}H_{90}Mo_4N_{12}O_{14}$	$C_{90}H_{90}Mo_4N_{12}O_{14}$
fw	2074.89	1986.32	1968.73	1962.79	1947.50	1947.50	1947.50	1947.50
space group	$P\bar{1}$ (No. 2)	$P\bar{1}$ (No. 2)	$P\bar{1}$ (No. 2)	$P\bar{1}$ (No. 2)	$P\bar{1}$ (No. 2)	$P\bar{1}$ (No. 2)	$P\bar{1}$ (No. 2)	$P\bar{1}$ (No. 2)
a (Å)	14.835(2)	14.758(3)	14.723(3)	14.702(3)	14.680(3)	14.674(2)	14.661(3)	14.736(3)
b (Å)	17.399(2)	17.262(4)	17.246(4)	17.244(4)	17.221(3)	17.232(3)	17.247(3)	17.278(4)
c (Å)	17.809(2)	17.517(4)	17.459(4)	17.449(4)	17.462(3)	17.483(3)	17.539(3)	17.590(4)
α (deg)	92.055(2)	92.301(4)	92.129(3)	91.797(3)	91.619(2)	91.549(2)	91.456(3)	91.605(4)
β (deg)	88.116(2)	91.046(4)	90.993(3)	90.969(3)	91.094(2)	91.144(2)	91.093(3)	90.926(4)
γ (deg)	93.027(2)	95.794(3)	95.741(3)	95.943(3)	96.315(2)	96.256(2)	95.972(3)	96.177(4)
V ($Å^3$)	4585.1(9)	4435(2)	4407(2)	4396.9(16)	4385(2)	4392(1)	4408(2)	4450(2)
Z	2	2	2	2	2	2	2	2
T (K)	213	213	213	213	213	213	213	213
d_{calcd} (g/cm^3)	1.503	1.487	1.484	1.483	1.475	1.473	1.467	1.453
μ (mm^{-1})	0.691	0.650	0.641	0.638	0.629	0.628	0.625	0.619
R1[c]	0.071	0.070	0.098	0.101	0.114	0.135	0.142	0.162
(wR2)[d]	(0.159)	(0.146)	(0.144)	(0.162)	(0.197)	(0.217)	(0.234)	(0.261)

[a] It should be noted that there is a gradual loss of CH_2Cl_2 molecules from the single crystal sample. The occupancies of the solvent CH_2Cl_2 molecules were refined for data set obtained from each time-dependent measurement. After about 160 h, the occupancy for CH_2Cl_2 was essentially zero and the CH_2Cl_2 molecules were no longer included in the structural refinement thereafter. [b] Data were obtained from PLATON/SQUEEZE program. [c] $R1 = \Sigma\|F_o\|-|F_c\|/\Sigma|F_o|$. [d] $wR2 = [\Sigma[w(F_o^2-F_c^2)^2]/\Sigma[w(F_o^2)^2]]^{1/2}$

Table XVII. Selected Bond Lengths (Å) and Angles (deg) for the Transformation of a Single Crystal of **5**·1.5CH_2Cl_2 to **6** upon Exposure to Air

compound	**5**·1.5CH_2Cl_2							**6**
cumulative time of exposure to air (h)	0	10	26	67	163	215	312	420
Mo(1)–Mo(2)	2.1053(6)	2.1082(6)	2.1128(7)	2.1267(8)	2.1398(9)	2.145(1)	2.151(2)	2.151(2)
Mo(3)–Mo(4)	2.1058(6)	2.1081(6)	2.1160(8)	2.1341(9)	2.146(1)	2.150(1)	2.153(2)	2.151(2)
Mo_2(1,2)··· Mo_2(1A,2A)	4.088	4.041	4.000	3.910	3.788	3.756	3.726	3.720
Mo_2(3,4)··· Mo_2(3A,4A)	4.083	4.052	3.992	3.859	3.738	3.725	3.719	3.720
Mo(1)–O(1)	2.146(4)	2.112(3)	2.089(4)	2.039(4)	1.968(5)	1.952(6)	1.935(8)	1.934(8)
Mo(2)–O(1)	2.145(4)	2.119(3)	2.098(4)	2.041(4)	1.972(5)	1.949(6)	1.929(7)	1.926(8)
Mo(3)–O(2)	2.130(4)	2.106(4)	2.068(4)	1.992(5)	1.932(5)	1.916(6)	1.909(8)	1.906(8)
Mo(4)–O(2)	2.135(4)	2.106(4)	2.075(5)	2.001(5)	1.932(5)	1.931(6)	1.930(8)	1.939(8)
Mo(1)–N(1)	2.170(4)	2.172(3)	2.174(4)	2.181(5)	2.180(5)	2.182(6)	2.176(8)	2.190(9)
Mo(1)–N(3)	2.131(4)	2.129(4)	2.131(4)	2.153(5)	2.159(6)	2.162(7)	2.169(9)	2.17(1)
Mo(1)–N(5)	2.166(4)	2.166(3)	2.161(4)	2.165(4)	2.160(5)	2.163(6)	2.180(8)	2.17(1)
Mo(2)–N(2)	2.152(4)	2.141(4)	2.145(4)	2.148(5)	2.149(6)	2.152(6)	2.163(8)	2.169(9)
Mo(2)–N(4)	2.121(4)	2.117(4)	2.119(4)	2.140(5)	2.154(6)	2.161(7)	2.17(1)	2.16(1)
Mo(2)–N(6)	2.155(4)	2.136(3)	2.141(4)	2.142(5)	2.136(5)	2.142(6)	2.143(8)	2.152(9)
Mo(3)–N(7)	2.156(4)	2.154(4)	2.150(4)	2.160(5)	2.158(6)	2.161(6)	2.162(9)	2.170(9)
Mo(3)–N(9)	2.139(4)	2.125(4)	2.139(5)	2.159(5)	2.172(6)	2.173(8)	2.16(1)	2.18(1)
Mo(3)–N(11)	2.149(4)	2.142(4)	2.142(5)	2.156(5)	2.158(6)	2.165(7)	2.172(9)	2.17(1)
Mo(4)–N(8)	2.153(4)	2.151(4)	2.145(5)	2.148(5)	2.151(6)	2.156(6)	2.171(9)	2.17(1)
Mo(4)–N(10)	2.122(4)	2.135(4)	2.153(5)	2.178(6)	2.189(6)	2.186(7)	2.18(1)	2.19(1)
Mo(4)–N(12)	2.141(4)	2.139(5)	2.134(5)	2.139(5)	2.142(6)	2.146(7)	2.137(9)	2.15(1)
Mo(1)–O(1) – Mo(2A)	144.6(2)	145.5(2)	145.6(2)	146.8(2)	148.0(3)	148.6(3)	149.2(4)	149.1(4)
Mo(3)–O(2) – Mo(4A)	146.4(2)	148.2(2)	149.0(2)	150.2(3)	150.6(3)	151.0(3)	151.4(4)	150.8(4)

VITA

Qinliang Zhao received her B.S. degree in Chemistry from Zhejiang University in July of 2003. She then moved to Texas A&M University and began her graduate study under the direction of Prof. F. A. Cotton. She received her Ph. D. in Chemistry at Texas A&M University in August, 2007.

Qinliang Zhao may be reached at Department of Chemistry, Texas A&M University, College Station, TX 77842 United States.

Email address: jzjxbd@gmail.com